Two Applications of a Spatial, Hybrid, Consumer–Resource Model

Elise Woodward

Thesis submitted to the University of Ottawa in partial fulfillment of the requirements for the degree of
Master of Science Mathematics and Statistics*

Department of Mathematics and Statistics
Faculty of Science
University of Ottawa

*The M.Sc. program is a joint program with Carleton University, administered by the Ottawa-Carleton Institute of Mathematics and Statistics

Abstract

Semi-discrete models provide unique insights into the dynamics of some biological populations that purely continuous or purely discrete models cannot. In this thesis, we formulate and analyze a semi-discrete consumer–resource model on two patches. We extend the model by Pachepsky et al. [34] to account for a spatial dimension and analyze equilibria and their stability. We perform an asymptotic analysis to determine the benefit of small dispersal on total asymptotic density and find that dispersal benefits one population while harming the other. We extend our results numerically to find novel responses to dispersal. We then use the Spruce Budworm and Fir Tree systems as inspiration to study the optimal control of the Budworm population. We determine that spatial heterogeneity and dispersal heterogeneity both lead to higher control intensity. We find interesting cyclic control dynamics in the case that the control is applied long-term.

Acknowledgements

Thank you to my supervisor, Dr. Frithjof Lutscher for making this thesis incredibly fun and teaching me all I know.

Contents

List of Figures

List of Tables

Chapter 1

Introduction

The goal of this thesis is to gain a deeper understanding of the dynamics that arise in two-patch consumer–resource models and examine two important applications. We begin with an analysis of the steady states and their stability, which establishes a theoretical foundation for the system. We then extend our focus to consider the two key applications of our model. First, we determine whether consumer dispersal can benefit the overall population densities in the long term; second, we determine the optimal control of a consumer in an extended consumer–resource model.

In many consumer–resource systems, the resource reproduces continuously while the consumer reproduces discretely. For example, the Broad-Footed Marsupial Mouse (*Antechinus stuartii*) is a marsupial native to Australia that reproduces in a short yearly burst in the spring. These mice feed on ground beetles such as those of the *Carabidae* variety that reproduce throughout the year [3]. These systems are ubiquitous in nature but cannot easily be described by either purely continuous or purely discrete dynamics. When this type of consumer and resource interacts, a semi-discrete model can more accurately describe the interactions between them [27]. A notable example of a semi-discrete consumer–resource model is the one derived and analyzed by Pachepsky et al. [34]. Their impulsive differential equations model consumer–resource dynamics using a semi-discrete formulation that combines 'within-year' continuous resource reproduction with 'between year' discrete consumer birth pulse. These equations determine this year's consumer and resource densities based on the previous year's densities. The consumer density is derived from the consumer's accumulated resource biomass in the previous year. This model highlights interesting dynamics that arise in semi-discrete systems that do not arise in their purely discrete or purely continuous analogues, such as shorter population cycles, ranging from two to six years.

While the model by Pachepsky et al. [34] exhibits new consumer–resource dynamics, it lacks a necessary spatial dimension. All interactions in ecology happen at some spatial scale, and, in spatial 'multi-patch models', novel population dynamics have been shown to arise [8]. For example, continuous models of a single species on two patches have shown that the total density of the species at steady state can be higher than the combined carrying capacity of the two patches [42]. While multi-patch models have been extensively studied in purely continuous or discrete time, few models currently exist for semi-discrete dynamics

of consumer–resource interactions on multiple patches. In this thesis, we formulate a model that addresses this gap by incorporating both spatial effects—through patches—and a semi-discrete structure. This model can be applied to various other biological systems.

For example, harp seals (*Pagophilus groenlandicus*) have highly synchronized births and migration, usually preferring local migration [38]. Harp seals consume large quantities of small fish such as sand lance (*Ammodytes hexapterus*), which reproduce throughout the year and do not migrate. This system is well described by population dynamics on coupled patches, where each patch represents an adjacent harbour or inlet. Another example is the spruce budworm (*Choristoneura fumiferana*), which feeds on North American spruce and fir trees. These trees produce needles that can be fed on year-round, so canopy availability is continuous. Spruce budworm reproduce in discrete annual bursts [32]. Often, two adjoining forests have different management strategies. By formulating a consumer–resource model on several patches with control of the consumer, we may then ask for the 'best' ways to apply management options.

To understand the 'best' management strategies, we use the foundation of *optimal control*. This framework uses Pontryagin's Maximum Principle (PMP) to find the optimal solution and optimal control [28]. PMP simplifies the problem of constrained optimization by introducing necessary conditions for an optimal control and trajectory. Optimal control has been applied to differential equations in the context of vaccination [2], finance [6] and species abundance [4]. More details and the mathematical background of optimal control will be explained further in Chapter 5.

This thesis is organized into four chapters. In Chapter 2, we introduce the background, the extended model, and all parameters. Our model set-up contains a set of continuous differential equations, combined with a set of discrete maps. As in the model by Pachepsky et al. [34], we solve our system of differential equations and, using the difference equations, derive stroboscopic maps describing consumer and resource density from year to year.

In Chapter 3, we analyze the existence and stability of equilibrium points and determine possible bifurcations. We first analyze the stability of the trivial equilibrium, then the stability boundaries for the semi-trivial equilibrium states. We use the boundaries of the semi-trivial states to determine conditions for consumer invasion. We next study the coexistence state, which introduces boundary coexistence equilibria. We determine the invasion conditions for the resource when the consumer and resource can coexist but one resource population is at low density. We next use a geometric approach to determine further coexistence fixed points. We use the same geometric approach to find conditions for both a transcritical and a saddle-node bifurcation. We then analyze how these bifurcations depend on dispersal. Finally, we illustrate numerical simulations that show classic consumer–resource behaviour.

In Chapter 4, we investigate the influence of dispersal on population density. Specifically, we analyze how small dispersal acts on total population density, using asymptotic methods. We find the first-order correction terms on each patch, which we use to determine the sign of small perturbations. We use the sum of the correction terms on both patches to determine the long-term benefit or detriment to consumer and resource populations globally. Finally, we remove the restriction of small dispersal and numerically study the dependence of asymptotic densities on dispersal probabilities.

In Chapter 5, we introduce control of the consumer to our model. The control represents aerial pesticide spraying in a discrete impulse once per year. We use the principles of optimal control to determine optimal spray trajectories for various heterogeneous environments.

While this thesis is motivated by ecological questions, we focus on the mathematical applications and outcomes. At the beginning of each chapter, we give relevant background and terminology. At the end of each chapter or section, we give a biological interpretation.

Chapter 2

Model Formulation

In this chapter, we first introduce the model by Pachepsky et al. [34]. Then we extend the model to account for spatial effects by introducing two patches. Next, we nondimensionalize the model to reduce the dimension of parameter space. Finally, we derive the stroboscopic maps that describe the changes in densities of consumers and resources from one year to the next.

2.1 Model Choice

In this thesis, we chose to implement a semi-discrete model. Semi-discrete models are characterized by having both continuous and discrete components. Specifically, we chose to represent birth and dispersal via a discrete impulse. Using discrete maps introduces a mathematical approximation of continuous biological processes. This approximation is justified in our case, as the species we consider have birth pulses and dispersal phases that are short relative to the length of the year. Alternatively, a purely continuous model could include a different timescale such as very fast or very slow dynamics, which would be implemented with very large or very small parameters, respectively. However, in the case of fast dispersal and birth, the complexity of such a purely continuous system is high, which reduces the tractability of the problem. By adopting a semi-discrete framework, we find stroboscopic maps which incorporate all the dynamics from the discrete and the continuous sections and allows all of the analysis that follows in Chapters 3, 4 and 5.

2.2 The Pachepsky Model

Our model is an extension of the semi-discrete model of consumers and resources by Pachepsky et al. [34]. Their model captures consumer–resource interactions within a year, then applies a map to represent the birth pulse of the consumer, illustrated in Figure 2.1. We introduce the Pachepsky model and relevant details here.

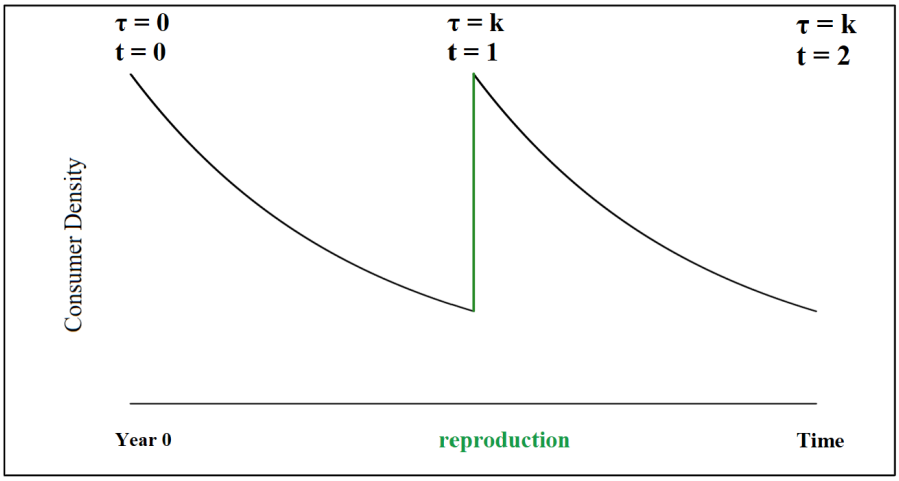

Figure 2.1: Illustration of example consumer dynamics of the Pachepsky consumer–resource model.

We denote the time within a year by τ, the duration of a year by k, and the years by t. At the start of the year ($\tau = 0$), there are resources and consumers present. Between $\tau = 0$ and $\tau = k^-$, consumers interact with the resource by consuming them and storing the energy from that consumption. Consumers die naturally, and the resource grows logistically. At the end of the year ($\tau = k^-$), the biomass stored in consumers is converted into offspring for the next year. The densities at the beginning of the next year are calculated from those at the end of the preceding year.

We call the continuous portion of the dynamics *within-year*. We denote the within-year density of the resource and consumers F_t and C_t, respectively, and the total biomass accumulated per consumer B_t, where $t = 0, 1, 2, 3, \ldots$ denotes the year. The units of B_t are resource density per consumer per time. We assume a fixed fraction of the biomass is stored for reproduction. When no confusion can arise, we will drop the index t to simplify notation. All parameter descriptions can be found in Table 2.1. For $\tau \in [0, k)$, the dynamics are given by the equations

$$\frac{dF}{d\tau} = r\left(1 - \frac{F}{K}\right)F - aFC, \tag{2.2.1}$$

$$\frac{dC}{d\tau} = -mC, \tag{2.2.2}$$

$$\frac{dB}{d\tau} = aF. \tag{2.2.3}$$

The initial conditions of the within-year dynamics in year t are $F_t(0)$, $C_t(0)$, and $B_t(0)$. We obtain these conditions from the system state at the end of the preceding year and the process of reproduction. We call the discrete maps that describe these processes *between-year*. We denote the density of the resource and consumers at the beginning of year t as V_t and W_t, respectively. Hence, we can write the initial conditions for the within-year dynamics

as

$$F_t(0) = V_t, \qquad C_t(0) = W_t, \qquad B_t(0) = 0. \tag{2.2.4}$$

The within-year dynamics start after reproduction, which we assume used all stored energy, and before new consumption occurs. Hence, the initial condition for B is zero, independent of the state of the previous year. The other two state variables are given by

$$\begin{aligned} V_{t+1} &= F_t(k^-), \\ W_{t+1} &= C_t(k^-)(\theta B_t(k^-) + 1). \end{aligned} \tag{2.2.5}$$

The term in parentheses in the second equation accounts for the conversion of biomass into new consumers and the survival of existing consumers during the birth pulse.

We then non-dimensionalize the model to reduce the number of parameters. For the *within-year* dynamics, we denote the scaled resource, consumer, and biomass density by f, c, and b, respectively. We denote the scaled time within a year by s. For the *between-year* dynamics, we denote resource and consumer density by v_t and w_t, respectively. We use the following scaling:

$$f = \frac{F}{K}, \quad c = \frac{C}{K\theta}, \quad b = \theta B, \quad s = \frac{\tau}{k}, \quad v_t = \frac{V_t}{K}, \quad w_t = \frac{W_t}{K\theta}. \tag{2.2.6}$$

Next, we define our nondimensional parameters as:

$$\mu = mk, \qquad \rho = rk, \qquad \alpha = a\theta kK. \tag{2.2.7}$$

With these nondimensional parameters and variables, we can rewrite our differential equations and maps. The *between-year* dynamics are given by the following equations:

$$\frac{df}{ds} = \rho(1-f)f - \alpha f c, \tag{2.2.8}$$

$$\frac{dc}{ds} = -\mu c, \tag{2.2.9}$$

$$\frac{db}{ds} = \alpha f \tag{2.2.10}$$

The *between-year* dynamics are given by the following maps:

$$v_{t+1} = f(1^-), \tag{2.2.11}$$

$$w_{t+1} = c(1^-)(b(1^-) + 1). \tag{2.2.12}$$

From these equations, Pachepsky et al. [34] calculate the stroboscopic maps that include the full dynamics from year to year, which allow easier analysis. The maps are the following:

$$v_{t+1} = v_t \frac{e^{\rho - \frac{\alpha w_t}{\mu}(1-e^{-\mu})}}{\rho v_t \int_0^1 e^{\rho\tau - \frac{\alpha w_t}{\mu}(1-e^{-\mu\tau})}\, d\tau + 1}, \tag{2.2.13}$$

$$w_{t+1} = \left[w_t e^{-\mu} \left(\alpha v_t \int_0^1 \frac{e^{\rho s - \frac{\alpha w_t}{\mu}(1-e^{-\mu s})}}{\rho v_t \int_0^s e^{\rho\tau - \frac{\alpha w_t}{\mu}(1-e^{-\mu\tau})}\, d\tau + 1}\, ds + 1 \right) \right]. \tag{2.2.14}$$

We will derive the corresponding maps for our model later and, in the process, explain how to derive such maps.

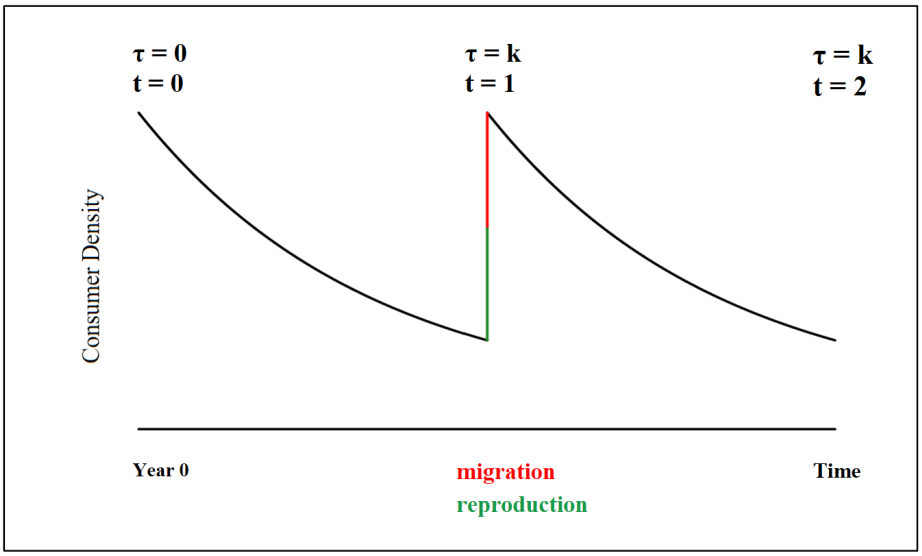

Figure 2.2: Illustration of example dynamics of the extended consumer–resource model. Example shown for one patch.

2.3 Extending the Model to Two Patches

We introduce our extended model with an illustration of the chronology of our model processes. In Figure 2.2, we represent an example of the dynamics of the consumer population on one patch.

In our extended model, we have two patches, each with a consumer and a resource population. The processes are the same as in the model by Pachepsky et al. [34], but we allow the consumers to migrate between patches with a certain probability immediately after reproduction. It is assumed that there are no losses in migration; therefore, the sum of consumers on both patches before and after migration remains constant. The densities at the beginning of the next year are calculated from those at the end of the preceding year by taking both reproduction and migration into account. The resource does not move between patches.

We denote the within-year density of the resource and consumers $F_{i,t}$ and $C_{i,t}$, respectively. The total biomass accumulated per consumer is $B_{i,t}$, where $i = 1, 2$ denotes the patch and $t = 0, 1, 2, 3, \ldots$ denotes the year. For $i = 1, 2$ and for $\tau \in [0, k)$ the dynamics of our model are given by the equations

$$\frac{dF_i}{d\tau} = r_i \left(1 - \frac{F_i}{K_i}\right) F_i - a_i F_i C_i, \tag{2.3.1}$$

$$\frac{dC_i}{d\tau} = -m_i C_i, \tag{2.3.2}$$

$$\frac{dB_i}{d\tau} = a_i F_i. \tag{2.3.3}$$

The initial conditions of the within-year dynamics in year t are $F_{i,t}(0)$, $C_{i,t}(0)$, and

Table 2.1: Descriptions of parameters in the dimensional two-patch model.

Parameters	Description	Units
K_i	carrying capacity	resource density
a_i	consumer attack rate	$\frac{1}{(\text{consumer})(\text{within-year time})}$
r_i	resource growth rate	$\frac{1}{\text{within-year time}}$
p_i	probability of non-dispersal	unitless
$1-p_i$	probability of dispersal	unitless
θ_i	biomass to offspring conversion efficiency	unitless
m_i	consumer death rate	$\frac{1}{\text{within-year time}}$

$B_{i,t}(0)$. We denote the density of the resource and consumers on patch i at the beginning of year t as $V_{i,t}$ and $W_{i,t}$, respectively. Hence, we can write the initial conditions for the within-year dynamics as

$$F_{i,t}(0) = V_{i,t}, \qquad C_{i,t}(0) = W_{i,t}, \qquad B_{i,t}(0) = 0. \tag{2.3.4}$$

We define p_i as the probability of remaining in patch i; i.e., of not dispersing. Then our maps become

$$\begin{aligned} V_{1,t+1} &= F_{1,t}(k^-), \\ V_{2,t+1} &= F_{2,t}(k^-), \\ W_{1,t+1} &= C_{1,t}(k^-)(\theta_1 B_{1,t}(k^-)+1)p_1 + C_{2,t}(k^-)(\theta_2 B_{2,t}(k^-)+1)(1-p_2), \\ W_{2,t+1} &= C_{2,t}(k^-)(\theta_2 B_{2,t}(k^-)+1)p_2 + C_{1,t}(k^-)(\theta_1 B_{1,t}(k^-)+1)(1-p_1). \end{aligned} \tag{2.3.5}$$

We also nondimensionalize our system to reduce the number of parameters. Descriptions of all parameters and variables are given in Table 2.2. We define our nondimensional variables in the same manner as Pachepsky et al. [34], namely

$$f_i = \frac{F_i}{K_i}, \quad c_i = \frac{C_i}{K_i\theta}, \quad b_i = \theta B_i, \quad s = \frac{\tau}{k}, \quad v_{i,t} = \frac{V_{i,t}}{K_i}, \quad w_{i,t} = \frac{W_{i,t}}{K_i\theta}, \tag{2.3.6}$$

and

$$\mu_i = m_i k, \qquad \rho_i = r_i k, \qquad \alpha_i = a_i \theta k K_i. \tag{2.3.7}$$

With these nondimensional parameters and variables, we can rewrite our differential equations and maps. The *between-year* dynamics are given by the following equations for $i = 1, 2$:

$$\frac{df_i}{ds} = \rho_i(1-f_i)f_i - \alpha_i f_i c_i, \tag{2.3.8}$$

$$\frac{dc_i}{ds} = -\mu_i c_i, \tag{2.3.9}$$

$$\frac{db_i}{ds} = \alpha_i f_i. \tag{2.3.10}$$

Table 2.2: Descriptions of variables and parameters in the nondimensional two-patch model.

Variable	**Description**
f_i	Resource density in patch i during the year
c_i	Consumer density in patch i during the year
b_i	Accumulated biomass patch i during the year per consumer
$v_{i,t}$	Resource density in patch i at the beginning of year t
$w_{i,t}$	Consumer density in patch i at the beginning of year t
Parameters	**Description**
ρ_i	Resource growth rate in patch i
α_i	Consumer conversion efficiency in patch i
μ_i	Consumer death rate in patch i
p_i	Probability of remaining in patch i

We update our initial conditions to reflect the new variables:

$$f_{i,t}(0) = v_{i,t}, \qquad c_{i,t}(0) = w_{i,t}, \qquad b_{i,t}(0) = 0. \tag{2.3.11}$$

The *between-year* dynamics are given by the following maps:

$$v_{1,t+1} = f_1(1^-), \tag{2.3.12}$$
$$v_{2,t+1} = f_2(1^-), \tag{2.3.13}$$
$$w_{1,t+1} = c_1(1^-)(b_1(1^-)+1)p_1 + c_2(1^-)(b_2(1^-)+1)(1-p_2), \tag{2.3.14}$$
$$w_{2,t+1} = c_2(1^-)(b_2(1^-)+1)p_2 + c_1(1^-)(b_1(1^-)+1)(1-p_1). \tag{2.3.15}$$

We derive our stroboscopic maps that map the density of consumers and resources in patch i at the beginning of year t to the consumer and resource density at the beginning of year $t+1$. To derive these maps, we begin by solving equation (2.2.9). We find that the consumer density at time $s = 1^-$ is

$$c_i(1^-) = w_{i,t}e^{-\mu_i}. \tag{2.3.16}$$

Equation (2.2.8) becomes a Bernoulli differential equation after Equation (2.3.16) is inserted. It can be solved by a change of variables and an integrating factor. The resource at time s is given by the expression,

$$f_i(s) = v_{1,t}\frac{e^{\rho_1 s - \frac{\alpha_i w_{i,t}}{\mu_i}(1-e^{-\mu_i s})}}{\int_0^s e^{\rho_i\tau - \frac{\alpha_i w_{i,t}}{\mu_i}(1-e^{-\mu_i\tau})}\,d\tau + 1}. \tag{2.3.17}$$

This expression can be used to find the biomass at time 1^- as

$$b_i(1^-) = \alpha_i v_{i,t}\int_0^1 \frac{e^{\rho_i s - \frac{\alpha_i w_{i,t}}{\mu_i}(1-e^{-\mu_i s})}}{\int_0^1 e^{\rho_i\tau - \frac{\alpha_i w_{i,t}}{\mu_i}(1-e^{-\mu_i\tau})}\,d\tau + 1}\,ds. \tag{2.3.18}$$

From here, we have all the ingredients necessary to derive the stroboscopic maps. The explicit expressions are:

$$v_{1,t+1} = v_{1,t}\frac{e^{\rho_1 - \frac{\alpha_1 w_{1,t}}{\mu_1}(1-e^{-\mu_1})}}{\rho_1 v_{1,t}\int_0^1 e^{\rho_1\tau - \frac{\alpha_1 w_{1,t}}{\mu_1}(1-e^{-\mu_1\tau})}\,d\tau + 1}, \tag{2.3.19}$$

$$v_{2,t+1} = v_{2,t}\frac{e^{\rho_2 - \frac{\alpha_2 w_{2,t}}{\mu_2}(1-e^{-\mu_2})}}{\rho_2 v_{2,t}\int_0^1 e^{\rho_2\tau - \frac{\alpha_2 w_{2,t}}{\mu_2}(1-e^{-\mu_2\tau})}\,d\tau + 1}, \tag{2.3.20}$$

$$\begin{aligned} w_{1,t+1} = &\left[w_{1,t}p_1 e^{-\mu_1}\left(\alpha_1 v_{1,t}\int_0^1 \frac{e^{\rho_1 s - \frac{\alpha_1 w_{1,t}}{\mu_1}(1-e^{-\mu_1 s})}}{\rho_1 v_{1,t}\int_0^s e^{\rho_1\tau - \frac{\alpha_1 w_{1,t}}{\mu_1}(1-e^{-\mu_1\tau})}\,d\tau + 1}\,ds + 1\right)\right] + \\ &\left[w_{2,t}(1-p_2)e^{-\mu_2}\left(\alpha_2 v_{2,t}\int_0^1 \frac{e^{\rho_2 s - \frac{\alpha_2 w_{2,t}}{\mu_2}(1-e^{-\mu_2 s})}}{\rho_2 v_{2,t}\int_0^s e^{\rho_2\tau - \frac{\alpha_2 w_{2,t}}{\mu_2}(1-e^{-\mu_2\tau})}\,d\tau + 1}\,ds + 1\right)\right], \end{aligned} \tag{2.3.21}$$

$$\begin{aligned} w_{2,t+1} = &\left[w_{2,t}p_2 e^{-\mu_2}\left(\alpha_2 v_{2,t}\int_0^1 \frac{e^{\rho_2 s - \frac{\alpha_2 w_{2,t}}{\mu_2}(1-e^{-\mu_2 s})}}{\rho_2 v_{2,t}\int_0^s e^{\rho_2\tau - \frac{\alpha_2 w_{2,t}}{\mu_2}(1-e^{-\mu_2\tau})}\,d\tau + 1}\,ds + 1\right)\right] + \\ &\left[w_{1,t}(1-p_1)e^{-\mu_1}\left(\alpha_1 v_{1,t}\int_0^1 \frac{e^{\rho_1 s - \frac{\alpha_1 w_{1,t}}{\mu_1}(1-e^{-\mu_1 s})}}{\rho_1 v_{1,t}\int_0^s e^{\rho_1\tau - \frac{\alpha_1 w_{1,t}}{\mu_1}(1-e^{-\mu_1\tau})}\,d\tau + 1}\,ds + 1\right)\right]. \end{aligned} \tag{2.3.22}$$

The maps derived above are explicit expressions that determine the density of consumers and resources at the beginning of year $t+1$ from those at the beginning of year t. These stroboscopic maps encompass the between-year and within-year dynamics. They transform the semi-discrete model into a fully discrete-time model. This reformulation then allows us to determine fixed points and perform stability analysis, which will be the subject of the next chapter.

Chapter 3

Model Analysis

In this chapter, we first introduce the relevant background on dynamical systems and two-patch models. We use this theory to explore the dynamics of our semi-discrete model in the context of equilibria and their stability. We find up to three positive coexistence equilibria and two boundary coexistence equilibria. We end this chapter with numerical simulations.

3.1 Background

We begin with key terminology and background information for the analysis of our model. This material is fairly standard and can be found in many books on the fundamentals of dynamical systems. We list a few common references. "Nonlinear Dynamics and Chaos" by Steven Strogatz provides an introduction to dynamical systems, fixed points, and bifurcations [40]. "A First Course in Discrete Dynamical Systems" by Richard Holmgren provides a comprehensive introduction to discrete systems and the most important theorems [22]. Mark Kot writes about key concepts, derivation, and analysis of mathematical models in "Elements of Mathematical Biology" [26].

The asymptotic behaviour of discrete maps can be analyzed in part by studying their fixed points. Consider the 1D map $x_{n+1} = f(x_n)$. A fixed point of f is any point x^* such that $f(x^*) = x^*$. Fixed points can be stable, asymptotically stable, or unstable. A fixed point is locally asymptotically stable if all nearby trajectories converge to this fixed point. In this thesis, *stable* is used as a shorthand for locally asymptotically stable.

Formally, a fixed point x^* is locally asymptotically stable if, given any $\epsilon > 0 \quad \exists \delta > 0$ such that if $||x_{n_0} - x^*|| < \delta$, then $||x_n - x^*|| < \epsilon \quad \forall n \geq n_0$, and if $||x_{n_0} - x^*|| < \delta$ implies $x_n \to x^*$ as $n \to \infty$. A fixed point is unstable if it is not stable. We use stable and unstable classification of fixed points in part to determine the long-term behaviour of our dynamical system.

We use linear stability analysis to determine the stability of fixed points. This analysis relies on the Jacobian matrix, which describes the local tangent plane (or hyperplane) of the map near a fixed point and thus is used to linearly approximate the system around the fixed

point. The entries of the Jacobian matrix are the partial derivatives of the maps. For two coupled maps $x_{n+1} = f(x_n, y_n)$ and $y_{n+1} = g(x_n, y_n)$, the Jacobian matrix is

$$J(x, y) = \begin{bmatrix} \frac{\partial f}{\partial x} & \frac{\partial f}{\partial y} \\ \frac{\partial g}{\partial x} & \frac{\partial g}{\partial y} \end{bmatrix}. \tag{3.1.1}$$

The dimension of the Jacobian matrix for a system of n equations is $n \times n$. We evaluate the Jacobian matrix at the fixed point. We then determine the eigenvalues of the Jacobian matrix by finding the roots of the characteristic polynomial $\det(J - \lambda I) = 0$. For a fixed point to be (locally asymptotically) stable, all eigenvalues must be strictly inside the unit circle; i.e., $|\lambda| < 1$. If one or more eigenvalues have modulus greater than one, $|\lambda| > 1$, the fixed point is unstable. If any eigenvalue has modulus equal to one, $|\lambda| = 1$, this is a marginal case and may represent a bifurcation.

A (local) bifurcation is a change in the number or the stability of steady states of the dynamical system caused by a parameter change. Bifurcations in discrete-time systems arise from eigenvalues of the Jacobian matrix crossing the unit circle. Depending on where an eigenvalue crosses, different bifurcations are possible. When an eigenvalue crosses -1, a flip bifurcation can occur. In this bifurcation, a stable fixed point becomes unstable and gives rise to a stable period-2 orbit. For this reason, it is also called a period-doubling bifurcation. When a pair of complex conjugate eigenvalues crosses the unit circle, a Neimark–Sacker bifurcation can occur. This bifurcation starts with a stable fixed point that turns unstable and is surrounded by a stable (or unstable) limit cycle. When an eigenvalue crosses $+1$, a saddle-node bifurcation or a transcritical bifurcation can occur. A saddle-node bifurcation occurs when two fixed points (one stable, one unstable) are created or annihilated. Transcritical bifurcations occur when two states collide and switch their stability.

In the context of population ecology, transcritical bifurcations commonly occur at the boundary of the biologically relevant phase space; i.e., where the density is zero. They can then be used to determine whether a species dies out or not. For example, in the case of a single population, if the zero state is stable, populations of small density will decline to zero and therefore die out, whereas if the zero state is unstable, populations of small density will grow and therefore survive. In population ecology, the ability of a population to grow from low density is called invasion. In multi-species systems, one can apply the same reasoning to any focal species by considering the stability of the state where all but the one focal species are present. Invasion analysis then produces conditions on the eigenvalues of the system, which determine whether the focal species will grow or fail. We will apply these ideas to both consumer and resource invasion in our system.

Pachepsky et al. [34] calculated steady states of their model and determined stability. They found three equilibria. First, a trivial state $(0, 0)$ that is unstable since the resource growth rate is positive ($\rho > 0$). Next, a semi-trivial state, $(1, 0)$, whose stability requires the consumer growth rate to be smaller than one, $\nu = (\alpha + 1)e^{-\mu} < 1$. Finally, a unique positive equilibrium, (v^*, w^*), with components

$$v^* = \frac{1}{\rho} \frac{e^{\frac{\rho(e^{\mu}-1)}{\alpha}} - 1}{\int_0^1 e^{\rho(s-(1-\frac{e^{\mu}-1}{\alpha})\frac{1-e^{-\mu s}}{1-e^{-\mu}})}}, \tag{3.1.2}$$

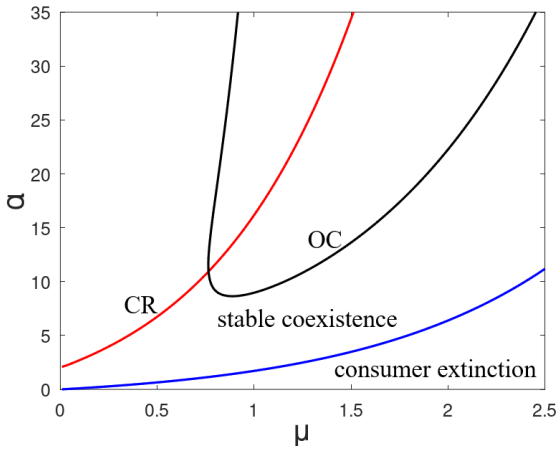

Figure 3.1: Illustration of the stability regions of the Pachepsky model. Reprinted from [1] with permission from Sarah Abel. CR denotes consumer–resource cycles and OC denotes overcompensation cycles.

$$w^* = \rho\mu \frac{1 - \frac{e^{\mu}-1}{\alpha}}{\alpha(1 - e^{-\mu})}. \tag{3.1.3}$$

We will derive this state in the context of our extended model and refer to it further in Chapter 4. Pachepsky et al. [34] utilized the eigenvalues of the Jacobian to determine when the fixed points were stable and unstable.

Fixed points are not the only behaviour that dynamical systems can exhibit. The Pachepsky model exhibits consumer–resource cycles, two-cycles, and other dynamics, including chaos. Two-cycles arise from period-doubling bifurcations, consumer–resource cycles occur through a Neimark–Sacker bifurcation, and consumer extinction occurs through a transcritical bifurcation. The boundaries of these behaviours in parameter space are illustrated in Figure 3.1. We use the stability boundaries in the Pachepsky model as a guide in order to study possible outcomes of our model, as shown in Section 3.6.

3.2 The Jacobian Matrix

We begin by calculating the Jacobian matrix in order to perform a linear stability analysis. We summarize the discrete maps described in (2.3.19)–(2.3.22) as

$$v_{1,t+1} = f_1(v_{1,t}, w_{1,t}), \tag{3.2.1}$$
$$v_{2,t+1} = f_2(v_{2,t}, w_{2,t}), \tag{3.2.2}$$
$$w_{1,t+1} = f_3(v_{1,t}, w_{1,t}, v_{2,t}, w_{2,t}), \tag{3.2.3}$$
$$w_{2,t+1} = f_4(v_{1,t}, w_{1,t}, v_{2,t}, w_{2,t}). \tag{3.2.4}$$

With this notation, we write the Jacobian matrix as

$$J(v_1, v_2, w_1, w_2) = \begin{bmatrix} \frac{\partial f_1}{\partial v_1} & \frac{\partial f_1}{\partial v_2} & \frac{\partial f_1}{\partial w_1} & \frac{\partial f_1}{\partial w_2} \\ \frac{\partial f_2}{\partial v_1} & \frac{\partial f_2}{\partial v_2} & \frac{\partial f_2}{\partial w_1} & \frac{\partial f_2}{\partial w_2} \\ \frac{\partial f_3}{\partial v_1} & \frac{\partial f_3}{\partial v_2} & \frac{\partial f_3}{\partial w_1} & \frac{\partial f_3}{\partial w_2} \\ \frac{\partial f_4}{\partial v_1} & \frac{\partial f_4}{\partial v_2} & \frac{\partial f_4}{\partial w_1} & \frac{\partial f_4}{\partial w_2} \end{bmatrix} = \begin{bmatrix} J_{1,1} & J_{1,2} \\ J_{2,1} & J_{2,2} \end{bmatrix}. \tag{3.2.5}$$

The Jacobian matrix is quite complicated, and the expressions are long. To simplify it, we introduce further notation as follows: For $i = 1, 2$, let

$$\sigma_i(w_i, s) \equiv e^{\rho_i s - \frac{\alpha_i w_i}{\mu_i}(1-e^{-\mu_i s})} \tag{3.2.6}$$

and

$$\beta_i(w_i, s) \equiv \int_0^s \sigma_i(w_i, \tau) d\tau = \int_0^s e^{\rho_i \tau - \frac{\alpha_i w_i}{\mu_i}(1-e^{-\mu_i \tau})} d\tau. \tag{3.2.7}$$

For simplicity of notation, we drop the dependency on w in σ and β if no confusion can arise. With this notation, we find the following expressions for the four sub-matrices of the Jacobian matrix:

$$J_{1,1} = \begin{bmatrix} \frac{\sigma_1(1)}{[\rho_1 v_1 \beta_1(1)+1]^2} & 0 \\ 0 & \frac{\sigma_2(1)}{[\rho_2 v_2 \beta_2(1)+1]^2} \end{bmatrix}, \tag{3.2.8}$$

$$J_{1,2} = \begin{bmatrix} \frac{v_1\left[\frac{\alpha_1}{\mu_1}(1-e^{-\mu_1})\sigma_1(1)\right]}{[\rho_1 v_1 \beta_1(1)+1]^2} & 0 \\ 0 & \frac{v_2\left[\frac{\alpha_2}{\mu_2}(1-e^{-\mu_2})\sigma_2(1)\right]}{[\rho_2 v_2 \beta_2(1)+1]^2} \end{bmatrix}, \tag{3.2.9}$$

$$J_{2,1} = \begin{bmatrix} w_1 p_1 e^{-\mu_1}\alpha_1 \int_0^1 \frac{\sigma_1(s)}{[\rho_1 v_1 \beta_1(s)+1]^2} ds & w_2(1-p_2)e^{-\mu_2}\alpha_2 \int_0^1 \frac{\sigma_2(s)}{[\rho_2 v_2 \beta_2(s)+1]^2} ds \\ w_1(1-p_1)e^{-\mu_2}\alpha_1 \int_0^1 \frac{\sigma_1(s)}{[\rho_1 v_1 \beta_1(s)+1]^2} ds & w_2 p_2 e^{-\mu_1}\alpha_2 \int_0^1 \frac{\sigma_2(s)}{[\rho_2 v_2 \beta_2(s)+1]^2} ds \end{bmatrix}, \tag{3.2.10}$$

$$J_{2,2} = \begin{bmatrix} p_1 e^{-\mu_1}\left(\alpha_1 v_1 \int_0^1 \frac{\sigma_1(s)}{\rho_1 v_1 \beta_1(s)+1}\, ds+1\right)+ & (1-p_2)e^{-\mu_2}\left(\alpha_2 v_2 \int_0^1 \frac{\sigma_2(s)}{\rho_2 v_2 \beta_2(s)+1}\, ds+1\right)+ \\ p_1 e^{-\mu_1} \frac{w_1 \frac{\alpha_1^2}{\mu_1} v_1^2 (1-e^{-\mu_1})\sigma_1(s)\rho_1}{[\rho_1 v_1 \beta_1(s)+1]^2} & (1-p_2)e^{-\mu_2} \frac{w_2 \frac{\alpha_2^2}{\mu_2} v_2^2 (1-e^{-\mu_2})\sigma_2(s)\rho_2}{[\rho_2 v_2 \beta_2(s)+1]^2} \\ (1-p_1)e^{-\mu_1}\left(\alpha_1 v_1 \int_0^1 \frac{\sigma_1(s)}{\rho_1 v_1 \beta_1(s)+1}\, ds+1\right)+ & p_2 e^{-\mu_2}\left(\alpha_2 v_2 \int_0^1 \frac{\sigma_2(s)}{\rho_2 v_2 \beta_2(s)+1}\, ds+1\right)+ \\ (1-p_1)e^{-\mu_1} \frac{w_1 \frac{\alpha_1^2}{\mu_1} v_1^2 (1-e^{-\mu_1})\sigma_1(s)\rho_1}{[\rho_1 v_1 \beta_1(1)+1]^2} & p_2 e^{-\mu_2} \frac{w_2 \frac{\alpha_2^2}{\mu_2} v_2^2 (1-e^{-\mu_2})\sigma_2(s)\rho_2}{[\rho_2 v_2 \beta_2(s)+1]^2} \end{bmatrix}. \tag{3.2.11}$$

3.3 Trivial Equilibrium

In this section, we determine the conditions for stability of the trivial equilibrium $(v_1, v_2, w_1, w_2) = (0, 0, 0, 0)$, which occurs when no resources or consumers are present on either patch. To determine its stability, we first evaluate the Jacobian matrix at the trivial state,

$$J(0,0,0,0) = \begin{bmatrix} e^{\rho_1} & 0 & 0 & 0 \\ 0 & e^{\rho_2} & 0 & 0 \\ 0 & 0 & p_1 e^{-\mu_1} & (1-p_2)e^{-\mu_2} \\ 0 & 0 & (1-p_1)e^{-\mu_1} & p_2 e^{-\mu_2} \end{bmatrix}. \tag{3.3.1}$$

This matrix has an upper block-triangular structure, so that the eigenvalues of the full matrix are given by the eigenvalues of the two sub-matrices that form the diagonal blocks. Therefore, the first two eigenvalues are simply the first two diagonal entries of the matrix. These eigenvalues are e^{ρ_1} and e^{ρ_2}. We could calculate the remaining two eigenvalues by finding the roots of the characteristic equation of the bottom sub-matrix, $J_{2,2}$, namely

$$(p_1 e^{-\mu_1} - \lambda)(p_2 e^{-\mu_2} - \lambda) - (1-p_2)(1-p_1)e^{-\mu_1} e^{-\mu_2} = 0. \tag{3.3.2}$$

However, since $\rho_i > 0$, the eigenvalues e^{ρ_1} and e^{ρ_2} are greater than unity; therefore, the equilibrium $(0, 0, 0, 0)$ is unstable. Biologically, this finding means that the resource populations on each patch are able to grow from low density. This result parallels that for the trivial equilibrium in the single-patch model by Pachepsky et al. [34].

3.4 Semi-Trivial Equilibria

There are three resource-only equilibria, which we call *semi-trivial*. Two of the three equilibria emerge when the resource is present in only one of the two patches, $(v_1, v_2, w_1, w_2) = (1, 0, 0, 0)$ and $(v_1, v_2, w_1, w_2) = (0, 1, 0, 0)$. Both of these states are unstable because the resource in the empty patch can grow from low density, as shown in Section 3.3. The third more interesting case is when $(v_1, v_2, w_1, w_2) = (1, 1, 0, 0)$. This corresponds to no consumers present on either patch, but the resources achieving their scaled carrying capacity.

3.4.1 Explicit Expressions of the Eigenvalues

The Jacobian matrix evaluated at this equilibrium is:

$$J(1,1,0,0) = \begin{bmatrix} e^{-\rho_1} & 0 & \frac{\alpha_1}{\mu_1}(1-e^{-\mu_1}) & 0 \\ 0 & e^{-\rho_2} & 0 & \frac{\alpha_2}{\mu_2}(1-e^{-\mu_2}) \\ 0 & 0 & p_1 e^{-\mu_1}(\alpha_1+1) & (1-p_2)e^{-\mu_2}(\alpha_2+1) \\ 0 & 0 & (1-p_1)e^{-\mu_1}(\alpha_1+1) & p_2 e^{-\mu_2}(\alpha_2+1) \end{bmatrix}. \tag{3.4.1}$$

This matrix is also upper block-triangular. The same process as in Section 3.3 can be applied to find the eigenvalues here. The first two eigenvalues are given by $\lambda_1 = e^{-\rho_1}$ and $\lambda_2 = e^{-\rho_2}$. Both of these are in the interval $(0,1)$. Hence, there is no instability associated with them. We define $\nu_i = e^{-\mu_i}(\alpha_i + 1)$. We consider ν_i to be the maximum growth rate of the consumer on the i-th patch in isolation. With this notation, the characteristic equation for the sub-matrix $J_{2,2}$ is then the quadratic equation

$$\lambda^2 - (p_1\nu_1 + p_2\nu_2)\lambda - (1-p_1-p_2)\nu_1\nu_2 = 0. \tag{3.4.2}$$

The remaining two eigenvalues are

$$\lambda_{3,4} = \frac{p_1\nu_1 + p_2\nu_2 \pm \sqrt{(p_1\nu_1+p_2\nu_2)^2 - 4(p_1+p_2)\nu_1\nu_2 + 4\nu_1\nu_2}}{2}. \tag{3.4.3}$$

By completing the square, we find that the discriminant is real and nonnegative. Specifically, for $\nu_1, \nu_2 > 0$ and $p_1, p_2 \in [0,1]$, the discriminant is

$$(\nu_1 p_1 - \nu_2(1-p_2))^2 + 4\,\nu_1\nu_2\,(1-p_1)(1-p_2) \geq 0. \tag{3.4.4}$$

This implies that $\lambda_{3,4}$ are real, $|\lambda_3| \geq |\lambda_4|$ and $\lambda_3 \geq 0$. Hence, the condition for stability of the semi-trivial equilibrium $(1,1,0,0)$ reduces to the condition $\lambda_3 < 1$. After some further calculations, we find that $\lambda_3 < 1$ if and only if

$$p_1\nu_1 + p_2\nu_2 + (1-p_1-p_2)\nu_1\nu_2 < 1. \tag{3.4.5}$$

If (3.4.5) is satisfied, the consumer cannot invade the system, i.e., grow from low density. If (3.4.5) is reversed, the consumer can invade the system at the semi-trivial state where the resource is at carrying capacity on both patches.

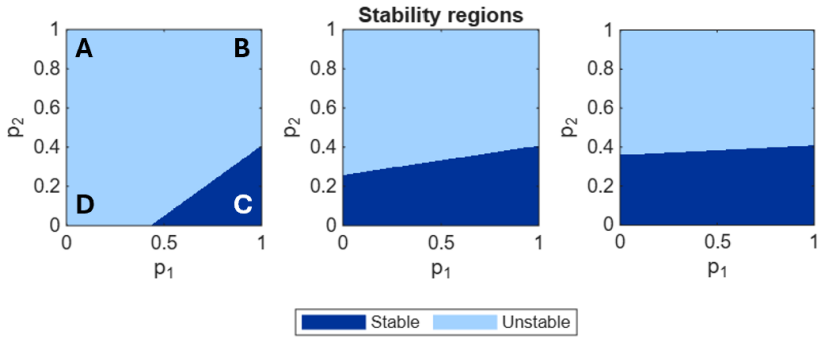

Figure 3.2: Illustration of the stability region of the semi-trivial equilibrium state in the p_1–p_2 plane. The plots have increasing values of μ_1 with $\mu_1 = 3$ (left), $\mu_1 = 4$ (middle) and $\mu_1 = 5$ (right). Other parameters are $\mu_2 = 1.5$, $\alpha_1 = \alpha_2 = 10$.

3.4.2 Stability Boundaries

We now investigate the stability boundary of this semi-trivial state and its relationship to model parameters. We rewrite condition (3.4.5) as

$$p_1\nu_1(1-\nu_2) + p_2\nu_2(1-\nu_1) < 1 - \nu_1\nu_2 \tag{3.4.6}$$

to find that the stability region is a half plane in p_1–p_2 parameter space.

In Figure 3.2, the regions where the semi-trivial equilibrium is stable are indicated in dark blue and regions where it is unstable are in light blue. Thus, the light blue regions are regions where the consumer can invade. The boundary is a straight line as predicted in (3.4.5). From the left plot to the right, the consumer death rate μ_1 is increased.

We first note that, since $\mu_1 > \mu_2$, the growth rate on patch 1 is lower than the growth rate on patch 2, i.e., $\nu_1 < 1 < \nu_2$. Patch 1 is a sink, as the growth rate is less than one, and patch 2 is a source, as the growth rate is greater than one. The contribution of the sink or source to the overall consumer growth rate depends on the movement probabilities. When $p_2 = 1$ and $p_1 = 0$, the contribution of the source is the largest, whereas when $p_1 = 1$, $p_2 = 0$, the contribution to the source is smallest. We can use Figure 3.2 to determine what values of p_1 and p_2 result in consumer invasion. In the next section, we study how λ_3 depends on the growth rate.

In Figure 3.2, the patches are isolated at (B) and switch patches entirely at (D). At both these points, consumer invasion is possible. At point (A), all individuals move towards the source, so invasion is possible. As the probability p_1 of staying on patch 1 increases, consumers can no longer invade. Thus, consumer invasion is only possible when migration away from the sink patch is high enough. One strategy for consumer persistence is the movement towards a good patch and away from a bad one.

As we increase the death rate of the consumer on the sink patch, migration away from a bad patch has less effect. The contribution of the source to the overall growth rate becomes more important. An increase in the probability of staying in the source patch is thus required

for invasion. In Figure 3.2, the slope of the stability boundary becomes less steep as the death rate of the consumer on patch one increases. When the death rate of the consumer on patch one goes to infinity, which represents instant extinction, we require $p_2 > 0.5$ for invasion to occur at all.

3.4.3 Monotonicity of λ_3

Next, we investigate how λ_3 depends on the growth rates ν_1 and ν_2. Since λ_3 is the overall growth rate of the consumer at low density (see [10]) and ν_1 and ν_2 are the maximum growth rates on patch one and patch two respectively, we expect that λ_3 is monotone increasing in ν_i. We will show that the derivative $\frac{\partial \lambda_3}{\partial \nu_i}$ is positive. We calculate

$$\frac{\partial \lambda}{\partial \nu_1} = p_1 + \frac{2(p_1\nu_1 + p_2\nu_2)p_1 - 4(p_1 + p_2 - 1)\nu_2}{2\sqrt{(p_1\nu_1 + p_2\nu_2)^2 - 4(p_1 + p_2 - 1)\nu_1\nu_2}}. \tag{3.4.7}$$

Note that if $p_1 + p_2 < 1$ then $\frac{\partial \lambda_3}{\partial \nu_1} > 0$. Otherwise, we require

$$p_1\sqrt{(p_1\nu_1 + p_2\nu_2)^2 - 4(p_1 + p_2 - 1)\nu_1\nu_2} \geq 2(p_1 + p_2 - 1)\nu_2 - p_1(p_1\nu_1 + p_2\nu_2). \tag{3.4.8}$$

If the left-hand side is negative, the inequality holds. If not, we continue by squaring both sides and simplifying the expressions. After some algebra, we find that the condition above is equivalent to

$$\nu_2^2(p_1 + p_2 - 1)[(p_1 - 1)(p_2 - 1)] \geq 0. \tag{3.4.9}$$

Since $p_1 + p_2 \geq 1$ and $p_i \in [0, 1]$, this condition is satisfied. Hence, λ_3 is a non-decreasing function of ν_1. Since λ_3 is symmetric in ν_1 and ν_2 with p_1 and p_2 exchanged, the same result holds with respect to ν_2. Thus, if the growth rate is increased on either patch, then λ_3 increases and the consumer grows more. Further, we expect that if $\max(\nu_i) < 1$—i.e., the patches are both sinks—then $\lambda_3 < 1$, so the population is not able to grow from low density. To see this, let $\nu_1 = \nu_2 = \nu$. Then

$$\lambda_3 = \frac{p_1\nu + p_2\nu \pm \sqrt{(p_1\nu + p_2\nu)^2 - 4(p_1 + p_2)\nu^2 + 4\nu^2}}{2} \tag{3.4.10}$$

reduces to $\lambda_3 = \nu$. Since $\frac{d\lambda_3}{d\nu_1} \geq 0$, we find that

$$\lambda_3(\nu_1, \nu_2) < 1 \quad \text{if} \quad \max\{\nu_1, \nu_2\} < 1. \tag{3.4.11}$$

Similarly, we find that

$$\lambda_3(\nu_1, \nu_2) > 1 \quad \text{if} \quad \min\{\nu_1, \nu_2\} > 1. \tag{3.4.12}$$

We are also interested in the derivative of λ_3 with respect to dispersal probability p_1. We expect that increasing the probability of remaining on the patch with the higher growth rate would lead to a higher invasion likelihood. To show this, we first assume, without loss of generality, that $\nu_1 > \nu_2$. The derivative is

$$\frac{\partial \lambda_3}{\partial p_1} = \frac{1}{2}\nu_1 + \frac{(p_1\nu_1 + p_2\nu_2)\nu_1 - 2\nu_1\nu_2}{2\sqrt{(p_1\nu_1 + p_2\nu_2)^2 - 4(p_1 + p_2 - 1)(\nu_1\nu_2)}}. \tag{3.4.13}$$

We note that $\nu_1 > 0$; thus, for this expression to be positive, we require

$$1 + \frac{(p_1\nu_1 + p_2\nu_2) - 2\nu_2}{\sqrt{(p_1\nu_1 + p_2\nu_2)^2 - 4(p_1 + p_2 - 1)(\nu_1\nu_2)}} \geq 0, \tag{3.4.14}$$

which reduces to the condition

$$\sqrt{(p_1\nu_1 + p_2\nu_2)^2 - 4(p_1 + p_2 - 1)(\nu_1\nu_2)} \geq 2\nu_2 - (p_1\nu_1 + p_2\nu_2). \tag{3.4.15}$$

Thus, if $2\nu_2 - (p_1\nu_1 + p_2\nu_2) \leq 0$, the condition is automatically satisfied, and λ_3 is an increasing function of p_1. Otherwise, if $2\nu_2 - (p_1\nu_1 + p_2\nu_2) > 0$, we apply a bit of algebra to condition (3.4.15) to find that it becomes

$$(1 - p_2)(\nu_1 - \nu_2) \geq 0. \tag{3.4.16}$$

Equation 3.4.16 quantifies how the overall growth rate responds to habitat retention p_1. The term $(1 - p_2)$ represents the proportion of individuals leaving patch two for patch one. The quality $\nu_1 - \nu_2$ measures the difference in patch quality, as ν is the low density growth rate of patch i. Thus, dispersal towards a higher quality patch cannot reduce the overall population growth rate when there is a difference in patch quality.

Since $p_2 \in [0, 1]$, the derivative of λ_3 with respect to p_1 is positive if $\nu_1 > \nu_2$. Thus, λ_3 is strictly increasing with respect to p_1 if the growth rate on patch one is higher than on patch two. If we instead assumed that $\nu_2 > \nu_1$, we would find that the derivative of λ_3 with respect to p_2 would be positive.

Finally, we show that if dispersal is symmetric (i.e., $p_1 = p_2 = p$) then the overall growth rate λ_3 is an increasing function with respect to the probability of dispersal, p. Under the condition on p_i, λ_3 becomes

$$\lambda_3 = \frac{1}{2}\left(p\nu_1 + \nu_2 + \sqrt{(p^2(\nu_1 + \nu_2)^2 - 4(2p - 1)\nu_1\nu_2}\right). \tag{3.4.17}$$

For $\frac{\partial \lambda_3}{\partial p} > 0$, we require that

$$\nu_1 + \nu_2 - \frac{4\nu_1\nu_2 - p(\nu_1 + \nu_2)^2}{\sqrt{p^2(\nu_1 + \nu_2)^2 - 4(2p - 1)\nu_1\nu_2}} > 0. \tag{3.4.18}$$

Multiplying by the denominator, we find

$$(\nu_1 + \nu_2)\sqrt{p^2(\nu_1 + \nu_2)^2 - 4(2p - 1)\nu_1\nu_2} > 4\nu_1\nu_2 - p(\nu_1 + \nu_2)^2. \tag{3.4.19}$$

Squaring both sides and simplifying, we find

$$4(\nu_1 + \nu_2)^2 > 16\nu_1\nu_2, \tag{3.4.20}$$

which simplifies to the requirement

$$(\nu_1 + \nu_2)^2 > 0. \tag{3.4.21}$$

Since we exclude the case that $\nu_1 = \nu_2 = 0$, we find this condition always satisfied.

We interpret the results of this section as follows: as the growth rate of either consumer population is increased, the overall growth rate of consumers also increases. Further, if we do not allow populations to be isolated ($p \neq 1$), we find that if invasion is possible in one patch, it occurs in both. This is a result of the coupling between patches. From this, we can further conclude that if the fastest-growing population has a growth rate less than one, both populations are sinks, and invasion becomes impossible. We note that the overall growth rate increases with an increasing probability of staying on the better-quality patch if the probability of staying on the other patch is constant. Populations thus benefit from individuals remaining on good patches when dispersal from the other patch is not affected. When we make the dispersal probabilities equal, increasing the probability of staying on a patch still increases the overall growth rate. Thus, the benefit from remaining on better-quality patches outweighs the detriment from also remaining on lower-quality patches.

3.5 Coexistence Equilibria

In this section, we study the coexistence equilibrium equations. First, we determine the general form of the equilibria, then we determine two subcases. One is when consumers are present on both patches, and one resource population has gone extinct. We call these equilibria the *boundary coexistence equilibria*. The second is when consumers and resources are present on each patch, which we call simply *coexistence equilibria*. We take a geometric approach to analyze the solutions of these coexistence equations. We find both a transcritical and a saddle-node bifurcation.

3.5.1 Coexistence Equations

The coexistence equilibria occur when consumers and resources are both present. We denote the densities of resources and consumers at equilibrium by $v_i > 0$ and $w_i > 0$, respectively. According to the dynamic equations (2.3.19)–(2.3.22), they satisfy the equations

$$v_1 = \frac{v_1 e^{\rho_1 - \frac{\alpha_1 w_1}{\mu_1}(1-e^{-\mu_1})}}{\rho_1 v_1 \int_0^1 e^{\rho_1 \tau - \frac{\alpha_1 w_1}{\mu_1}(1-e^{-\mu_1 \tau})}\, d\tau + 1}, \tag{3.5.1}$$

$$\begin{aligned} w_1 = &\left[w_1 p_1 e^{-\mu_1} \left(\alpha_1 v_1 \int_0^1 \frac{e^{\rho_1 s - \frac{\alpha_1 w_1}{\mu_1}(1-e^{-\mu_1 s})}}{\rho_1 v_1 \int_0^s e^{\rho_1 \tau - \frac{\alpha_1 w_1}{\mu_1}(1-e^{-\mu_1 \tau})}\, d\tau + 1}\, ds + 1 \right) \right] + \\ &\left[w_2 (1-p_2) e^{-\mu_2} \left(\alpha_2 v_2 \int_0^1 \frac{e^{\rho_2 s - \frac{\alpha_2 w_2}{\mu_2}(1-e^{-\mu_2 s})}}{\rho_2 v_2 \int_0^s e^{\rho_2 \tau - \frac{\alpha_2 w_2}{\mu_2}(1-e^{-\mu_2 \tau})}\, d\tau + 1}\, ds + 1 \right) \right], \end{aligned} \tag{3.5.2}$$

and similarly for v_2 and w_2.

From (3.5.1) and symmetry considerations, we find

$$\rho_i v_i \int_0^1 e^{\rho_i \tau - \frac{\alpha_i w_i}{\mu_i}(1-e^{-\mu_i \tau})}\, d\tau + 1 = e^{\rho_i - \frac{\alpha_i w_i}{\mu_i}(1-e^{-\mu_i})}, \tag{3.5.3}$$

for $i = 1, 2$, which we solve for v_i to obtain

$$v_i = \frac{e^{\rho_i - \frac{\alpha_i w_i}{\mu_i}(1-e^{-\mu_i})} - 1}{\rho_i \int_0^1 e^{\rho_i \tau - \frac{\alpha_i w_i}{\mu_i}(1-e^{-\mu_i \tau})}\, d\tau}. \tag{3.5.4}$$

With the notation from (3.2.6) and (3.2.7), this expression simplifies to

$$v_i = \frac{\sigma_i(w_i, 1) - 1}{\rho_i \beta_i(w_i, 1)}. \tag{3.5.5}$$

Next, we turn to the equations for w_i. We begin by simplifying the integral terms, namely

$$I = \alpha_1 v_1 \int_0^1 \frac{e^{\rho_1 s - \frac{\alpha_1 w_1}{\mu_1}(1-e^{-\mu_1 s})}}{\rho_1 v_1 \int_0^s e^{\rho_1 \tau - \frac{\alpha_1 w_1}{\mu_1}(1-e^{-\mu_1 \tau})}\, d\tau + 1}\, ds. \tag{3.5.6}$$

With the notation introduced in (3.2.6) and (3.2.7), this term becomes

$$I = \alpha_1 \int_0^1 \frac{v_1 \sigma_1(w_1, s)}{\rho_1 v_1 \beta_1(w_1, s) + 1}\, ds = \frac{\alpha_1}{\rho_1} \int_0^1 \frac{\rho_1 \sigma_1(w_1, s)}{\rho_1 \beta_1(w_1, s) + 1/v_1}\, ds. \tag{3.5.7}$$

Since $\beta_i = \int \sigma_i(\cdot, s) ds$, we can integrate to obtain

$$\frac{\alpha_1}{\rho_1} \ln\left(\rho_1 \beta_1(w_1, s) + 1/v_1\right) \Big|_{s=0}^{s=1} = \frac{\alpha_1}{\rho_1} \left[\ln(\rho_1 \beta_1(w_1, 1) + 1/v_1) - \ln(1/v_1)\right], \tag{3.5.8}$$

since $\beta_i(w_i, 0) = 0$. Hence, we have simplified the integral to

$$I = \frac{\alpha_1}{\rho_1} \ln\left(\frac{\rho_1 \beta_1(w_1, 1) + 1/v_1}{1/v_1}\right) = \frac{\alpha_1}{\rho_1} \ln(\rho_1 v_1 \beta_1(w_1, 1) + 1). \tag{3.5.9}$$

After substituting the expression for v_1 in (3.5.5), we have

$$I = \frac{\alpha_1}{\rho_1} \ln(\sigma_1(w_1, 1)) = \frac{\alpha_1}{\rho_1} \left(\rho_1 - \frac{\alpha_1 w_1}{\mu_1}(1 - e^{-\mu_1})\right). \tag{3.5.10}$$

We now return to the equilibrium equation (3.5.2). We substitute the expression for the integral in the first parenthesis with (3.5.10), and similarly in the second parenthesis with the same expression but with index 1 replaced by 2. We obtain

$$w_1 = w_1 p_1 e^{-\mu_1} \left(\alpha_1 + 1 - \frac{\alpha_1^2 w_1}{\mu_1 \rho_1}(1 - e^{-\mu_1})\right) + w_2(1 - p_2) e^{-\mu_2} \left(\alpha_2 + 1 - \frac{\alpha_2^2 w_2}{\mu_2 \rho_2}(1 - e^{-\mu_2})\right). \tag{3.5.11}$$

We observe that we can separate the terms with w_1 from those with w_2. We substitute again the expression of the growth rate $\nu_i = e^{-\mu_i}(\alpha_i + 1)$; see (3.4.3). We obtain the corresponding equation for w_2 by symmetry. Then we have the following quadratic system to solve:

$$w_1 - w_1 p_1 \left(\nu_1 - e^{-\mu_1} \frac{\alpha_1^2 w_1}{\mu_1 \rho_1}(1 - e^{-\mu_1})\right) = w_2(1 - p_2) \left(\nu_2 - e^{-\mu_2} \frac{\alpha_2^2 w_2}{\mu_2 \rho_2}(1 - e^{-\mu_2})\right), \tag{3.5.12}$$

$$w_2 - w_2 p_2 \left(\nu_2 - e^{-\mu_2} \frac{\alpha_2^2 w_2}{\mu_2 \rho_2}(1 - e^{-\mu_2})\right) = w_1(1 - p_1) \left(\nu_1 - e^{-\mu_1} \frac{\alpha_1^2 w_1}{\mu_1 \rho_1}(1 - e^{-\mu_1})\right). \tag{3.5.13}$$

We continue the study of these equations in Section 3.5.3.

3.5.2 Boundary Coexistence Equilibrium

We now consider a boundary coexistence equilibrium where the consumers are sustained on both patches, but one of the resource populations has died out. This corresponds to the equilibria $(0,v_2^*,w_1^*,w_2^*)$ and $(v_1^{**},0,w_1^{**},w_2^{**})$.

We use equations (2.3.21) and (2.3.22) and set $v_1 = 0$ to find an equation for the exact values of the consumer and non-extinct resource. The equations are:

$$w_1 = w_1p_1e^{-\mu_1} + w_2(1-p_2)e^{-\mu_2}\left(\alpha_2v_2\int_0^1 \frac{e^{\rho_2 s - \frac{\alpha_2 w_2}{\mu_2}(1-e^{-\mu_2 s})}}{\rho_2 v_2\int_0^s e^{\rho_2\tau - \frac{\alpha_2 w_2}{\mu_2}(1-e^{-\mu_2\tau})}\,d\tau + 1}\,ds + 1\right), \tag{3.5.14}$$

$$w_2 = w_2p_2e^{-\mu_2}\left(\alpha_2v_2\int_0^1 \frac{e^{\rho_2 s - \frac{\alpha_2 w_2}{\mu_2}(1-e^{-\mu_2 s})}}{\rho_2 v_2\int_0^s e^{\rho_2\tau - \frac{\alpha_2 w_2}{\mu_2}(1-e^{-\mu_2\tau})}\,d\tau + 1}\,ds + 1\right) + w_1(1-p_1)e^{-\mu_1}. \tag{3.5.15}$$

We again apply the notation as in (3.2.6) and (3.2.7) to find:

$$w_1 = w_1p_1e^{-\mu_1} + w_2(1-p_2)e^{-\mu_2}\left(-\frac{\alpha_2^2w_2}{\mu_2\rho_2}(1-e^{-\mu_2}) + (\alpha_2+1)\right), \tag{3.5.16}$$

$$w_2 = w_2p_2e^{-\mu_2}\left(-\frac{\alpha_2^2w_2}{\mu_2\rho_2}(1-e^{-\mu_2}) + (\alpha_2+1)\right) + w_1(1-p_1)e^{-\mu_1}. \tag{3.5.17}$$

Letting $\nu_2 = e^{-\mu_2}(1+\alpha_2)$, we obtain:

$$w_1 = w_1p_1e^{-\mu_1} - (1-p_2)\left[e^{-\mu_2}\frac{\alpha_2^2}{\mu_2\rho_2}(1-e^{-\mu_2})\right]w_2^2 + w_2(1-p_2)\nu_2, \tag{3.5.18}$$

$$w_2 = \left[-p_2e^{-\mu_2}\frac{\alpha_2^2}{\mu_2\rho_2}(1-e^{-\mu_2})\right]w_2^2 + w_2p_2\nu_2 + w_1(1-p_1)e^{-\mu_1}. \tag{3.5.19}$$

Applying some algebra, we are able to reduce the system to a quadratic in w_2 of the form:

$$Aw_2^2 + Bw_2 = 0,$$

where

$$A = e^{-\mu_2}\frac{\alpha_2^2}{\mu_2\rho_2}(1-e^{-\mu_2})\left[p_2 + \frac{(1-p_1)e^{-\mu_1}(1-p_2)}{1-p_1e^{-\mu_1}}\right], \tag{3.5.20}$$

$$B = 1 - p_2\nu_2 - \frac{(1-p_1)e^{-\mu_1}(1-p_2)\nu_2}{1-p_1e^{-\mu_1}}. \tag{3.5.21}$$

The solutions for w_2 are therefore

$$w_2^* = 0 \quad \text{or} \quad w_2^* = -\frac{B}{A}. \tag{3.5.22}$$

We exclude the solution $w_2 = 0$ to find that the consumer density on patch one is

$$w_1^* = \frac{1-p_2}{1-p_1 e^{-\mu_1}} \left[-\nu_2 \frac{B}{A} - e^{-\mu_2} \frac{\alpha_2^2}{\mu_2 \rho_2} (1 - e^{-\mu_2}) \frac{B^2}{A^2} \right]. \tag{3.5.23}$$

Next, we are interested in whether the resource is able to invade patch one. To find this condition, we require some elements of the Jacobian matrix. The Jacobian matrix has the following block structure:

$$J(0, v_2^*, w_1^*, w_2^*) = \begin{bmatrix} \sigma_1(w_1^*, 1) & 0 & 0 & 0 \\ 0 & a_{22} & a_{23} & a_{24} \\ a_{31} & a_{32} & a_{33} & a_{34} \\ a_{41} & a_{42} & a_{43} & a_{44} \end{bmatrix}$$

Hence, $\sigma_1(w^*, 1)$ is an eigenvalue of the Jacobian. Thus, for the equilibrium to be unstable, we require $\sigma_1(w^*, 1) > 1$ or

$$\rho_1 > \alpha_1 \frac{w_1^*}{\mu_1} (1 - e^{-\mu_1}). \tag{3.5.24}$$

Condition (3.5.24) indicates that the resource can invade if the total consumption pressure on the right-hand side is lower than the resource growth rate ρ_i.

3.5.3 Bifurcations of Coexistence Equilibria

The set of coupled equations (3.5.12) and (3.5.13) proves difficult to solve analytically. It is, in fact, equivalent to a quartic polynomial and can therefore have at most four solutions. Since $(0, 0)$ is a solution, we could obtain a cubic polynomial for which explicit solution formulas exist. We will use these formulas later, but first, for simplicity and insight, we look at their geometric interpretation.

Equations (3.5.12) and (3.5.13) represent equations of conic sections. We use this structure to determine equilibrium points and bifurcations. For ease of notation, we introduce the parameters

$$a = (1 - p_1\nu_1), \quad b = p_1 \frac{e^{-\mu_1}\alpha_1^2}{\mu_1\rho_1}(1 - e^{-\mu_1}), \quad c = (1 - p_2)\nu_2, \quad d = (1 - p_2)\frac{e^{-\mu_2}\alpha_2^2}{\mu_2\rho_2}(1 - e^{-\mu_2}) \tag{3.5.25}$$

and

$$e = (1 - p_2\nu_2), \quad f = p_2 \frac{e^{-\mu_2}\alpha_2^2}{\mu_2\rho_2}(1 - e^{-\mu_2}), \quad g = (1 - p_1)\nu_1, \quad h = (1 - p_1)\frac{e^{-\mu_1}\alpha_1^2}{\mu_1\rho_1}(1 - e^{-\mu_1}).$$

With these, we can rewrite our coupled quadratic equations as:

$$w_1(a + bw_1) = w_2(c - dw_2), \tag{3.5.26}$$

$$w_2(e + fw_2) = w_1(g - hw_1). \tag{3.5.27}$$

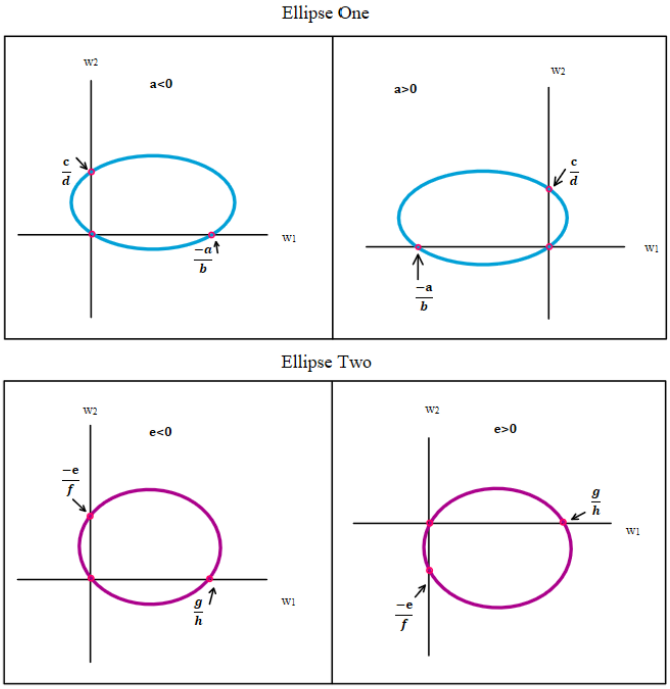

Figure 3.3: Diagram representations of the ellipses in (3.5.26) and (3.5.27) and their intercepts.

We know that $b, c, d, f, g > 0$. Only a and e can change signs. The standard form of the conic section (3.5.26) is

$$aw_1 + bw_1^2 - cw_2 + dw_2^2 = 0. \tag{3.5.28}$$

We require $-4bc < 0$ for the conic section to be an ellipse. This condition is satisfied as $b, c > 0$. A similar argument can be made for equation (3.5.13). Ellipse one and Ellipse two will refer to both the set of points satisfying (3.5.26) and (3.5.27) or the equations (3.5.26) and (3.5.27) themselves depending on the context.

Clearly, the two ellipses intersect at $(0, 0)$. We note that since there are no mixed terms (i.e., terms that contain the product w_1w_2), the axes of the ellipses are parallel to the coordinate axes. Where each intersects the w_1 and w_2 axes depends on the signs of a and e. In total, four different combinations emerge; see Figure 3.3. We now study how varying parameters changes the intersections of the ellipses, thus creating bifurcations.

Transcritical Bifurcation

We begin by describing a transcritical bifurcation that introduces one positive steady state. A transcritical bifurcation occurs when two steady states collide and their stability switches. For example, Figure 3.4 illustrates how two ellipses that must go through the origin can produce such a bifurcation. This bifurcation is created by varying the parameters of the conic sections described in equations (3.5.26) and (3.5.27). These parameters are complicated

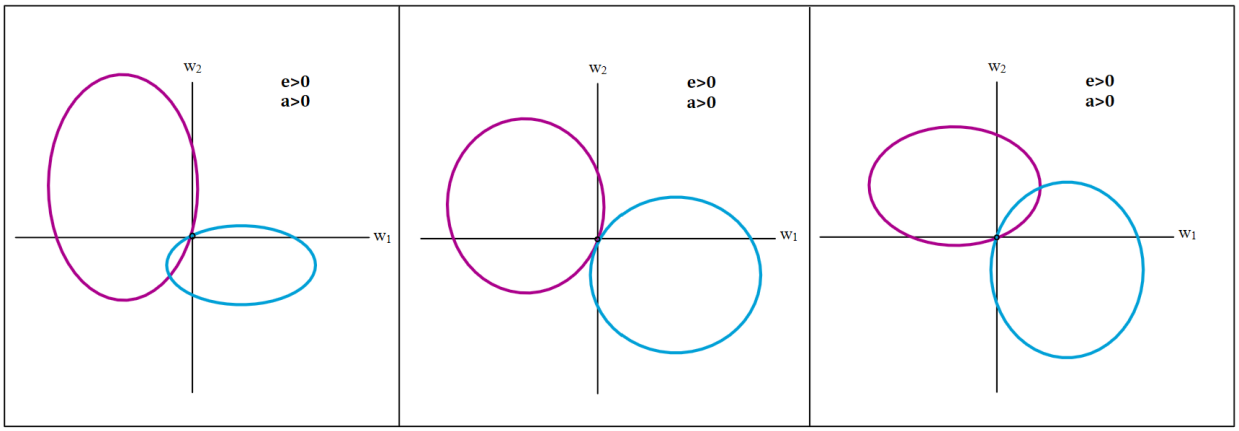

Figure 3.4: Representative diagram of possible intersections of equations (3.5.26) and (3.5.27), showing a transcritical bifurcation. Ellipse one is blue and Ellipse two is purple.

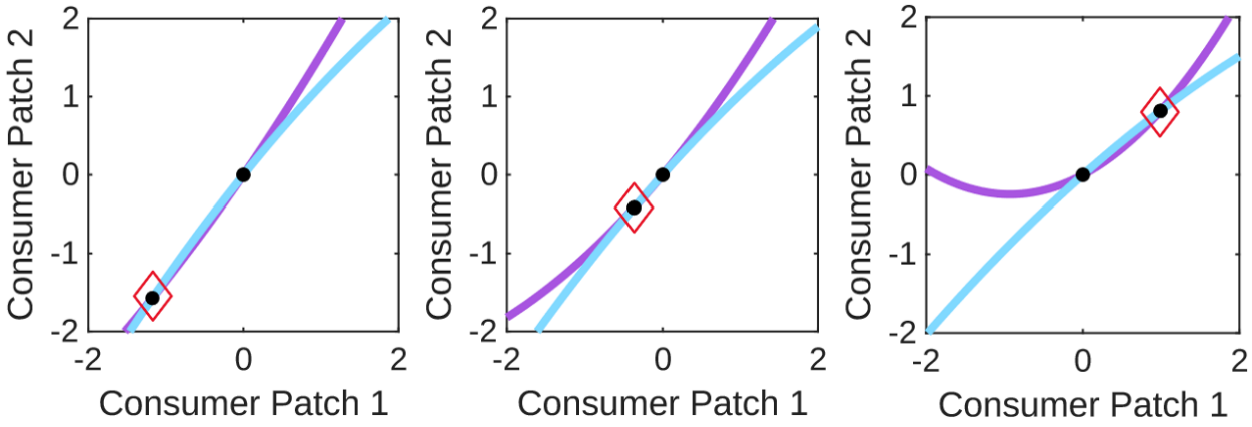

Figure 3.5: Diagram of intersections of equations (3.5.26) and (3.5.27) showing a transcritical bifurcation as $p_1 = p_2$ increase from 0.3 (left) via 0.42 (middle) to 0.5 (right). Ellipse one is blue and Ellipse two is purple. Other parameters are $\rho_{1,2} = 20$, $\mu_{1,2} = 1$, $\alpha_1 = 3$, and $\alpha_2 = 0.5$. The diamond follows one equilibrium through the transcritical bifurcation.

expressions of the model parameters. In Figure 3.5, we show that we can find this same bifurcation with respect to our model parameters. It turns out that we can analytically determine the condition for this bifurcation and its dependence on model parameters. To find this condition, we perform an analysis of the slopes at zero to determine when the slopes exchange sign.

We first calculate the slope of each ellipse at the origin. Locally we can write $w_2 = F_1(w_1)$. Using implicit differentiation and the chain rule, we have

$$\frac{dE(w_1, F_1(w_1))}{dw_1} = a + 2bw_1 - cF_1'(w_1) + 2dF_1(w_1)F_1'(w_1). \tag{3.5.29}$$

Evaluating at $(0,0)$ gives $a - cF_1'(0) = 0$. We solve for $F_1'(0)$ to find

$$F_1'(0) = \frac{a}{c} = \frac{1 - p_1\nu_1}{(1-p_2)\nu_2}. \tag{3.5.30}$$

Similarly, from the second ellipse (writing $w_2 = F_2(w_1)$), we find

$$F_2'(0) = \frac{g}{e} = \frac{(1-p_1)\nu_1}{1 - p_2\nu_2}. \tag{3.5.31}$$

Then we find that the bifurcation occurs when the two slopes coincide—i.e., $F_1'(0) = F_2'(0)$—which gives

$$\frac{1 - p_1\nu_1}{(1-p_2)\nu_2} = \frac{(1-p_1)\nu_1}{1 - p_2\nu_2}, \tag{3.5.32}$$

or, equivalently,

$$p_1\nu_1 + p_2\nu_2 + (1 - p_1 - p_2)\nu_1\nu_2 = 1. \tag{3.5.33}$$

This is exactly the threshold where the semi-trivial state loses stability; see (3.4.5). It is thus the condition for a transcritical bifurcation to occur.

Saddle-Node Bifurcation

Similar to the transcritical bifurcation, we can use the geometric interpretation of the co-existence equations to predict the existence of a saddle-node bifurcation. A saddle-node bifurcation occurs when two equilibria become one, then one equilibrium disappears. We construct a saddle-node configuration from transformations of our conic sections, as shown in Figure (3.6). To find this bifurcation with our original model parameters, we use the following analysis. Neither ellipse has mixed terms, so each has one axis parallel to the coordinate axis w_1 and one parallel to the coordinate axis w_2. For example, ellipse two has a vertical axis parallel to the w_2 axis. The uppermost point of ellipse two is on this parallel axis. Thus, this point satisfies

$$w_2(e + fw_2) = h\left(\frac{g}{2h}\right)\left(\frac{g}{h} - \frac{g}{2h}\right) = \frac{g^2}{h}. \tag{3.5.34}$$

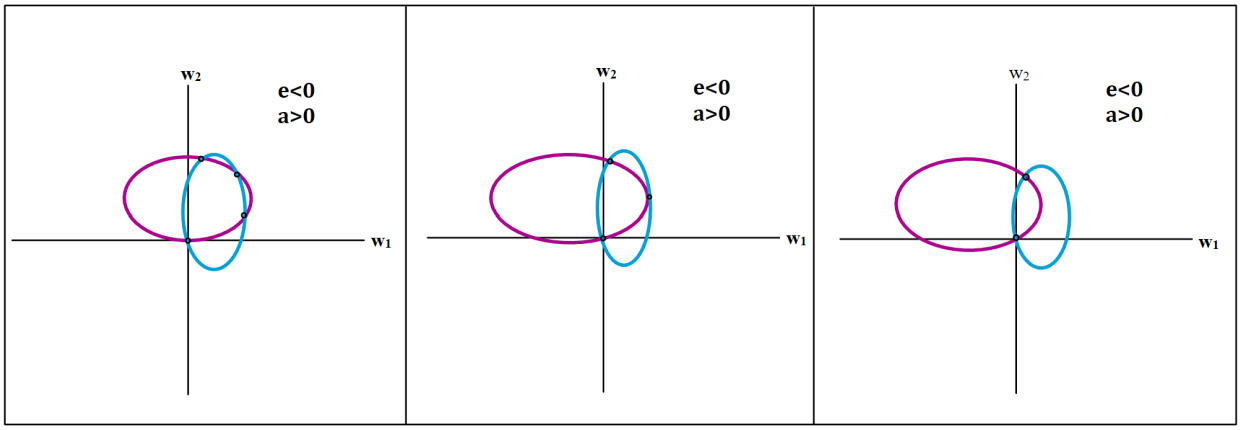

Figure 3.6: Representative diagram of possible intersections of equations (3.5.26) and (3.5.27), showing a saddle-node bifurcation. Ellipse one is purple and Ellipse two is blue.

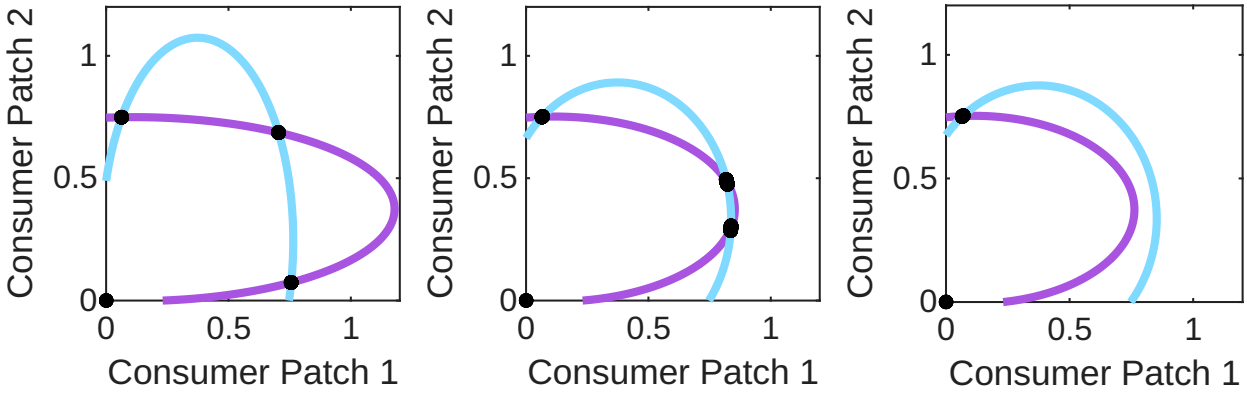

Figure 3.7: Diagram of intersections of equations (3.5.26) and (3.5.27) showing a saddle-node bifurcation as p_2 increases from 0.2 (left) via 0.62 (middle) to 0.71 (right). Other parameters are $\mu_{1,2} = 0.1$, $\rho_{1,2} = 10$, $\alpha_{1,2} = 15$, and $p_1 = 0.1$.

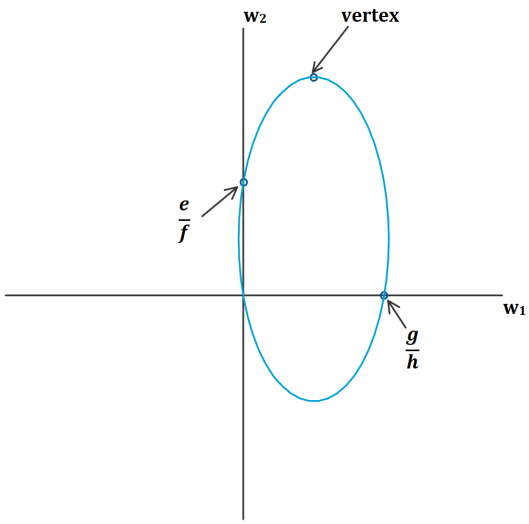

Figure 3.8: Illustration of how the vertex of Ellipse two can be moved without changing the intersections with the axes; see (3.5.35).

This is a quadratic equation that we can solve for w_2. We find

$$w_{2,vertex} = \frac{-1}{2}\left(\frac{e}{f}\right) \pm \frac{1}{2}\sqrt{\left(\frac{e}{f}\right)^2 + \left(\frac{g}{h}\right)\left(\frac{g}{f}\right)}. \tag{3.5.35}$$

Hence, we can make the vertex of w_2 large while keeping the positive intersection of the ellipse at $\frac{g}{h}$. Using Figure 3.6 as a guide, we can achieve the geometry of the left-most plot by making $\frac{g}{f}$ large, which stretches the first ellipse vertically. We keep $\frac{e}{f}$ and $\frac{g}{h}$ constant to fix the intersection of the ellipses with the coordinate axes. See Figure 3.8.

Using this information, we are able to find the same saddle-node bifurcation predicted by Figure 3.6, using our model parameters, which we display in Figure 3.7. In the left-most plot of both figures, three equilibrium points exist. In the middle plot, two equilibrium points collide into one, which forms the saddle-node bifurcation. In the final plot, the equilibrium point has disappeared. Finally, we find an analytic condition for which a saddle-node bifurcation arises. To do so, we first convert our two coupled quadratic equations into a single quartic equation. Let $A_i = \frac{e^{-\mu_i}\alpha_i^2}{\mu_i\rho_i}(1-e^{-\mu_i})$. Then our equations become

$$w_1 - w_1 p_1 \left(\nu_1 - w_1 A_1\right) - w_2(1-p_2)\left(\nu_2 - w_2 A_2\right) = 0, \tag{3.5.36}$$
$$w_2 - w_2 p_2 \left(\nu_2 - w_2 A_2\right) - w_1(1-p_1)\left(\nu_1 - w_1 A_1\right) = 0. \tag{3.5.37}$$

We multiply Equation (3.5.36) by $(1-p_1)$ and Equation (3.5.37) by p_1 to find

$$w_1(1-p_1) - w_1 p_1(1-p_1)\left(\nu_1 - w_1 A_1\right) - w_2(1-p_2)(1-p_1)\left(\nu_2 - w_2 A_2\right) = 0, \tag{3.5.38}$$
$$w_2 p_1 - w_2 p_2 p_1 \left(\nu_2 - w_2 A_2\right) - w_1 p_1(1-p_1)\left(\nu_1 - w_1 A_1\right) = 0. \tag{3.5.39}$$

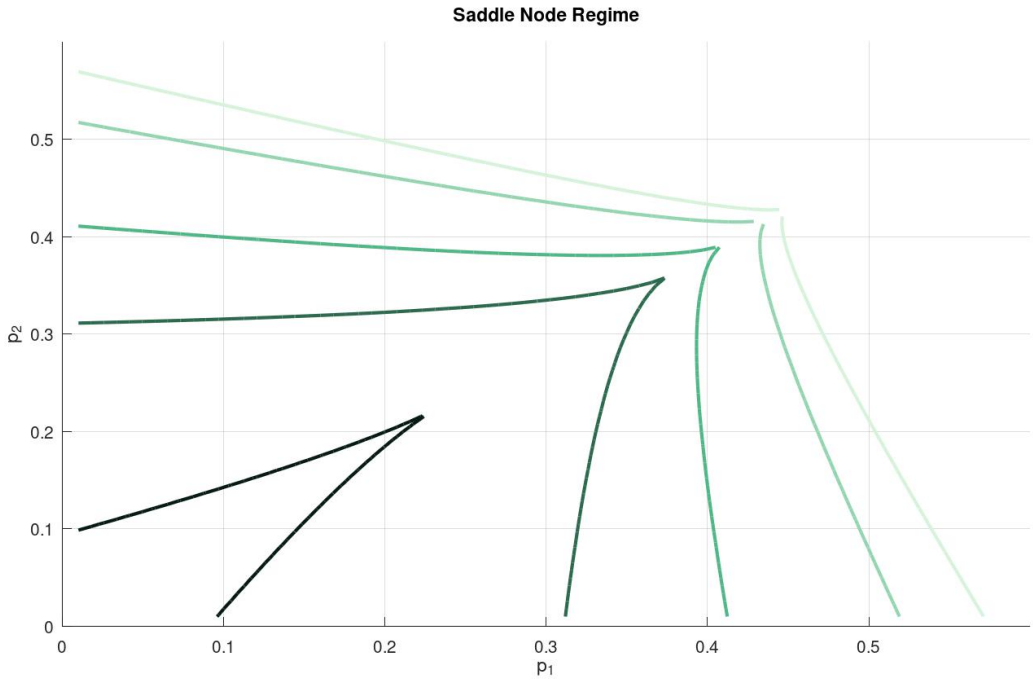

Figure 3.9: Curve in p_1-p_2 space where the discriminant of Equation (3.5.46) is zero. Parameters are $\rho_{1,2} = 20$, $\mu_1 = 0.5$, $\mu_2 = 0.4$. Increasing brightness indicates increasing α for $\alpha_{1,2} = 5, 8, 10, 13, 15$.

Expanding both, we find

$$w_1(1-p_1) - w_1p_1(1-p_1)\nu_1 + p_1(1-p_1)A_1w_1^2 - w_2(1-p_2)(1-p_1)\left(\nu_2 - w_2A_2\right) = 0 \tag{3.5.40}$$

$$w_2p_1 - w_2p_2p_1\left(\nu_2 - w_2A_2\right) - w_1p_1(1-p_1)\nu_1 + p_1(1-p_1)A_1w_1^2 = 0. \tag{3.5.41}$$

We subtract Equation (3.5.41) from Equation (3.5.40) so that the quadratic w_1 terms cancel:

$$(1-p_1)w_1 = (1-p_1)(1-p_2)\nu_2w_2 - (1-p_1)(1-p_2)A_2w_2^2 + p_1p_2A_2w_2^2 + p_1w_2 - p_1p_2\nu_2w_2. \tag{3.5.42}$$

Dividing by $(1-p_1)$ to isolate for w_1 we find

$$w_1 = (1-p_2)\nu_2w_2 - (1-p_2)A_2w_2^2 + \frac{p_1p_2A_2w_2^2}{1-p_1} + \frac{p_1w_2}{1-p_1} - \frac{p_1p_2v_2w_2}{1-p_1}. \tag{3.5.43}$$

We define $\hat{a} = (1-p_2)\nu_2 + \frac{p_1(1-p_2\nu_2)}{1-p_1}$ and $\hat{b} = -(1-p_2)A_2 + \frac{p_1p_2A_2}{1-p_1}$. Equation (3.5.43) has the form

$$w_1 = \hat{a}w_2 + \hat{b}w_2^2, \tag{3.5.44}$$

which we substitute into our first equation. Expanding squares, we find

$$p_1A_1(\hat{a}^2w_2^2 + 2\hat{a}\hat{b}w_2^3 + \hat{b}^2w_2^4) + (1-p_1\nu_1)(\hat{a}w_2 + \hat{b}w_2^2) - (1-p_2)\nu_2w_2 + (1-p_2)A_2w_2^2 = 0. \tag{3.5.45}$$

Thus, we have a quartic function in w_2. One root is zero, as we expect, so we factor it out and arrange terms based on degree. We obtain the cubic equation

$$[p_1A_1\hat{b}^2]w_2^3+[2p_1A_1\hat{a}\hat{b}]w_2^2+[(1-p_1\nu_1)(b)+(1-p_2)A_2+p_1A_1(\hat{a}^2)]w_2+[\hat{a}(1-p_1\nu_1)-(1-p_2)\nu_2]=0. \tag{3.5.46}$$

A saddle-node bifurcation can occur when there is a double root of this cubic function, which occurs when there is a root that is also a local maximum or minimum. We compute the derivatives of Equation (3.5.46) and set them to zero to find

$$[3p_1A_1\hat{b}^2]w_2^2 + [4p_1A_1\hat{a}\hat{b}]w_2 + [(1-p_1\nu_1)\hat{b} + (1-p_2)A_2 + p_1A_1\hat{a}^2] = 0, \tag{3.5.47}$$

$$[6p_1A_1b^2]w_2 + [4p_1A_1\hat{a}\hat{b}] = 0. \tag{3.5.48}$$

Thus, a double root occurs for a value w_2^* such that w_2^* is a root of (3.5.46) and its derivative (3.5.47) but not its second derivative (3.5.48).

From here, we can solve Equation (3.5.47) for w_2 using the quadratic formula and use the solution to get a parametric curve from Equation (3.5.46). We show this curve in p_1-p_2 space in Figure 3.9, using a level-zero contour plot.

We expected that, based on the parameter region in which the saddle-node bifurcation arises, the fixed points might both be unstable. We then tried to find the steady states in phase space using numerical simulations but found that these states were most likely unstable. An area of future research is to determine if any saddle-node bifurcations with stable steady states exist in the model.

We now interpret the results of Section 2.5. Coexistence equilibria arise when both species, consumer and resource, are present. Coexistence can involve either three or all four persisting populations. In the case where three persist, we note that only one population of resource may die out, as it does not disperse. Boundary coexistence equilibria, where one population dies out while the others persist, are a common phenomenon in meta-population models. For example, Haygood [21] found that the dynamics of a system of initially two resource and two consumer populations could remain stable even if the one resource population has died out. Further, Haygood found that this requires that the growth rate of the resource population on the surviving patch to be higher than the pressure from the consumers on both patches. We find a similar result and determine when a resource population avoids extinction and can invade. We find that invasion occurs when the resource growth rate exceeds the total consumption pressure. Consumption pressure can be viewed as the attack rate scaled by the consumer death rate multiplied by the probability of survival for the consumer.

In our model, positive coexistence through a transcritical bifurcation at the zero state occurs. This bifurcation occurs at a critical threshold, which accounts for the scaled local growth rate by patch ($p_i\nu_i$) of those remaining on the patch, and the effect of those dispersing ($p_1\nu_1\nu_2 + p_2\nu_1\nu_2$). Low $p_i\nu_i$ means either individuals are leaving their patches too fast (low p_i) or have a low growth rate ν_i. If the contribution from the local growth rate is too low—i.e., the patches are of poor quality—then dispersal effects must compensate for invasion to occur. If the sum of the local contributions from each patch is high enough, the population can persist, which leads to a positive steady state.

Table 3.1: Parameter values used for Figure 3.10.

Plot	α	ρ	μ	p_1	p_2
a	10	20	1.5	0.5	0.55
b	12	22	1	0.5	0.55
c	11	25	0.8	0.5	0.55
d	2.88	20	0.1	0.5	0.505
e	20	13.5	0.8	0.9	0.7
f	18/5	20/10	1	0.2	0.8

The model also displays a saddle-node bifurcation in the consumer–resource parameter regime. There may be other types of saddle-node bifurcations that arise in the model, but the one found in this section was composed of two unstable equilibria. Around the bifurcation, we find large amplitude consumer–resource cycles on patch one and resource extinction on patch two (simulations not shown).

3.6 Numerical Simulations

We created all numerical simulations using Octave 8.4.0. We used both an integral solver and an ODE solver to independently simulate the model. We then validated the two methods against each other. The ODE solver uses the built-in function *ode23* to calculate the densities within year. For the ODE solver *ode23*, we used the preset tolerances and settings. We collected these densities at the end of the year and passed them to the maps described in (2.3.5). This process was iterated.

In the second method, the stroboscopic maps given in Equations (2.3.19) through (2.3.22) were numerically approximated using numerical quadrature. The integral solver uses the trapezoid rule (*trapz*) with 100 nodes to approximate the integral representing consumer growth over one year. The code calculates the nested integral in the consumer equations. To calculate the outer integral, which we integrate with respect to ds, we need to first evaluate the inner integral whose upper bound is the integration variable s. The inner integral is evaluated 100 times, each with a slightly higher bound s. In each iteration, we evaluate the integral using the built-in Octave function (*integral*), which is an adaptive Gauss–Kronrod Scheme.

In Figure 3.10, we illustrate some dynamical behaviour of the model. Some typical behaviours that result from consumer–resource dynamics are (a) stable dynamics, (b) two-cycle dynamics, and (d) consumer–resource cycles. We can also find four and six cycles, but we choose to display the six-cycle dynamics in (c). We are also able to display chaotic dynamics, as shown in panel (e). Panel (f), where a single resource extinction is shown, is not possible in the Pachepsky equations because it is a consequence of dispersal.

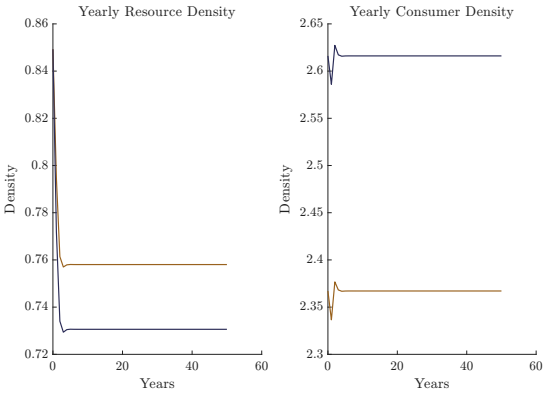

(a) Stable dynamics

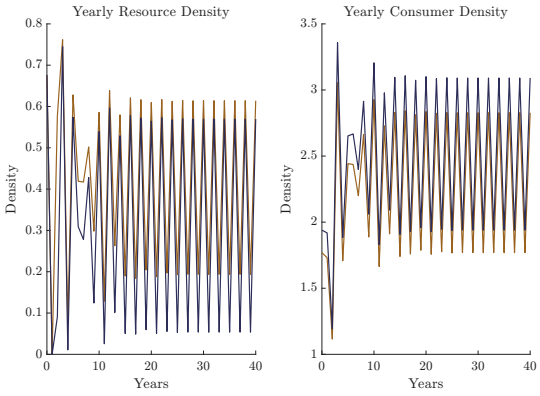

(b) Two-cycle dynamics

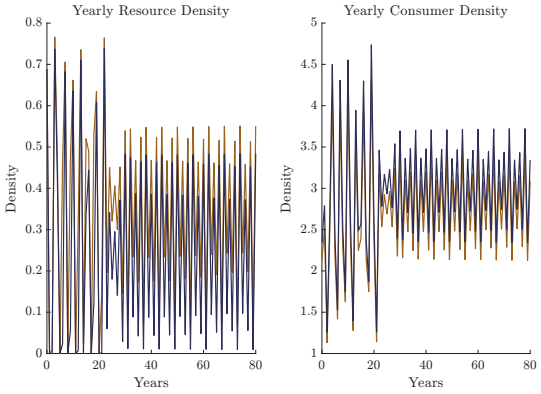

(c) Six-cycle dynamics

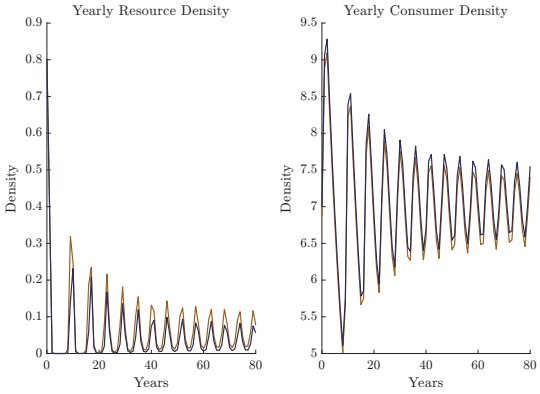

(d) Consumer-resource Cycles

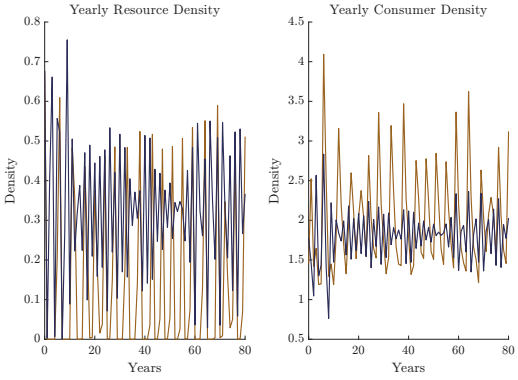

(e) Chaotic dynamics

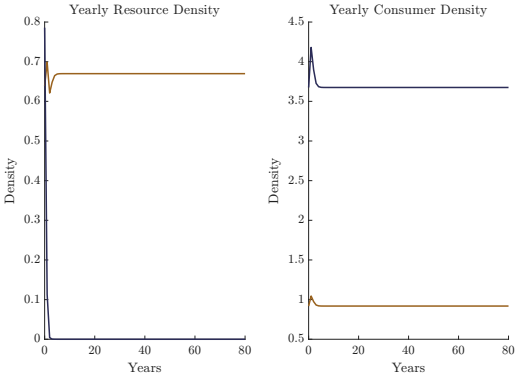

(f) Single Resource Extinction

Figure 3.10: Dynamics of the semi-discrete model. See Table 3.1 for parameter values. Initial conditions: $v_1 = 1, v_2 = 1, w_1 = 0.2, w_2 = 0.2$ used for all plots. Blue is patch one and brown is patch two.

Chapter 4

Influence of Dispersal

In this chapter, we investigate the influence of dispersal on the population dynamics of consumers and resources. We begin by citing the relevant background. Next, we investigate the role of dispersing consumers on the overall population abundance of both consumers and their resource. We first perform an asymptotic expansion from the known equilibrium solution in Pachepsky et al. [34] and determine conditions for when increasing dispersal leads to increasing population density at low dispersal. We then explore the same question beyond the validity of the asymptotic expansion. We say that dispersal is beneficial to a population if the steady-state density of the population on both patches combined is higher with dispersal than without.

4.1 Background

The benefits of dispersal have been widely studied. Freedman and Waltman (1977) were the first to discover the benefits of dispersal in a two-patch model in continuous time. They studied a single species with two non-competing populations x_1 and x_2, each on its respective patch, which move between patches (disperse) with rate ϵ. They focused only on the limiting case when $\epsilon \to \infty$. They called the patch-specific growth rates α_i and the carrying capacities K_i. Their model is given by

$$\frac{dx_1}{dt} = \alpha_1 x_1 \left(1 - \frac{x_1}{K_1}\right) - \epsilon x_1 + \epsilon x_2, \tag{4.1.1}$$

$$\frac{dx_2}{dt} = \alpha_2 x_2 \left(1 - \frac{x_2}{K_2}\right) - \epsilon x_2 + \epsilon x_1. \tag{4.1.2}$$

Freedman and Waltman found an explicit expression of the unique positive steady state in terms of the dispersal rate, $(x_1^*(\epsilon), x_2^*(\epsilon))$. Without dispersal (i.e., when $\epsilon = 0$), the steady state of this model is simply the carrying capacity: $(x_1^*(0), x_2^*(0)) = (K_1, K_2)$. The authors showed that when $\epsilon \to \infty$, the steady-state densities in the two patches become equal; i.e., $(x_1^*(\epsilon), x_2^*(\epsilon)) \to (x^*, x^*)$, where

$$x^* = \frac{\alpha_1 + \alpha_2}{\frac{\alpha_1}{K_1} + \frac{\alpha_2}{K_2}}. \tag{4.1.3}$$

They then then showed that $K_1 + K_2 - 2x^* < 0$ if either $K_1 > K_2$ and $\frac{\alpha_1}{K_1} > \frac{\alpha_2}{K_2}$ or $K_2 > K_1$ and $\frac{\alpha_2}{K_2} > \frac{\alpha_1}{K_1}$. Hence, in those cases, the total consumer population at steady state is higher with large dispersal than without [18].

We note that when $\alpha_1 = \alpha_2$, the expression for x^* is the harmonic mean of the carrying capacities. At $\epsilon = 0$, the density is the sum of the carrying capacities, so twice the arithmetic mean. The AM-HM inequality says that the arithmetic mean is greater than the harmonic mean [9]. Hence, only if the populations on two patches have different growth rates can the phenomenon occur that dispersal can increase the total population density at steady state.

The steady-state density for models with dispersal has since been named *TRAPA* — Total Realized Asymptotic Population Abundance. How *TRAPA* depends on dispersal has been studied in the context of many different models. For the continuous-time case, DeAngelis et al. [15] investigated a seed-dispersal model and derived how TRAPA depends on dispersal. They determined that including dispersal in a heterogeneous model meant the seed populations could benefit or could be reduced depending on the asymmetry in the model. In the discrete case, Arditi et al. [5] found that for a two-patch model with a Beverton–Holt growth function, dispersal was not always beneficial. They found that the benefit can exhibit a unimodal dependence on dispersal probability.

Further, predator–prey models [36], PDE models [29]and [42], consumer–resource models [41] and other meta-community models have investigated the dependence of dispersal on *TRAPA*. Huang and Wang [24] determined that intermediate dispersal promotes persistence in two-patch systems, but large dispersal can lead to extinction. Few studies have been conducted on the effects of consumer dispersal on resource dynamics, but Hu and Wangshi find that in a MacArthur-type model, the resource always has a higher *TRAPA* when consumers disperse [23]. These results highlight that dispersal can heavily influence *TRAPA*, and that dispersal may, under certain conditions, promote higher *TRAPA*.

Grumbach et al. [20] studied a discrete-time population dynamic model of a single species on two patches and defined a way to evaluate the effect of dispersal with what they called the *H-index*. They started with two populations, $N_{A,t}(\delta)$ and $N_{B,t}(\delta)$, which represent the populations on two patches at time t for a given value of dispersal δ. They defined ξ_i as the strength of intraspecific competition, and the Beverton–Holt growth functions $f_i(N) = \frac{r_i N}{1+\xi_i N}$ as population dynamics on each patch. Their equations become:

$$N_{A,t+1}(\delta) = (1-\delta) f_A(N_{A,t}(\delta)) + \delta f_B(N_{B,t}(\delta)), \tag{4.1.4}$$

$$N_{B,t+1}(\delta) = (1-\delta) f_B(N_{B,t}(\delta)) + \delta f_A(N_{A,t}(\delta)), \tag{4.1.5}$$

where δ is the probability of moving between patches. The steady-state values of this map with respect to time are denoted by $N_A^*(\delta)$ and $N_B^*(\delta)$, and they exist for all δ. The H-index $H : [0,1] \to \mathbb{R}$, as defined in [20], measures the difference between the asymptotic population density at steady state with dispersal and without dispersal. Specifically, the H-index is

$$H(\delta) = N_A^*(\delta) + N_B^*(\delta) - (N_A^*(0) + N_B^*(0)). \tag{4.1.6}$$

Clearly $H(0) = 0$. Hence, the sign of the H-index determines when the population has a higher or lower *TRAPA* with dispersal. In the absence of dispersal, the asymptotic density

of the population on patch A is $N_A^*(0) = K_A \equiv (r_A - 1)/\xi_A$, and similarly on patch B. Grumbach et al. [20] found four qualitatively different shapes of their H-index in their model. They called these shapes (1) monotonically beneficial, (2) unimodally beneficial, (3) beneficial turning detrimental, and (4) monotonically detrimental; see Figure 4.1. The authors compared their results with a continuous analogue of their model and find the same four response scenarios.

In the models by Freedman and Waltman [18] and by Grumbach et al. [20], the authors determine an explicit expression for the positive steady state as a function of dispersal. Our model differs because we have two interacting species, while we do not have explicit expressions for the positive steady states, and, in fact, do not necessarily have uniqueness. However, to understand whether dispersal benefits the global populations of consumers and resources, we must determine these expressions. We approach this problem in two ways. We first use a perturbation method, which is feasible because we have an explicit expression for the equilibrium without dispersal. This method is valid only for small dispersal probabilities. Second, we calculate the solutions to the coupled equations (3.5.12) and (3.5.13) numerically for each dispersal probability, as in the paper by Grumbach et al. [20]. This approach is valid for all dispersal probabilities.

The first approach uses perturbation analysis to approximate the solution by expressing it as an infinite power series with respect to a small parameter. This parameter perturbs the equation from its solvable form and builds on the known solution. We use the probability of dispersal as the small parameter. Then we can use the zeroth-order solution to find higher-order correction terms. An introduction to asymptotic analysis and perturbation methods can be found in [7]. The asymptotic series can be truncated at any order but provides a better approximation with each higher order (except when the series diverges). Generally, calculating higher-order terms is more complicated at each step. In the context of this thesis, we focus on the zeroth-order term and first-order correction term. We can interpret the first-order correction as the direction that dispersal influences population density. Thus, if the sum of the first corrections from patches one and two is positive, small dispersal is beneficial.

Representing the solution as an asymptotic expansion relies on using known quantities to calculate the corrections to a more complicated model. In the absence of dispersal, we can use the positive equilibrium expressions found in Pachepsky et al. [34] as the zeroth-order solution. For the asymptotic expansion to be valid, we implicitly assume that our extended model also has a positive, unique steady state by restricting parameter space to the region where we observe only one steady state. In the following calculations, we use the bifurcation diagram 3.1 to guide the restriction of parameter space. We verify uniqueness by checking the intersection of the ellipses found in section 3.5.3.

The second approach calculates *H-index*. To do so, we determine the steady state density with dispersal numerically. We use the positive equilibrium expression found in the paper by Pachepsky et al. [34] to represent the density without dispersal on either patch. We then find the same four response scenarios for the consumer population as in [20]. We also extend this work to determine the corresponding response scenarios for the resource.

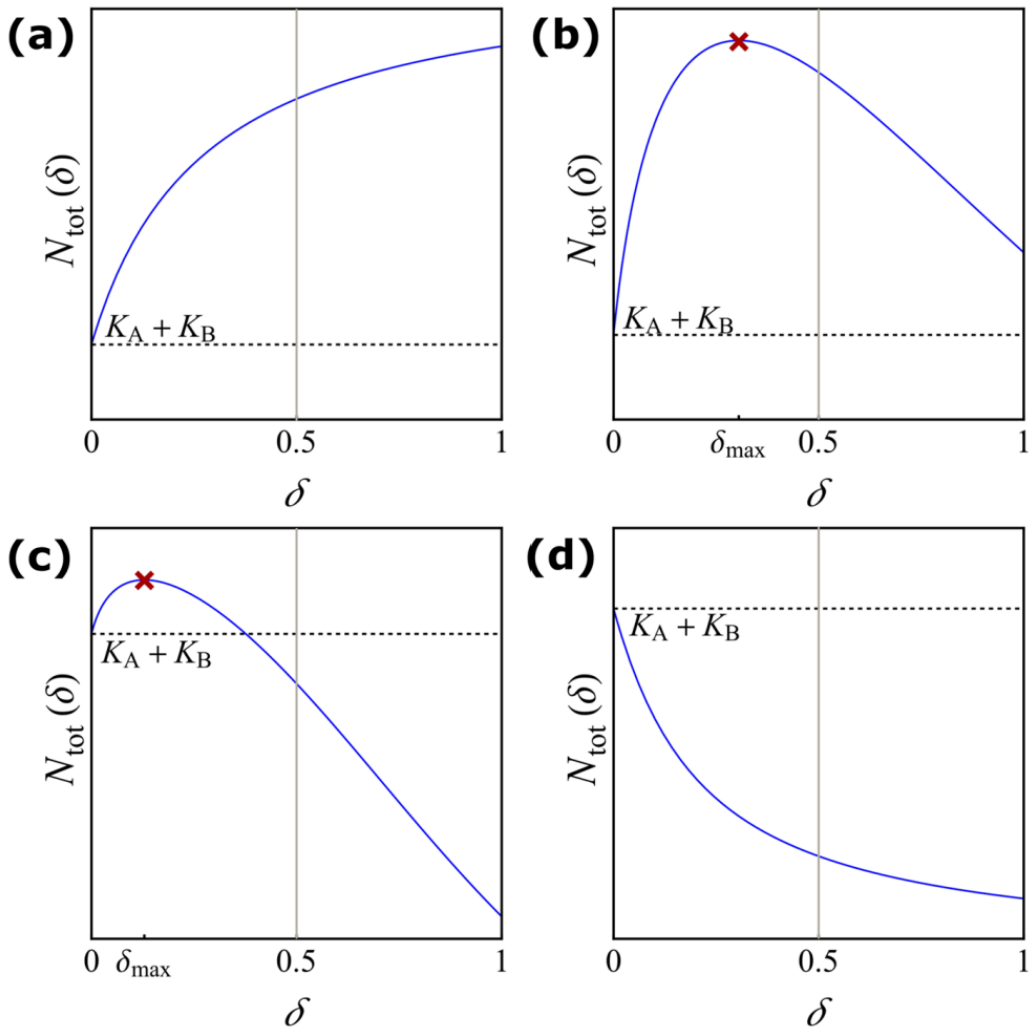

Figure 4.1: Description of the four response scenarios detailed in Grumbach et al. [20]. $N_{\text{tot}}(\delta)$ is the density of the population at steady state with dispersal, and $K_1 + K_2$ (dashed line) is the density without it. The four plots show: (a) monotonically beneficial, (b) unimodally beneficial, (c) beneficial turning detrimental, and (d) monotonically detrimental H-index. Reprinted with permission from "Grumbach, C., Reurik, F. N., Segura, J., Franco, D., and Hilker, F. M. (2023). The effect of dispersal on asymptotic total population size in discrete- and continuous-time two-patch models. Journal of Mathematical Biology, 87(4), 60."

4.2 Asymptotic Expansion

The goal of this asymptotic expansion is to calculate the first-order correction to the positive equilibrium in our model, using the known coexistence equilibrium from Pachepsky et al. [34]. This linear correction will allow us to determine the sign of the slope of the equilibrium density. Given the sign of the slope, we are able to determine whether small dispersal increases or decreases consumer equilibrium density.

We start by introducing a small parameter ϵ by setting

$$p_1 = p_2 = p = 1 - \epsilon. \tag{4.2.1}$$

Since p_i represent the probability of staying on a patch, ϵ represents dispersal. We expand w_1 and w_2 as a power series so that:

$$w_1 = w_{1,0} + \epsilon w_{1,1} + \epsilon^2 w_{1,2} + \dots \quad , \tag{4.2.2}$$

$$w_2 = w_{2,0} + \epsilon w_{2,1} + \epsilon^2 w_{2,2} + \dots \quad . \tag{4.2.3}$$

We also expand the parameters containing p as functions of ϵ, with $a(\epsilon) = a_0 + \epsilon a_1$, and similarly for the other parameters. We substitute our expansions for w_1 and w_2 into the coexistence equation (3.5.26) and find

$$\begin{aligned}(a_0 + \epsilon a_1)(w_{1,0} + \epsilon w_{1,1}) + (b_0 + \epsilon b_1)(w_{1,0} + \epsilon w_{1,1})^2 \\ -(c_0 + \epsilon c_1)(w_{2,0} + \epsilon w_{2,1}) + (d_0 + \epsilon d_1)(w_{2,0} + w_{2,1})^2 = 0.\end{aligned} \tag{4.2.4}$$

We begin with the zeroth-order calculations. In this case, we set $\epsilon = 0$, which reduces our model to the model in Pachepsky et al. [34], separately on the two patches. The zeroth-order equation is

$$a_0 w_{1,0} + b_0 w_{1,0}^2 - c_0 w_{2,0} + d_0 w_{2,0}^2 = 0. \tag{4.2.5}$$

We note that $c_0 = 0$ and $d_0 = 0$ (see below). The solution becomes

$$w_{1,0} = 0 \quad \text{or} \quad w_{1,0} = -\frac{a_0}{b_0}, \tag{4.2.6}$$

and similarly

$$w_{2,0} = 0 \quad \text{or} \quad w_{2,0} = -\frac{e_0}{f_0}. \tag{4.2.7}$$

We take the nonzero expressions and assume that $a_0, e_0 < 0$ (see below). This is the positive equilibrium density found in [34]. This equilibrium occurs in our model when the two patches are isolated (i.e., there is no dispersal).

We now consider the first-order approximation, which is the next term in the asymptotic expansion. We calculate the correction term for patch one only to simplify calculations. Substituting in the known zeroth-order term, we find:

$$(a_0 + \epsilon a_1)\left(\frac{-a_0}{b_0} + \epsilon w_{1,1}\right) + (b_0 + \epsilon b_1)\left(\frac{-a_0}{b_0} + \epsilon w_{1,1}\right)^2 \tag{4.2.8}$$

$$-(c_0+\epsilon c_1)\left(\frac{-e_0}{f_0}+\epsilon w_{2,1}\right)+(d_0+\epsilon d_1)\left(\frac{-e_0}{f_0}+\epsilon w_{2,1}\right)^2=0,$$

which, expanded, gives

$$\begin{aligned}(a_0+\epsilon a_1)\left(\frac{-a_0}{b_0}+\epsilon w_{1,1}\right)+(b_0+\epsilon b_1)\left(\frac{a_0^2}{b_0^2}-2\epsilon\frac{a_0}{b_0}w_{1,1}+O(\epsilon^2)\right)\\ -(\epsilon c_1)\left(\frac{-e_0}{f_0}+\epsilon w_{2,1}\right)+(\epsilon d_1)\left(\frac{e_0^2}{f_0^2}-2\epsilon\frac{e_0}{f_0}w_{2,1}+O(\epsilon^2)\right)=0,\end{aligned} \tag{4.2.9}$$

We find that taking only order-ϵ terms results in

$$a_0w_{1,1}-\frac{a_0a_1}{b_0}-2a_0w_{1,1}+b_1\frac{a_0^2}{b_0^2}+c_1\frac{e_0}{f_0}+d_1\frac{e_0^2}{f_0^2}=0. \tag{4.2.10}$$

We note that $a_0\neq 0$, so that

$$w_{1,1}=\frac{1}{a_0}\left(-\frac{a_0a_1}{b_0}+b_1\frac{a_0^2}{b_0^2}+c_1\frac{e_0}{f_0}+d_1\frac{e_0^2}{f_0^2}\right). \tag{4.2.11}$$

Then we write our parameters in terms of model parameters as

$$\begin{aligned}&a_0=1-\nu_1, && a_1=\nu_1, && b_0=\frac{e^{-\mu_1}\alpha_1^2}{\mu_1\rho_1}(1-e^{-\mu_1}), && b_1=-b_0,\\ &c_0=0, && c_1=\nu_2, && d_0=0, && d_1=\frac{e^{-\mu_2}\alpha_2^2}{\mu_2\rho_2}(1-e^{-\mu_2}),\\ &e_0=1-\nu_2, && f_0=d_1.\end{aligned}$$

Simplifying, we find

$$w_{1,1}=\frac{c_1e_0+e_0^2}{a_0d_1}-\frac{a_1+a_0}{b_0}=\frac{(\nu_2-1)}{(\nu_1-1)(\frac{e^{-\mu_2}\alpha_2^2}{\mu_2\rho_2}(1-e^{-\mu_2}))}-\frac{(1-\nu_1)+\nu_1}{\frac{e^{-\mu_1}\alpha_1^2}{\mu_1\rho_1}(1-e^{-\mu_1})}. \tag{4.2.12}$$

We factor out $\frac{1}{\nu_i-1}$ to arrive at

$$w_{1,1}=\frac{1}{\nu_1-1}\left(\frac{\nu_2-1}{\frac{e^{-\mu_2}\alpha_2^2}{\mu_2\rho_2}(1-e^{-\mu_2})}-\frac{\nu_1-1}{\frac{e^{-\mu_1}\alpha_1^2}{\mu_1\rho_1}(1-e^{-\mu_1})}\right). \tag{4.2.13}$$

After inspection, this expression simplifies to

$$w_{1,1}=\frac{1}{\nu_1-1}\left(w_{2,0}-w_{1,0}\right). \tag{4.2.14}$$

The term for $w_{2,1}$ follows by symmetry:

$$w_{2,1}=\frac{1}{\nu_2-1}\left(w_{1,0}-w_{2,0}\right). \tag{4.2.15}$$

In summary, we find that w_1 and w_2 up to a first-order correction are given by

$$w_1 = -\frac{1-\nu_1(\mu_1\rho_1)}{e^{-\mu_1}\alpha_1^2(1-e^{-\mu_1})} + (1-p)\frac{1}{\nu_1-1}(w_{2,0}-w_{1,0}), \tag{4.2.16}$$

$$w_2 = -\frac{1-\nu_2(\mu_2\rho_2)}{e^{-\mu_2}\alpha_2^2(1-e^{-\mu_2})} + (1-p)\frac{1}{\nu_2-1}(w_{1,0}-w_{2,0}). \tag{4.2.17}$$

We note that $w_{1,1} > 0$ precisely when $w_{2,1} < 0$. Thus, to benefit one consumer population, the other consumer population is harmed.

Dispersal is beneficial to consumers when $W \equiv w_{1,1} + w_{2,1} > 0$. We find

$$W = \left(\frac{\nu_1-\nu_2}{(\nu_1-1)(\nu_2-1)}\right)(w_{2,0}-w_{1,0})\,. \tag{4.2.18}$$

We note that the net effect W is positive if both $\nu_1 > \nu_2$ and $w_{2,0} > w_{1,0}$ or if $\nu_1 < \nu_2$ and $w_{2,0} < w_{1,0}$.

We can perform the same asymptotic analysis with the resource, since the resource is a function of the consumer density $v_i = G_i(w_i)$; see Equation (3.5.4). We write again $\epsilon = 1-p$. We expand v_i as a power series $v_i = v_{i,0} + \epsilon v_{i,1} + \cdots$. Then

$$v_i = G_i(w_{i,0} + \epsilon w_{i,1} + \cdots). \tag{4.2.19}$$

By comparing the expressions

$$v_{i,0} + \epsilon v_{i,1} + \cdots = G_i(w_{i,0}) + G_i'(w_{i,0})\epsilon w_{i,1} + \cdots\,, \tag{4.2.20}$$

we find that

$$v_1 = G'(w_{1,0})w_{1,1}. \tag{4.2.21}$$

We can express $G_i'(w_i)$ using the functions σ_i and β_i as

$$G_i'(w_i) = \frac{-\frac{\alpha_i}{\mu_i}(1-e^{-\mu_i})\sigma_i(1)\beta_i(1) + \frac{\alpha_i}{\mu_i}[\sigma_i(1)-1]\int_0^1(1-e^{-\mu_i\tau})\sigma_i(\tau)d\tau}{\rho_i[\beta_i(1)]^2}. \tag{4.2.22}$$

Dispersal is beneficial to the resources when $V \equiv v_{1,1} + v_{2,1} > 0$.

Figure 4.2 shows the benefit of dispersal as a function of parameters μ_1 and μ_2. Blue indicates that dispersal is predicted to be beneficial by asymptotic approximation as $w_{1,1} + w_{2,1} > 0$. Red indicates predicted detriment, where $w_{1,1} + w_{2,1} < 0$. Overlaid on the same plot are simulation results, wherein the summed density of consumers is compared with and without small dispersal. To create the simulations to calculate consumer dispersal benefit, the maps in equations (2.3.19)-(2.3.22) are iterated for 2000 years. The final densities are collected for the simulation with $\epsilon = 0$ or $p = 1$ (no dispersal) and with $\epsilon = 0.01$ or $p = 0.99$ (small dispersal). The sign of W is calculated for each grid point. Then the simulation results are compared to the asymptotic results. Agreement between methods is shown when dots are only in blue regions and crosses are only in red regions. We note that in our figures,

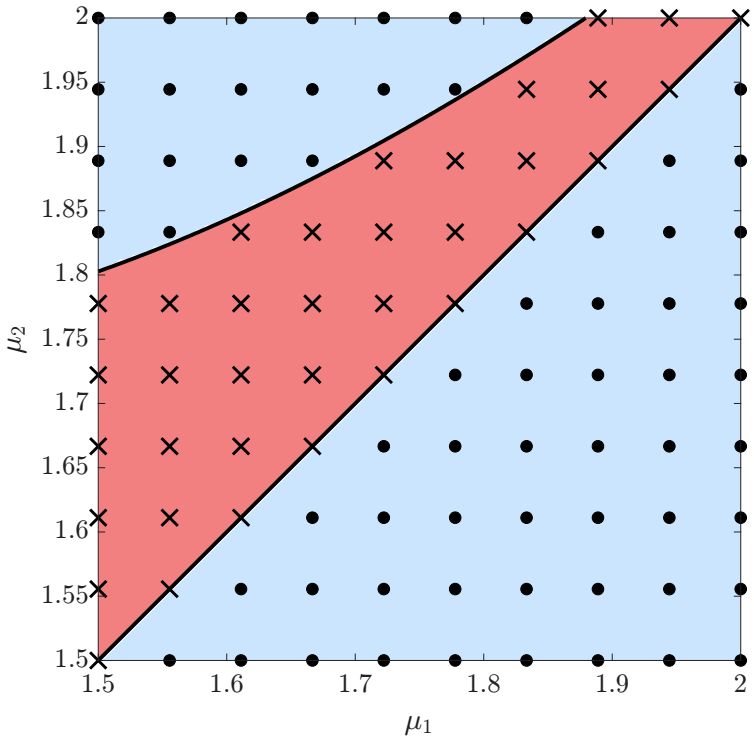

Figure 4.2: Comparison of asymptotic results (blue/red) with numerical simulations (dots/crosses). Blue and dots represent a benefit. Red or cross markings indicate a detriment. Fixed parameters are $\rho_1 = 22, \rho_2 = 26$, $\alpha_1 = \alpha_2 = 10$, and $\epsilon = 0.01$ or $p = 0.99$.

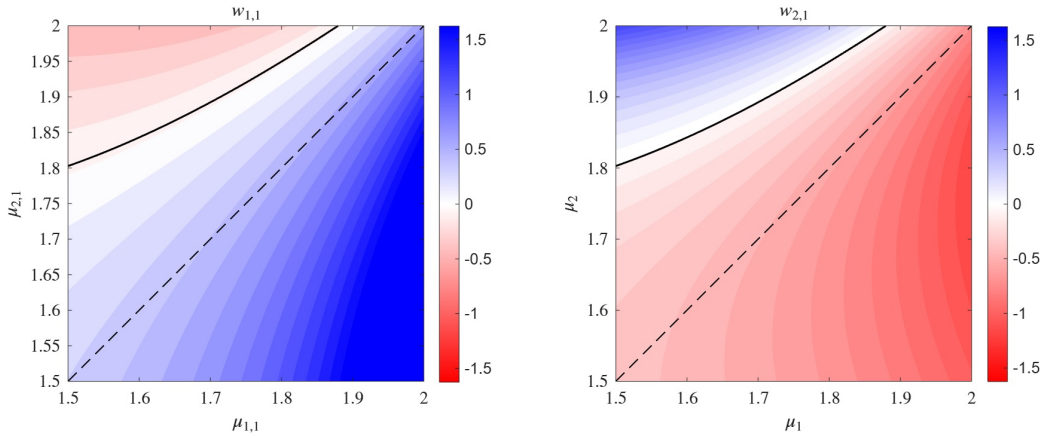

Figure 4.3: Results of the plotting the sign of the components of W. Left plot: $w_{1,1}$. Right plot: $w_{2,1}$. Blue represents a benefit, while red indicates a detriment. Fixed parameters are as in Figure 4.2.

simulations agree with asymptotic predictions. We investigated a large variety of parameters, and all showed good agreement between simulation and asymptotics. We choose to display a case of parameter values that lead to an interesting and biologically relevant pattern in Figure 4.2.

In Figure 4.3, we perform the same analysis but instead split the sum W into its components $w_{1,1}$ and $w_{2,1}$. Red indicates that dispersal is detrimental, $w_{i,1} < 0$, and blue indicates that dispersal is beneficial, $w_{i,1} > 0$. The black lines indicate when dispersal has no effects. We note that, as expected, the plots have opposite colours in each of the regions.

In Figure 4.4, we show a region where there is only detriment (red) of consumer dispersal on the resource density according to the sign of V. The plot is the same style and for the same parameters as Figure 4.2. While for this region of parameter space, consumer dispersal is only detrimental to resource density, this is not always the case. In Figure 4.5 we show one region of parameter space where the resource benefits from consumer dispersal.

We interpret the results of this section as follows. The equilibrium solution found in the Pachepsky model is recovered in our model to zeroth-order, as expected; see equation (3.1.3). We note that in this section, dispersal is symmetric and small, thus the probability of remaining on a patch is large. At first order, the correction term, we find that W has two components. The first is the difference in consumer population without dispersal: $w_{2,0} - w_{1,0}$. This factor is zero if the patches are identical with respect to the resources, when $\nu_1 = \nu_2$. This zero contour is represented by the dashed diagonal line in Figures 4.2 and 4.3. It represents dispersal having no effect on population density in either patch. The second component is the difference in the populations without dispersal. Thus, when $w_{1,0} = w_{2,0}$, we find the curved solid line in Figures 4.2 and 4.3. This line represents a transition between dispersal benefit and detriment.

We note that if $w_{1,1} > 0$ then $w_{2,1} < 0$, and vice-versa. So the benefit of dispersal is never

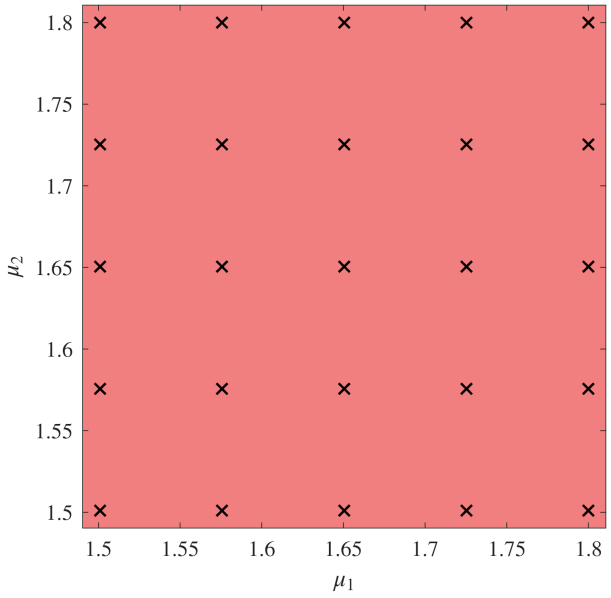

Figure 4.4: Comparison of asymptotic results (red) with numerical simulations (crosses) for the resource. Fixed parameters are $\rho_1 = 22, \rho_2 = 26$, $\alpha_1 = \alpha_2 = 10$. The growth parameters are $\nu_i > 1$.

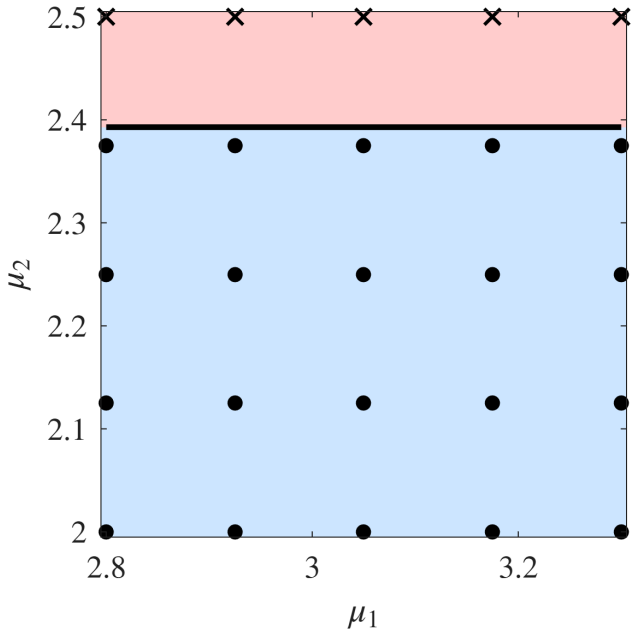

Figure 4.5: Comparison of asymptotic results (red/blue) with numerical simulations (crosses/dots) for the resource. Fixed parameters are $\rho_1 = 20, \rho_2 = 26$, $\alpha_1 = \alpha_2 = 10$. The growth parameters are $\nu_i > 1$. The solid line represents when the parameters are symmetric, so no benefit or detriment occurs.

more than $\max\{w_{1,1}, w_{2,1}\}$. Thus, the correction terms distribute the effects of dispersal and induce a net directional flow. Figure 4.3 helps us determine what compensation occurs to achieve a net positive result. In the region plotted, patch one compensates for patch two when the death rate of consumers on patch one is lower than on patch two. When the death rate is higher on patch one, the consumer population on patch two does not compensate enough, and small dispersal is detrimental. For the resource, we find that small dispersal is often detrimental to the resource. Figure 4.4 shows one case where all parameter space is detrimental, while the same parameter space has both beneficial and detrimental regions for the consumers. We calculated the resource benefit for several parameter regimes and found that the resource density was consistently harmed by small dispersal. We now look at the full range of dispersal to determine if dispersal is always detrimental for the resource, and what patterns can emerge for the consumer.

4.3 H-Index

For simplicity, we assume again that the dispersal probability is symmetric. We define $\delta = 1-p$ as the dispersal, v_i as the resource density and w_i as the consumer density at steady state. We denote by H_w and H_v the consumer and resource benefit-index, respectively. They are defined as:

$$H_v(\delta) \equiv v_1(\delta) + v_2(\delta) - (v_1(0) + v_2(0)), \tag{4.3.1}$$
$$H_w(\delta) \equiv w_1(\delta) + w_2(\delta) - (w_1(0) + w_2(0)). \tag{4.3.2}$$

If no confusion can arise, we simply refer to both as H-index.

We do not have an explicit expression for the coexistence equilibrium, so we cannot determine an analytic expression for $H(\delta)$. We plot $H(\delta)$ for a range of dispersal probabilities and determine patterns of detriment and benefit from the sign of $H(\delta)$. These response scenarios are compared with those from Grumbach et al. [20]. As our model can have more than one positive steady state, we consider only parameters within the range that provide stable, unique equilibria.

In Figure 4.6, we find four basic response scenarios, along with the trivial response scenario $H = 0$ and an extinction-response scenario. In plot (a), we find the *monotonically detrimental* case for the consumer population. In our model, we find that monotonic detriment occurs when the death rate is low on both patches, and the patch with the smaller death rate has the lowest resource growth rate. We note that the lowest H-index value is -0.142.

The extinction state is reached in plot (b), where the patch with the higher death rate also has the lowest resource growth rate, so dispersing between these patches at high probabilities is strongly detrimental to the population density. The largest valid H-index is -2.2, which is a much stronger effect than in plot (a). In plot (b), the population reaches extinction when the H curve is horizontal and at an approximate density of -2.22, which is simply the density of consumers without dispersal.

Table 4.1: Parameter values used for Figure 4.6.

Plot	**Parameters**					
	ρ_1	ρ_2	α_1	α_2	μ_1	μ_2
a	22	26	10	10	1.6	1.7
b	22	26	10	10	3	2
c	22	26	10	10	2	1.9
d	20	21	11	11	2	1.9
e	20	21	9	11	2	1.9
f	20	20	10	10	2	2

The corresponding response for the resource in plot (a) shows that low and median dispersal has no benefit, but large dispersal, and thus a large detriment to the consumer population benefits the resource. In plot (b), the consumers are harmed more than in plot (a), so the effect is compounded, and the resources can benefit at a lower dispersal probability. A larger range of consumer dispersal values lead to a higher benefit for the resource.

Plot (c) shows consumer *benefit turned detriment*. This scenario emerges when the consumer death rate is just slightly lower than the monotone detriment case. Thus, small dispersal is beneficial to the consumers experiencing a higher death rate, but too much dispersal leads to consumer detriment. The response of the resource is that in the region where dispersal is beneficial to the consumer, and slightly beyond, the resource is harmed. Once dispersal harms the consumer enough, the resource can benefit again.

Plot (d) shows *unimodal benefit* to the consumer population with resource detriment turned benefit. This case shows small consumer benefit, and where the benefit starts to decrease for the consumer, the resource benefits. This is the one case where the resource and the consumer can both benefit from dispersal. We note that the benefit is extremely small to the resource, and also small to the consumer.

Plot (e) shows *monotone benefit* to the consumer with resource detriment. In this case, as the consumers always benefit, and as the benefit is not marginal, the resource cannot benefit. In this case, the patch with the higher resource growth rate has the higher attack rate and lower death rate of consumers, making one patch better than the other, promoting high values of dispersal. Finally, plot (f) shows the case where consumers and resources are not affected by dispersal. This is expected when parameters are symmetric.

One biological application of this chapter is in the context of native plants. In some systems, the consumer is invasive and feeds on native plants (resource), and this system can be described by a semi-discrete system. For example, the emerald ash borer (*Agrilus planipennis*) feed on native ash trees (specifically *Fraxinus pennsylvanica*) and has highly synchronized emergence under certain weather conditions [31]. By determining when the emerald ash borer benefits from dispersal, we can understand what ecological conditions are favourable for protecting native species using tools to interrupt dispersal, such as tree thinning and barrier zones [11], [37]. Tree thinning increases the distance between stands, manipulating dispersal patterns, whereas barrier zones interrupt human dispersal of infected trees, which interrupts borer dispersal in turn.

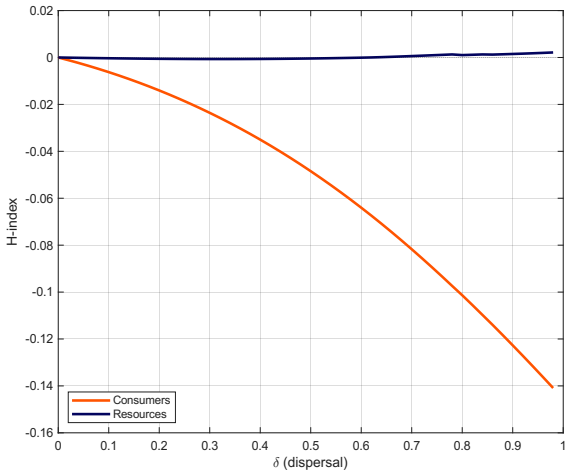

(a) monotone detriment

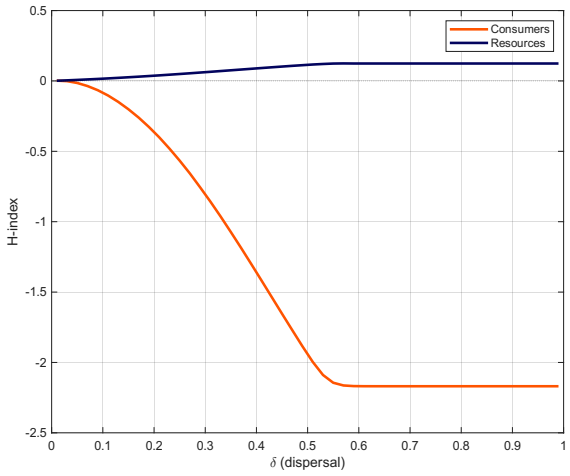

(b) monotone detriment to extinction

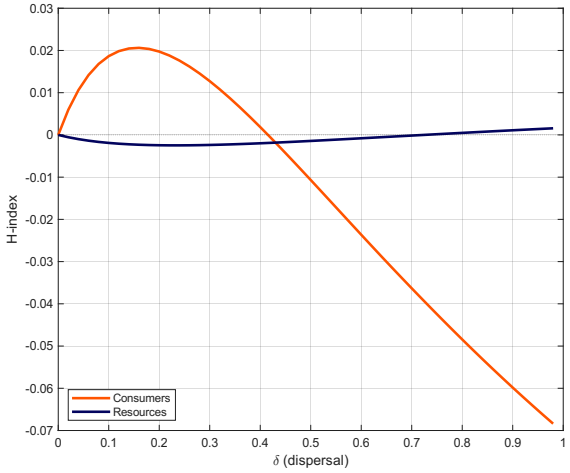

(c) Benefit to detriment

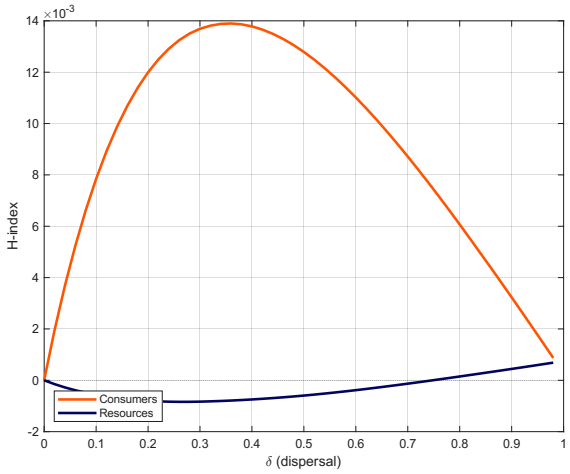

(d) unimodal benefit

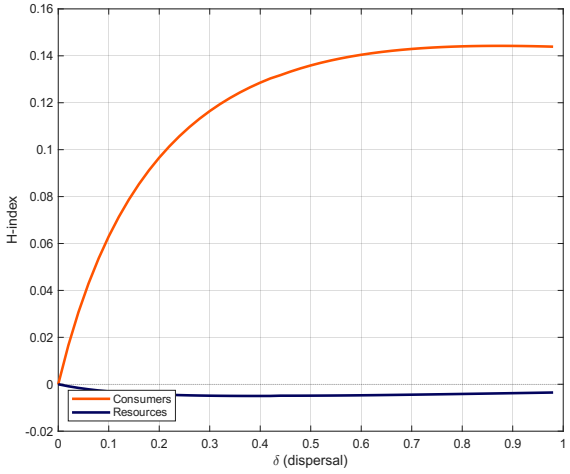

(e) monotone benefit

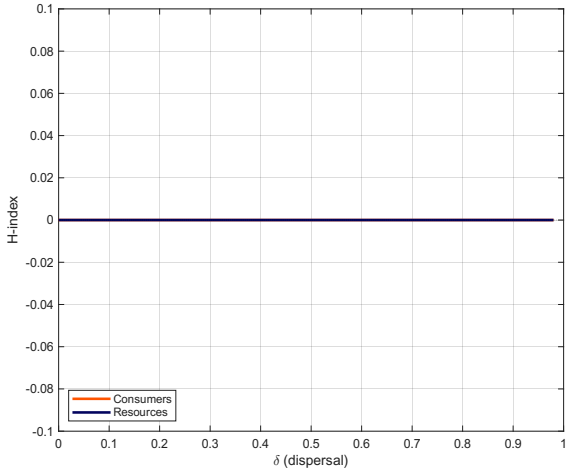

(f) no benefit or detriment

Figure 4.6: H-index for the semi-discrete model. Blue represents the resource and orange represents the consumer. Figure parameters are listed in Table 4.1.

In this chapter, we have explored the effect of dispersal on our two-patch consumer–resource model. We determined that for small dispersal, there can be a net benefit if the population on one patch benefits more than the other patch population is harmed. We then extended the analysis to account for all possible dispersal values and found four distinct response scenarios consistent with literature. In the next chapter, we are interested in the optimal control of the consumer population.

Chapter 5

Optimal Control

In this chapter, we are inspired by the problem of managing the spruce budworm in Canada. We introduce relevant background and methods. Then we formulate an optimal control problem to address aerial spraying of a pesticide over two patches. We study how the optimal control depends on differences in patch quality and movement between patches. We conclude with determining the long-term optimal-control schedule for two adjacent stands with different management strategies.

5.1 Managing Spruce Budworms in Canada

Spruce budworms (SBWs), or *Choristoneura fumiferana*, is the most costly and destructive species affecting Eastern Canadian forests today [32]. If left unmanaged, SBWs consume the needles of white spruce (*Picea glauca*) and balsam fir (*Abies balsamea*), causing vast tree mortality [13]. A popular strategy to manage SBWs is the use of bacillus thuringiensis kurstaki (Bt_k) pesticide. This pesticide can be sprayed aerially over affected forest regions, and acts on the spruce budworm by infecting the gut lining, which induces rapid mortality [39].

Often, two adjacent environments have different management strategies. The Canadian provinces of New Brunswick and Quebec are one example: while forest managers in New Brunswick spray pesticides on a large percentage of its forests and have done so since the most recent outbreak started in 2009, their counterparts in Quebec spray very little because of the much larger landmass and its remoteness. Another example is Gros Morne National Park (NL), which is pesticide-free, while its surrounding areas are actively sprayed against SBWs. A map of the sprayed areas around Gros Morne National Park is shown in Figure 5.1. Similar situations occur for other protected areas and their surroundings and for other forest pest species [16]. Aerial application of pesticides is, of course, costly [19]. It is thus of great importance to find the 'best' ways to apply management options, such as spraying, in situations where only a portion of the area is being managed. In this chapter, we use the theory of optimal control to explore various such strategies.

Figure 5.1: A map of Newfoundland showing a portion of Gros Morne National Park (in green), and the areas sprayed by Btk (in × marks). Taken from gov.nl.ca 2025 Forest Insect Control Program Interactive Map.

5.2 Background on Optimal Control

Optimal control begins with the construction of a difference equation and the choice of control. We denote by $x \in \mathbb{R}^n$ the state variable and by $x_t \in \mathbb{R}^n$ the state variable at time t. We consider a time horizon of T years, so that $t = 0, 1, \ldots, T$. For the purpose of optimal control, it is useful to consider the entire system state over the entire time horizon. For that, we use the vector notation $\vec{x} = [x_0, x_1, \ldots x_T]$ and define the state space $X \in \mathbb{R}^{n\times(T+1)}$. At times, it will become necessary to refer to component i of the state variable x at time t. For that, we write $x_{i,t}$, where the first index always refers to the i-th component in the vector x_t.

Next, we write $u_t \in \mathbb{R}^m$ for the vector of controls at time t and $\vec{u} = [u_0, u_1, \ldots u_{T-1}]$ for the collection of controls over the time horizon. Hence, the control space is $U \in \mathbb{R}^{m\times T}$. Note that since controls are applied between two time steps of the state variable, there is one less component (in time) of the control. Note that the number of controls in each time step does not have to match the number of state variables, as it is not necessarily possible to control each state variable, whereas some state variables could have more than one control.

The dynamics of the system are governed by the difference equation

$$x_{t+1} = f(x_t, u_t, t), \quad t = 0, 1, 2, \ldots, T. \tag{5.2.1}$$

The *cost functional*, also called an *objective function*, defines the quantity that we want to optimize. This function typically includes the 'cost' associated with the control, which we would like to minimize, and the desired system state, which we would like to achieve. The

functional can be written as

$$J(\vec{x}, \vec{u}, T) = \sigma(x_T) + \sum_{t=0}^{T-1} g_t(x_t, u_t, t), \tag{5.2.2}$$

where σ indicates the *payoff term* for the final time and g_t contains the cost and desired system state at time $t = 0, 1, \ldots, T-1$. Once the components of optimal control have been collected, the goal is to find a sequence $(\vec{x}^*, \vec{u}^*)$ that maximizes or minimizes the functional (5.2.2) and satisfies the difference equation (5.2.1). To simplify this complex optimization problem, we use Pontryagin's Maximum Principle.

Pontryagin's Maximum Principle transforms complex optimization over function spaces to point-wise optimization of a Hamiltonian. The Hamiltonian is a function that couples the control to the state equations via some adjoint functions $\lambda_{i,t}$, where $i = 1, \ldots, n$ and $t = 0, \ldots, T$. These adjoint functions are analogous to Lagrange multipliers from multivariable optimization. The Hamiltonian contains the right-hand side of the difference equation, $f(x_t, u_t, t)$, weighted by the adjoints, and the cost function, $g(x_t, u_t, t)$. It is defined as

$$H_t(x_t, u_t, \lambda_{t+1}) = g(x_t, u_t, t) + \lambda_{t+1}^\top f(x_t, u_t, t) = g(x_t, u_t, t) + \sum_{i=1}^{n} \lambda_{i,t+1} f_i(x_t, u_t, t), \tag{5.2.3}$$

where we have used the notation $\lambda_t = [\lambda_{1,t}, \ldots, \lambda_{n,t}]^\top$. Pontryagin's Maximum Principle for discrete systems gives necessary conditions for the existence of an optimal control sequence and optimized state vectors.

Theorem 5.2.1. *Pontryagin's Maximum Principle* [35] Suppose that $(\vec{x}^*, \vec{u}^*)$ is an optimal trajectory-control sequence for the difference equation (5.2.1) with the objective function (5.2.2) for the state variable x and control variable u. Then

1. For $t = 0, 1, \ldots, T-1$, (5.2.3) is satisfied at $(\vec{x}^*, \vec{u}^*)$.
2. For $t = T-1, \ldots, 0$, we have

$$\lambda_{i,t} = \frac{\partial H_t}{\partial x_{i,t}}(x_t^*, u_t^*, \lambda_{t+1}) \tag{5.2.4}$$

   with terminal condition

$$\lambda_T = \frac{\partial \sigma}{\partial x}(x_T^*). \tag{5.2.5}$$

3. For each $t = 0, \ldots, T-1$,

$$\frac{\partial H_t(x^*, u^*, \lambda_{t+1})}{\partial u_{i,t}} = 0. \tag{5.2.6}$$

Pontryagin's Maximum Principle gives three necessary conditions that define an optimal trajectory and optimal controls. The terminal condition $\lambda_T = \sigma'(x^*(T))$ is also called the transversality condition. The payoff function is σ, which is the term that in the objective

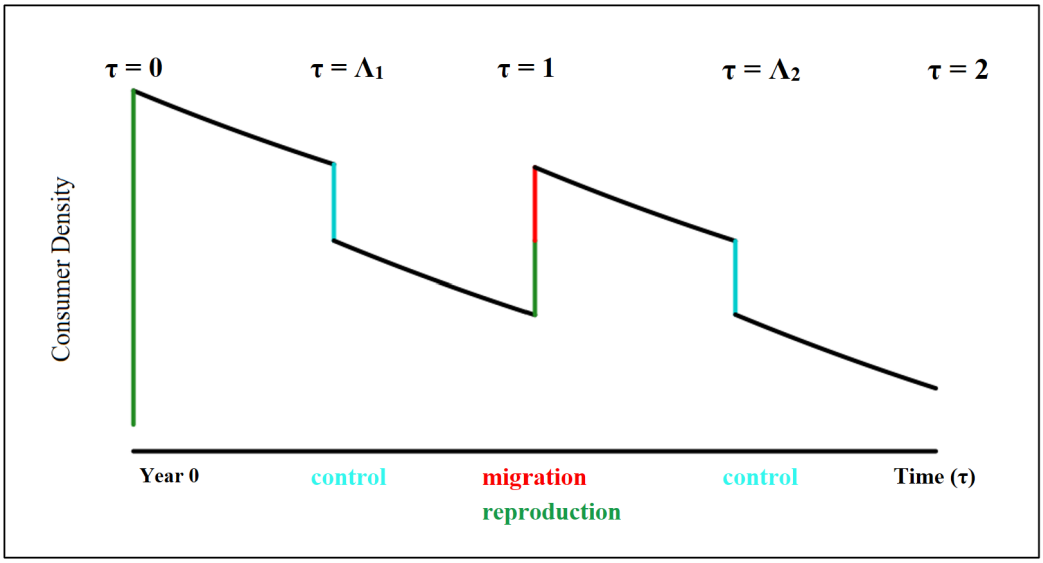

Figure 5.2: Illustration of example dynamics of the extended consumer–resource model including control. Example shown for one patch.

function J dictates what the objective final state of the system should be at time T. The adjoint equation is $\lambda_{i,t} = \frac{\partial H_t}{\partial x_{i,t}}$, which is a backward difference equation. The optimality condition characterizes the optimal control, and is determined by the condition $\frac{\partial H_t}{\partial u_{i,t}} = 0$ at u^*.

We next introduce the Forward Backward Sweep (FBS) algorithm [30]. This algorithm solves the necessary conditions iteratively and outputs the optimal control and the corresponding optimized state within a given tolerance. The FBS algorithm begins with the user choosing an initial guess for the control $\vec{u} \in U$. Next, the user sets an initial condition x_0, and, using $\vec{u}$, solves the stroboscopic maps forward in time. This gives $\vec{x} \in X$. Using this information, one then solves the adjoint difference equation backwards in time for $\vec{\lambda}$ using the transversality condition for the final adjoint value. Then the algorithm checks for convergence: if the difference between the new calculated control and the initial control guess is below some tolerance (δ), the algorithm completes, and outputs the optimal control schedule and the dynamics associated with it. If the difference is larger than the tolerance, the algorithm chooses an average between the initial guess and the new calculated control as the new initial guess and repeats. One typically limits the maximum number of iteration steps in order to prevent the algorithm from running forever. The pseudocode for FBS is given in Algorithm 1.

5.3 Formulating the Model with Control

We begin with the model in Chapter 2 and include a control measure of one pesticide spraying per year. We incorporate the effects of spraying as an additional source of mortality at the time of spraying. Since spraying happens over a very short period of time and since consumer

Algorithm 1 Forward Backward Sweep

procedure FBS(params,T)

set δ and $I_{\max}$ ▷ initialize threshold and max iterations

$\vec{u} = [u_0, u_1, u_2, ..., u_{T-1}]$ ▷ make an initial guess for control

$x_0 \in \mathbb{R}^n$ ▷ set initial conditions

$\lambda_T \in \mathbb{R}^n$ ▷ set final adjoint conditions

while not converged and iterations $< I_{\max}$ **do**

1. Apply Φ to x_0 for T steps ▷ solve state equation forward
2. Solve $\lambda_{i,t} = \frac{\partial H_t(x_t, u_t, \lambda_{t+1})}{\partial x_{i,t}}$ for $i = 1, \dots n$ and $t = T-1, \dots 0$ from λ_T

▷ solve adjoint equation backward

3. Find $\vec{u}^*$ such that $\frac{\partial H_t(x_t^*, u_t^*, \lambda_{t+1})}{\partial u_{i,t}} = 0$ for all $t = 0, \dots T$, and $i = 1...n$

▷ calculate new control and optimal state

if $|\vec{u}^* - \vec{u}| < \delta$ **then**

return $\vec{x}^* = \vec{x}$, $\vec{u}^*$

else

$\vec{u}_{\text{new}} = 0.5(\vec{u}^* - \vec{u})$

end if

end while

return *did not converge*

end procedure

death is very fast compared to the length of the season, we model control as an impulse. We denote the time of spraying within year t by $\Lambda_t \in (0,1)$. The time line in Figure 5.2 illustrates the consumer density on one patch over two years. We work directly with the nondimensionalized model, where the densities of resource and consumer on patch i at the beginning of year t are denoted as $v_{i,t}$ and $w_{i,t}$, respectively.

In year t, the equations for $s \in [0, \Lambda_t)$ and $s \in [\Lambda_t, 1]$ are given by equations (2.3.8)–(2.3.10), namely for patch number $i = 1, 2$. The initial conditions in year t at $s = 0$ are $f_i(0) = v_{i,t}$, $c_i(0) = w_{i,t}$, and $b_i(0) = 0$. At time $s = \Lambda_t$, we apply the control, which removes a fraction $u_{i,t}$ of consumers on patch i in year t but leaves the resource and the energy stored per consumer unchanged. Hence, the initial condition for the above equations in the interval $s \in [\Lambda_t, 1]$ are

$$f_i(\Lambda_t^+) = f_i(\Lambda_t^-), \tag{5.3.1}$$
$$c_i(\Lambda_t^+) = (1 - u_{i,k})c_i(\Lambda_t^+), \tag{5.3.2}$$
$$b_i(\Lambda_t^+) = b_i(\Lambda_t^-). \tag{5.3.3}$$

Migration and reproduction at the end of a year are unaffected by the control intervention. Hence, the corresponding maps remain the same as (2.3.12)–(2.3.15). As already discussed in Chapter 2, the functions on the right-hand side depend on t via the initial conditions of the differential equations that they satisfy. We make this dependence on initial conditions explicit and use the resulting notation to write the stroboscopic map from one year to the next in a compact form.

We denote by x_t the vector of densities of all state variables on both patches at the beginning of year t; i.e.,

$$x_t = \left[v_{1,t}, w_{1,t}, 0, v_{2,t}, w_{2,t}, 0\right]^\top \in \mathbb{R}^6. \tag{5.3.4}$$

Then the initial conditions of (2.3.8)–(2.3.10) at $s = 0$ can be written as

$$x_t(0) = \left[f_1(0), c_1(0), b_1(0), f_2(0), c_2(0), b_2(0)\right]^\top.$$

We denote the solution operator of system (2.3.8)–(2.3.10) in $\mathbb{R}^6$ at time s by $\phi_1(s) = \phi_1(s; x)$ (where the latter argument indicates the initial condition). Thanks to the explicit solution that we derived in Section 2.3 of system (2.3.8)–(2.3.10), we have an explicit representation

of ϕ_1 as

$$\phi_1(s;x) = \begin{bmatrix} v_1 \frac{e^{\rho_1 s - \frac{\alpha_1 w_1}{\mu_1}(1-e^{-\mu_1 s})}}{\rho_1 v_1 \int_0^s e^{\rho_1 \tau - \frac{\alpha_1 w_1}{\mu_1}(1-e^{-\mu_1 \tau})} d\tau + 1} \\ w_1 e^{-\mu_1 s} \\ \alpha_1 v_1 \int_0^s \frac{e^{\rho_1 s - \frac{\alpha_1 w_1}{\mu_1}(1-e^{-\mu_1 s})}}{\rho_1 v_1 \int_0^s e^{\rho_1 \tau - \frac{\alpha_1 w_1}{\mu_1}(1-e^{-\mu_1 \tau})} d\tau + 1} \\ v_2 \frac{e^{\rho_2 s - \frac{\alpha_2 w_2}{\mu_2}(1-e^{-\mu_2 s})}}{\rho_2 v_2 \int_0^s e^{\rho_2 \tau - \frac{\alpha_2 w_2}{\mu_2}(1-e^{-\mu_2 \tau})} d\tau + 1} \\ w_2 e^{-\mu_2 s} \\ \alpha_2 v_2 \int_0^s \frac{e^{\rho_2 s - \frac{\alpha_2 w_2}{\mu_2}(1-e^{-\mu_2 s})}}{\rho_2 v_2 \int_0^s e^{\rho_2 \tau - \frac{\alpha_2 w_2}{\mu_2}(1-e^{-\mu_2 \tau})} d\tau + 1} \end{bmatrix}. \tag{5.3.5}$$

Hence, the system state in year t immediately before the control measure is given by $\phi_1(\Lambda_t^-; x_t)$.

Next, we introduce the matrix

$$\phi_2 = \begin{bmatrix} 1 & 0 & 0 & 0 & 0 & 0 \\ 0 & 1-u_{1,t} & 0 & 0 & 0 & 0 \\ 0 & 0 & 1 & 0 & 0 & 0 \\ 0 & 0 & 0 & 1 & 0 & 0 \\ 0 & 0 & 0 & 0 & 1-u_{2,t} & 0 \\ 0 & 0 & 0 & 0 & 0 & 1 \end{bmatrix}, \tag{5.3.6}$$

which expresses the effect of the control as stated in equations (5.3.1)–(5.3.3). Then we can write the initial conditions of (2.3.8)–(2.3.10) at $s = \Lambda_t$ as

$$\begin{bmatrix} f_1(\Lambda_t) \\ c_1(\Lambda_t) \\ b_1(\Lambda_t) \\ f_2(\Lambda_t) \\ c_2(\Lambda_t) \\ b_2(\Lambda_t) \end{bmatrix} = \hat{x}_t \equiv \phi_2 \phi_1(\Lambda_t^-; x_t) = \phi_2 \begin{bmatrix} f_1(\Lambda_t^-) \\ c_1(\Lambda_t^-) \\ b_1(\Lambda_t^-) \\ f_2(\Lambda_t^-) \\ c_2(\Lambda_t^-) \\ b_2(\Lambda_t^-) \end{bmatrix} = \begin{bmatrix} f_1(\Lambda_t^-) \\ (1-u_{1,t})c_1(\Lambda_t^-) \\ b_1(\Lambda_t^-) \\ f_2(\Lambda_t^-) \\ (1-u_{2,t})c_2(\Lambda_t^-) \\ b_2(\Lambda_t^-) \end{bmatrix}.$$

Since the differential equations for $s \in [0, \Lambda_t)$ are the same as for $s \in [\Lambda_t, 1^-)$, the solutions are again given by the solution operator $\phi_1(\cdot)$ as above, but with initial conditions $\hat{x}_t$ and for time $s = 1 - \Lambda_t$. Hence, we can write the density of all state variables at the end of year t, before reproduction and migration, as

$$\begin{bmatrix} f_1(1^-) \\ c_1(1^-) \\ b_1(1^-) \\ f_2(1^-) \\ c_2(1^-) \\ b_2(1^-) \end{bmatrix} = \phi_1(1-\Lambda_t^-; \hat{x}_t) = \phi_1(1-\Lambda_t^-; \phi_2\phi_1(\lambda_t^-; x_t)). \tag{5.3.7}$$

Reproduction is again a nonlinear operator. We have $\phi_3 \colon \mathbb{R}^6 \to \mathbb{R}^6$, with

$$\phi_3 : \begin{bmatrix} f_1 \\ c_1 \\ b_1 \\ f_2 \\ c_2 \\ b_2 \end{bmatrix} \mapsto \begin{bmatrix} f_1 \\ (1+b_1)c_1 \\ 0 \\ f_2 \\ (1+b_2)c_2 \\ 0 \end{bmatrix}. \tag{5.3.8}$$

Finally, migration between the two patches is a linear process, which is described by the matrix

$$\phi_4 = \begin{bmatrix} 1 & 0 & 0 & 0 & 0 & 0 \\ 0 & p_1 & 0 & 0 & 1-p_2 & 0 \\ 0 & 0 & 1 & 0 & 0 & 0 \\ 0 & 0 & 0 & 1 & 0 & 0 \\ 0 & 1-p_1 & 0 & 0 & p_2 & 0 \\ 0 & 0 & 0 & 0 & 0 & 1 \end{bmatrix}. \tag{5.3.9}$$

With this notation, we can write the year-to-year map of our system with control as

$$x_{t+1} = \Phi(x_t; \Lambda_t, u_{1,t}, u_{2,t}) = \phi_4\phi_3(\phi_1(1-\Lambda_t^-; \phi_2\phi_1(\Lambda_t^-; x_t))), \tag{5.3.10}$$

where, as mentioned above, Λ_t is the time of control in year t and $u_{i,t}$ is the control intensity on patch i in year t.

5.4 A Simple Example on One Patch

In this section, we work through a simple example with one patch before presenting more complicated cases over two patches. In the case presented, we are interested in controlling the population of consumers in the one patch after ten years, while keeping the cost minimal. For simplicity and in line with many other applications (e.g., [14, 17, 25]), we choose a quadratic cost function for the control. We denote resources by v_t, consumers by w_t, and biomass by b_t. We write the difference equation for this system as

$$x_{t+1} = \begin{bmatrix} v_{t+1} \\ w_{t+1} \\ b_{t+1} \end{bmatrix} = \Phi(x_t) = \begin{bmatrix} \Phi_v(x_t) \\ \Phi_w(x_t) \\ \Phi_b(x_t) \end{bmatrix} \tag{5.4.1}$$

and the cost functional as

$$J(u_t) = \sum_{t=0}^{T-1} u_t^2 + w_T. \tag{5.4.2}$$

This cost functional represents the quadratic cost of spraying the pesticide during the ten years and the density of consumers at the final time T, which will be minimized. We note that the control has one less component than the state, as the control is applied between the

years. The timing of the impulsive control in year t is $\Lambda_t = \Lambda$, which, for this example, we set as $\Lambda = 0.5$. The resulting Hamiltonian for year t does not contain the payoff term w_T:

$$H_t = u_t^2 + \lambda_{v,t+1}\Phi_v + \lambda_{w,t+1}\Phi_w. \tag{5.4.3}$$

The adjoint equations for this optimal-control problem have functions that are all evaluated at (v_t^*, w_t^*, u_t^*, t). The equations are

$$\lambda_{1,t} = \frac{\partial H_t}{\partial v_t} = \frac{\partial g}{\partial v_t} + \frac{\partial \Phi_v}{\partial v_t}\lambda_{t+1} = \frac{\partial \Phi_v}{\partial v_t}\lambda_{t+1}, \tag{5.4.4}$$

$$\lambda_{2,t} = \frac{\partial H_t}{\partial w_t} = \frac{\partial g}{\partial w_t} + \frac{\partial \Phi_w}{\partial w_t}\lambda_{t+1} = \frac{\partial \Phi_w}{\partial w_t}\lambda_{t+1}. \tag{5.4.5}$$

With final time T, the components of the transversality condition are

$$\lambda_{w,T} = 1, \tag{5.4.6}$$

$$\lambda_{v,T} = 0. \tag{5.4.7}$$

Finally, the optimality condition is

$$\frac{\partial H_t}{\partial u_t} = 0 \text{ at } u_t^*. \tag{5.4.8}$$

To find the optimal control and optimal state, we apply the FBS algorithm. We note that, since this is a constrained optimal-control problem, with $0 \leq u_t \leq 0.9$, the absolute minimum may lie on the boundary. We thus use the argmin instead of the zero derivative condition in Theorem 5.2.1.

We plot the results of the FBS sweep algorithm in Figure 5.3. The optimal control is on the right, and the corresponding dynamics of the populations are on the left. The controls for this example show no or very-low-intensity control applied in the first seven years before an increase in intensity in year eight. Finally, in year nine, a large control is applied to reduce the population in year ten. The sudden decrease of the consumer population as a result of the final control can be seen in the left plot of Figure 5.3, with the population of consumers (in green) dropping to less than half the stable density reached without control. This set of controls is expected, as the consumer density was only minimized in the final year.

5.5 Two-Patch Control

The aim of this section is to determine the optimal control of a consumer population on two non-identical patches with asymmetric dispersal. We do so by building up the complexity of the model with four cases. Each case will allow us to better analyze the most complex case. Figure 5.4 illustrates the four cases for which we will find the optimal control. We begin by finding the control that minimizes consumer density in identical patches with symmetric migration, plot (a). We then introduce two sources of heterogeneity: asymmetric migration,

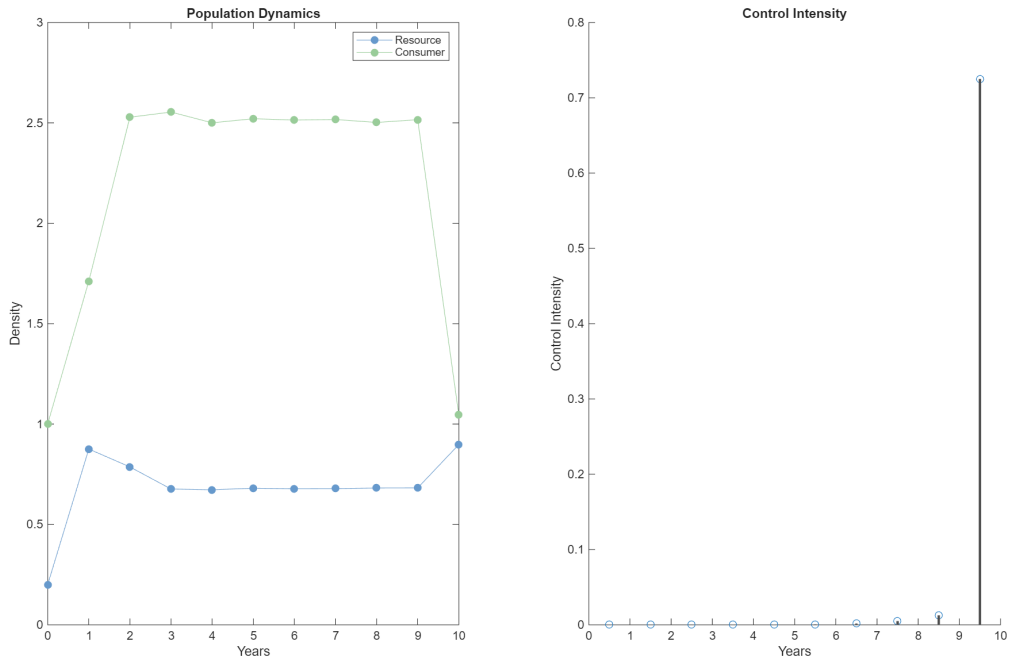

Figure 5.3: Left plot: Density of consumer (green) and resource (blue) population on one patch over 10 years. Right plot: optimal control intensity for the simple example.

and non-identical patches. In case two, we investigate asymmetric migration but identical patches, plot (b). In case three, we investigate symmetric migration but non-identical patches, plot (c). Finally, in case four, we investigate both non-identical patches and asymmetric migration, plot (d). We end this section by addressing the effects of heterogeneous landscapes.

5.5.1 Set-up

The set-up of each case is similar. We give a general set-up for all cases here, and give specifics and results about each case in Subsection 5.5.2.

For all simulations, we have chosen a finite time horizon of ten years. For the objective function, we have chosen to minimize the square of the costs and the density of consumers. The functions $\Phi_{i,v}$ and $\Phi_{i,w}$ represent the map associated with the resources and the consumers on patch i, respectively, as in (5.3.10). For control variables $u_{1,t}$ and $u_{2,t}$ we chose our objective function to be the following:

$$J(u) = \sum_{t=0}^{T-1} u_{1,t}^2 + u_{2,t}^2 + w_{1,t}^2 + w_{2,t}^2. \tag{5.5.1}$$

Then the Hamiltonian for year t becomes:

$$H_t = u_{1,t}^2 + u_{2,t}^2 + w_{1,t}^2 + w_{2,t}^2 + \lambda_{v_1,t+1}\Phi_{1,v} + \lambda_{v_2,t+1}\Phi_{2,v} + \lambda_{w_1,t+1}\Phi_{1,w} + \lambda_{w_2,t+1}\Phi_{2,w}. \tag{5.5.2}$$

The necessary conditions for this case become, for $i = 1, 2$:

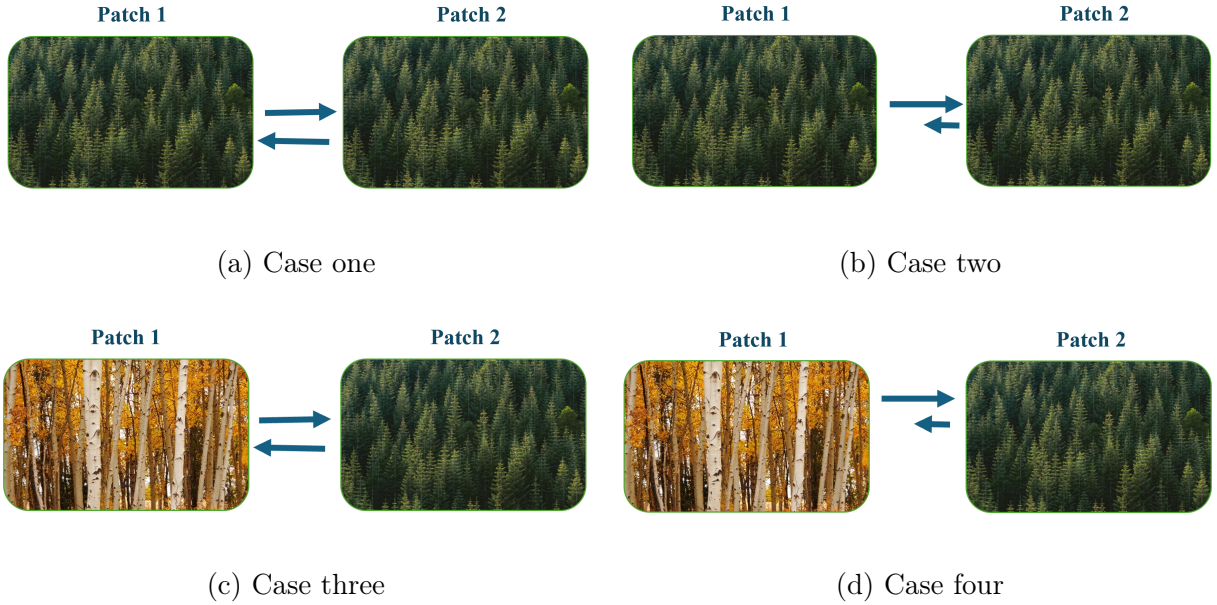

(a) Case one (b) Case two

(c) Case three (d) Case four

Figure 5.4: Illustration of the set-up of each case. Green coniferous forests represent the better-quality patches, whereas birch forests represent the lower-quality patches for our species. Arrows indicate the direction and intensity of dispersal.

$$\lambda_{w_i,t} = \frac{\partial \Phi_{i,w}}{\partial w_i} + 2w_{i,t}, \tag{5.5.3}$$

$$\lambda_{v_i,t} = \frac{\partial \Phi_{i,v}}{\partial v_i} + 2w_{i,t}. \tag{5.5.4}$$

Then as there is no payoff term, the transversality conditions become:

$$\lambda_{w_i,T} = 0, \tag{5.5.5}$$

$$\lambda_{v_i,T} = 0. \tag{5.5.6}$$

The optimality condition is:

$$\frac{\partial H_t}{\partial u_t} = 0 \text{ at } u_t^*. \tag{5.5.7}$$

We note that, for all the cases, we bound the controls such that $0 \leq u \leq 0.9$. We chose 0.9 as an upper bound of control to represent the biological fact that SBW control is not absolute, and perfect eradication is practically impossible. In each case, we apply the FBS algorithm 1 with slight modification in our model parameters. The algorithm returns the optimal-control-intensity schedule and the corresponding optimal consumer and resource density over the T-year time horizon.

5.5.2 Results

In this subsection, we give specifications and the results of the four cases and use the findings to better understand the biologically motivated control of SBWs in Canadian forests. In all cases, we choose the initial conditions to be $v_1 = v_2 = 0.7$, $w_1 = w_2 = 2.5$, which is close to the steady-state densities of resources and consumers without dispersal or control.

In case one, we minimize consumers in each year across two identical patches with symmetric migration. To represent identical patches, all of the parameters have been set equal across patches. Thus, the resource growth rate is $\rho_1 = \rho_2 = 20$, the attack rate is $\alpha_1 = \alpha_2 = 10$, and the death rate is $\mu_1 = \mu_2 = 1.5$. This symmetry can be interpreted as equal patch quality, which is represented by the forest type in Figure 5.4. We let $p_1 = p_2 = 0.5$ to represent symmetric migration, where $p = 0.5$ is chosen for simplicity. The results of this experiment are described in the top two rows of Figure 5.5. The optimal control used to minimize consumer density is symmetric, as is expected with symmetric migration, patch quality and also cost. The control is applied with maximal intensity ($p = 0.9$) for three years before reducing to a low of approximately 25% control reduction between years three and four. Control is slowly decreasing every year thereafter. The control intensity drops because around year three, the consumer is almost at extinction. We note that the consumer population has a density much lower than that without control, as expected. We note also that the resource population has a density slightly higher than without control, but generally remains constant. This dynamic will serve as the baseline for cases two, three, and four, which include some heterogeneity.

In case two, we minimize consumers in each year across two identical patches, but include asymmetric dispersal. All parameters are set equal, $\rho_1 = \rho_2 = 20$, $\alpha_1 = \alpha_2 = 10$, and $\mu_1 = \mu_2 = 1.5$, but we set $p_1 = 0.15$ and $p_2 = 0.65$ to represent the asymmetry. The results of this experiment are shown in the bottom two rows of Figure 5.5. The consumer population does much worse on patch one than on patch two, even though the patch quality is the same. Since the consumers leave patch one with a much higher probability than remaining there, the consumer population is already lower. After the first strong application of controls, fewer controls are necessary to reach a low density of consumers on patch one. In contrast, more individuals reside and stay on patch two, so more control is needed. Thus, control can be reduced if migration acts as a controlling mechanism itself.

In case three, we minimize consumers in each year across two different patch qualities with symmetric migration. In the higher-quality patch, patch two, the attack rate is higher, $\alpha_1 = 10, \alpha_2 = 12$, the resource growth rate is higher, $\rho_1 = 20, \rho_2 = 22$, and the death rate is lower, $\mu_1 = 1.5, \mu_2 = 1$. The results are displayed in the top two rows of Figure 5.6. We note that, unlike case two, which includes asymmetric dispersal, the dynamics on both patches are quantitatively similar. The control is applied more heavily to the better-quality patch, after the initial full intensity four-year control schedule. Thus, a better quality patch requires more control than a lower quality patch if dispersal is symmetric.

We now reach our most complex model, that of asymmetric migration in a heterogeneous landscape, which we model in case four. This includes asymmetric patch quality, with patch two as the better patch. We chose a higher resource growth rate in patch two, $\rho_1 = 20, \rho_2 =$

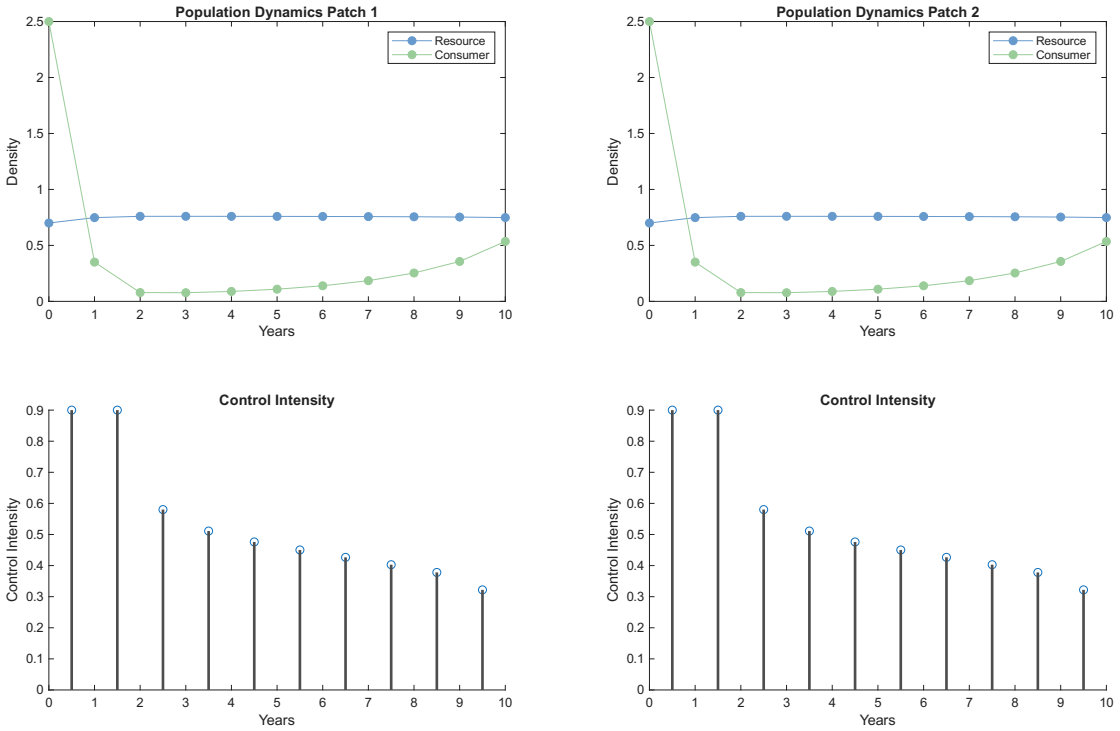

(a) Case one

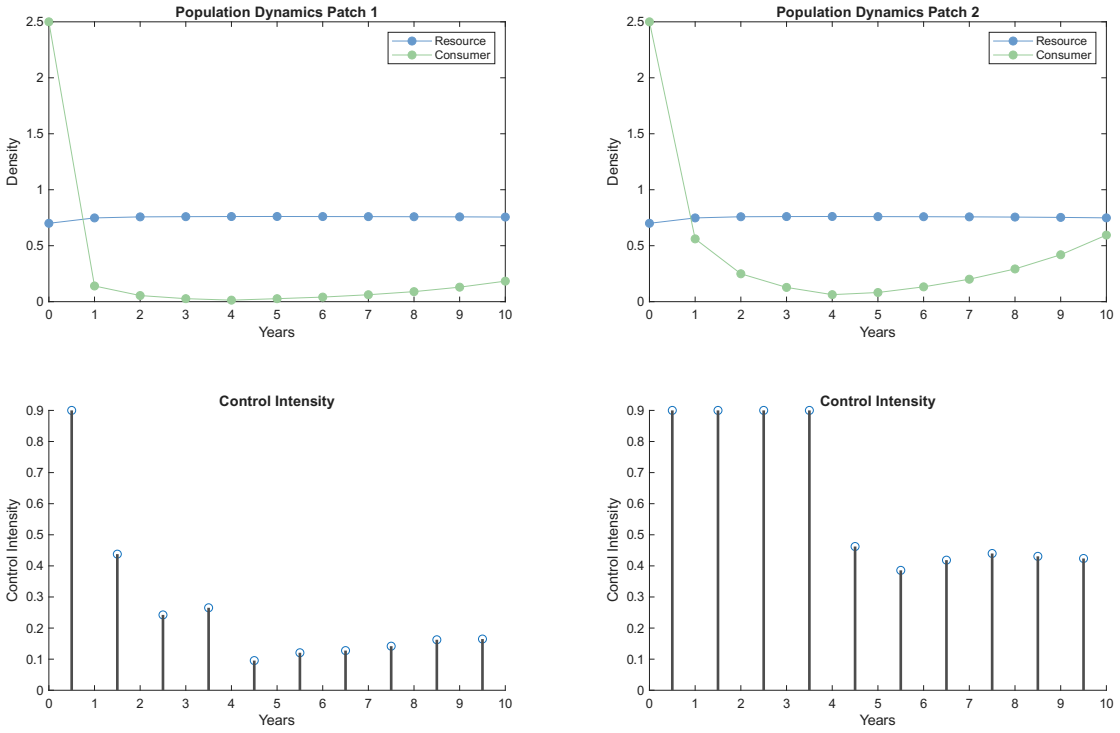

(b) Case two

Figure 5.5: Rows one and three: Dynamics of the symmetric model with symmetric and asymmetric migration at the start of each year for consumers (green) and resources (blue) under optimal control. Rows two and four: corresponding control-intensity schedule.

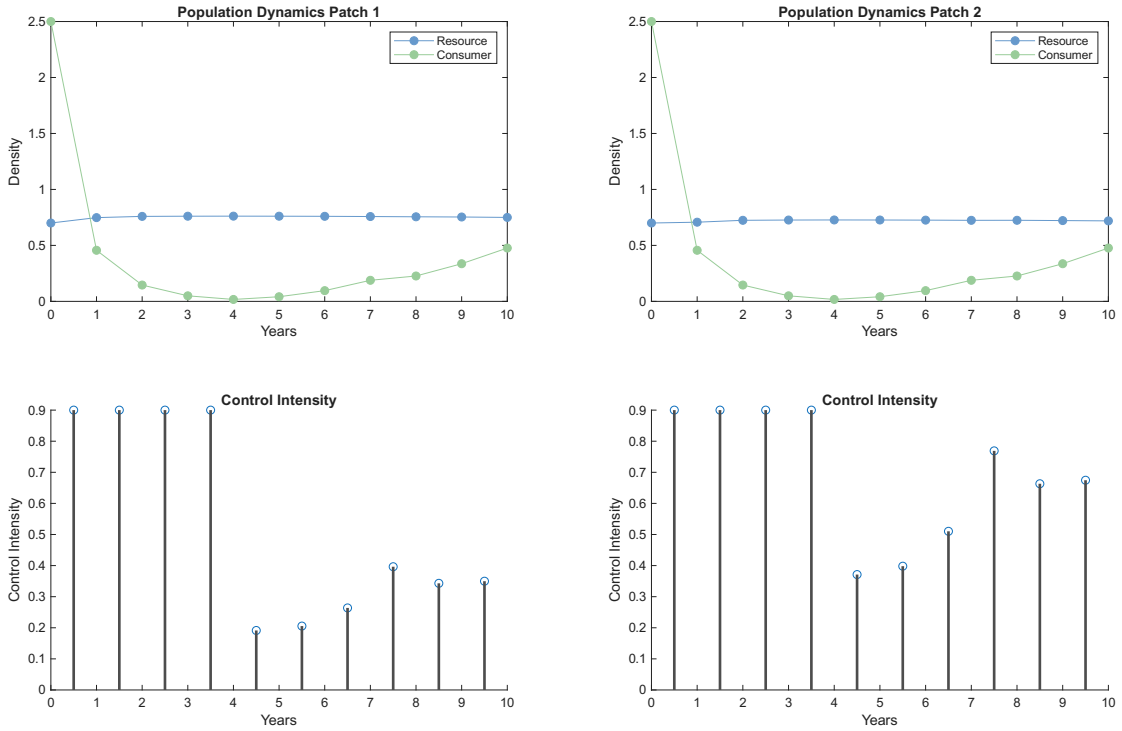

(a) Case three

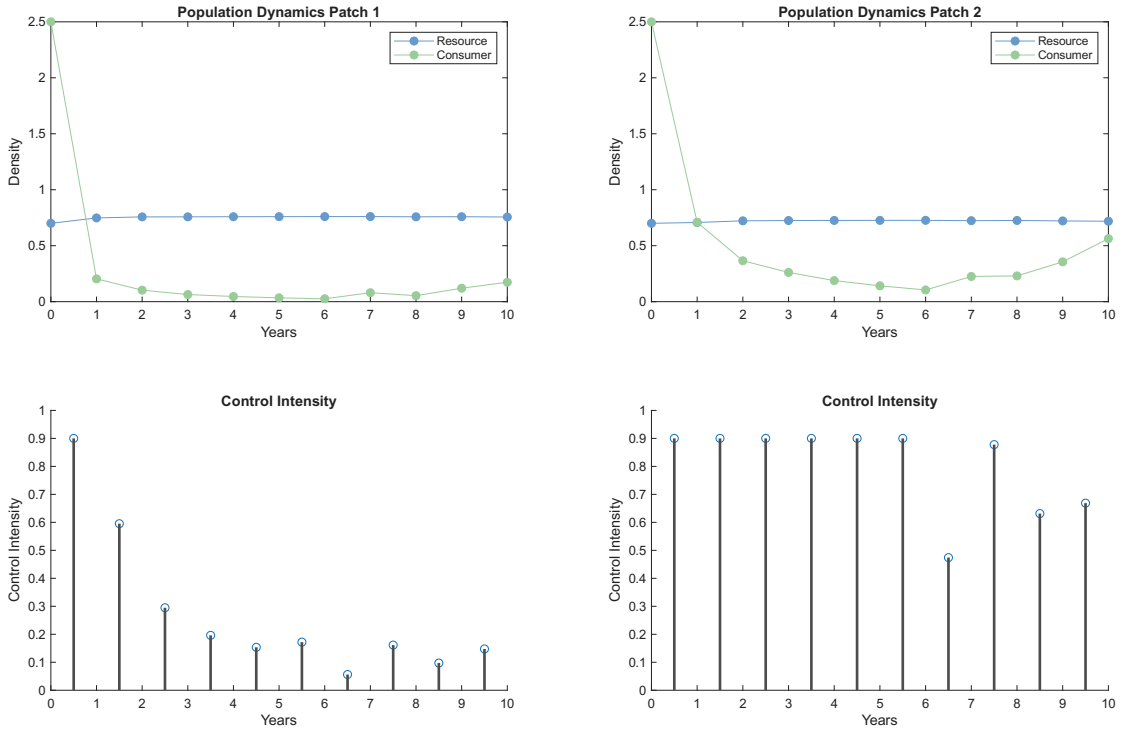

(b) Case four

Figure 5.6: Rows one and three: Dynamics of the symmetric and asymmetric model both with asymmetric migration at the start of each year for consumers (green) and resources (blue). Rows two and four: corresponding control-intensity schedule.

22, a lower consumer death rate, $\mu_1 = 1.5, \mu_2 = 1$, and a higher attack rate $\alpha_1 = 10, \alpha_2 = 12$. Accordingly, we chose retention to be low on patch one and high on patch two, by setting $p_1 = 0.15$ and $p_2 = 0.65$. We would expect, based on case two, that the patch to which more individuals disperse has higher control. We also expect that the patch of better quality has more control. The results of this experiment are shown in the bottom two rows of Figure 5.6.

We note that, as expected, there is a large asymmetry in the control and the dynamics in patch one versus patch two. Patch one has few individuals after the initial control pulse of one year, so it needs very little control in subsequent years. There are more individuals on patch two due to migration, so more control is applied. Also, since the patch quality is higher, more individuals thrive and so the patch has more control applied. The effects of dispersal and better patch quality in patch two are shown by high control intensity over the first six years. After which, the controls remain high on patch two and lower on patch one.

Altogether, we find that dispersal asymmetry and patch quality asymmetry reinforce one another, producing a strong and more intense control schedule. We also find that the resource population does not experience large changes due to the control of the consumer, even though the two dynamics are linked through the attack term. This may be a result of the objective function, which frames the optimal-control problem to minimize the running costs and minimize the consumer density and does not reward higher resource density.

5.6 Spruce Budworm Management

In this section, we now return to our original issue, that of SBWs in Canadian forests. To approach this problem, we consider two patches that have distinct management strategies. We consider one patch located on the parkland of Gros Morne National Park, which allows little to no control. Thus, the cost of spraying the parkland is scaled very high. We consider control on the surrounding land to be of lower cost and thus scale it appropriately. We consider the surrounding land to be less habitable for SBWs; thus the quality of the patch within the park is higher than that surrounding it. Finally, we consider heterogeneous movement in and out of the park to simulate directed migration west or east. We include a payoff term, which reflects the fact that the final condition for the system should also minimize the SBW population at the final time and reduce the chances of future outbreaks. We set a final time of 35 years, which is the average length of a SBW outbreak. Our cost function is

$$J(u) = 10w_{1,T} + 10w_{2,T} + \sum_{t=0}^{T-1} 5u_{1,t}^2 + 30u_{2,t}^2 + w_{1,t}^2 + w_{2,t}^2. \tag{5.6.1}$$

The weights are chosen so that spraying in the parkland is much more costly than outside. We chose a high weight for the final year to ensure the system ends in less than endemic population size, reducing the chances of another outbreak. Then the Hamiltonian for year t becomes:

$$H_t = 5u_{1,t}^2 + 30u_{2,t}^2 + w_{1,t}^2 + w_{2,t}^2 + \lambda_{v_1,t+1}\Phi_{1,v} + \lambda_{v_2,t+1}\Phi_{2,v} + \lambda_{w_1,t+1}\Phi_{1,w} + \lambda_{w_2,t+1}\Phi_{2,w}. \tag{5.6.2}$$

The necessary conditions for this case become for $i = 1, 2$:

$$\lambda_{w_i,t} = \frac{\partial \Phi_{i,w}}{\partial w_i} + 20w_{i,t}, \tag{5.6.3}$$

$$\lambda_{v_i,t} = \frac{\partial \Phi_{i,v}}{\partial v_i} + 20w_{i,t}. \tag{5.6.4}$$

Then unlike before, we include a payoff term, so that the transversality conditions become:

$$\lambda_{w_i,T} = 20w_1, \tag{5.6.5}$$

$$\lambda_{v_i,T} = 20w_2. \tag{5.6.6}$$

The optimality condition is:

$$\frac{\partial H_t}{\partial u_t} = 0 \text{ at } u_t^*. \tag{5.6.7}$$

Figures 5.7 and 5.8 display the results of these experiments. We note that in the figures, the left two plots represent the surrounding forest, and the right two plots represent the parkland. We chose the parkland to have a higher resource growth rate ($\rho_1 = 20, \rho_2 = 25$), a higher attack rate ($\alpha_1 = 10, \alpha_2 = 11$) and a lower consumer-death rate ($\mu_1 = 1.5, \mu_2 = 1$).

For the first experiment, we let $p_1 = 0.15$ and $p_2 = 0.65$. This means that dispersal is directed toward the parkland. This scenario may occur because the consumers direct their movement towards the better-quality patch, or winds transport them into the park. We find that, even though control on the parkland (right plots) costs six times that of the surrounding forest, the optimal control is still to spray in both the lower-cost and the higher-cost patch. The optimal control is to apply cyclic controls on each patch, with lower-intensity controls on the higher-cost parkland. When higher-intensity controls are applied in patch one, patch two has two lower-intensity years. Similarly, when patch two applies a higher-intensity control, patch one applies a lower-intensity control. We also note the difference in scales, where the intensity of most controls on patch one are three times higher or more than on patch two, as expected since the control is much more costly on patch two. Finally, we note that the resource population cycles in both patches when the consumer populations are being controlled with cyclic intensity.

For the second experiment, we let $p_1 = 0.65$ and $p_2 = 0.15$. This means that dispersal is directed away from the parkland (i.e., consumers predominately move away from the better-quality patch). We find that the optimal-control schedule of the consumer is somewhat opposite to the control schedule of the first experiment. We note that the control of the consumer is higher on patch two, and lower on patch one than the first experiment. In this scenario, the optimal outcome is to heavily control the population on the parkland, and let the consumers on the private forests die naturally due to the higher death rate on that patch. In this scenario, the private forests end up with a higher density of consumers than on the parkland. In the last few years, there are slightly higher controls applied in order to account for the requirement that the final consumer density be minimized.

In both cases, control on the costly patch is always part of the optimal control, but the manner in which it is applied depends on the direction of dispersal.

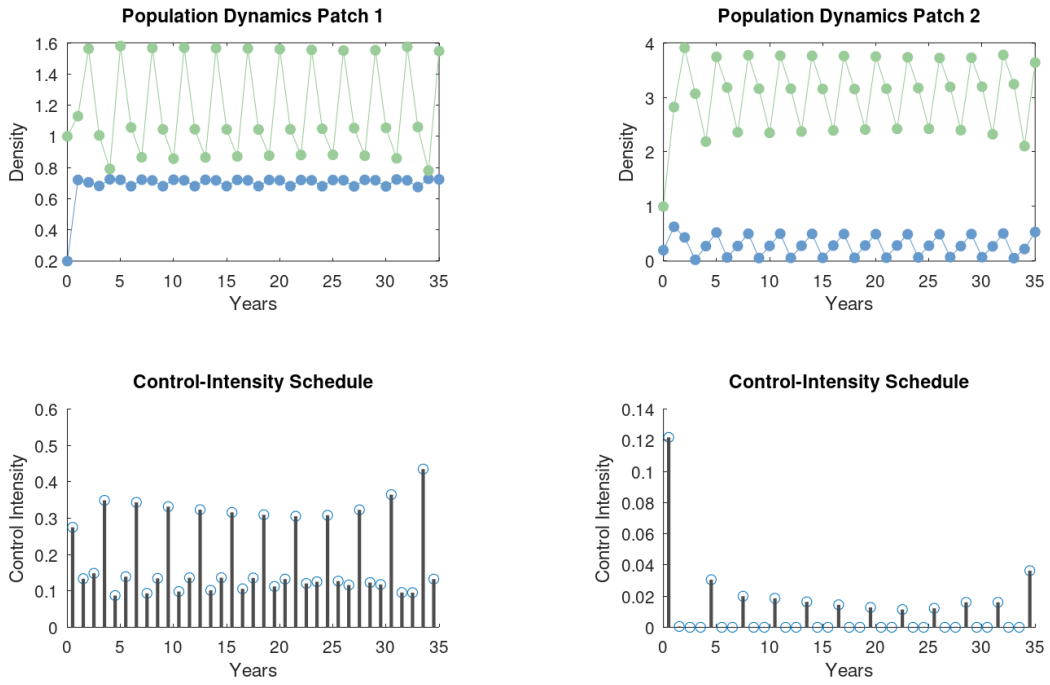

Figure 5.7: Top plot: density of consumer (green) and resource (blue) population on one patch over 35 years. Bottom plots: control intensity when control intensity applied halfway through each year. Left plots: surrounding stands. Right plots: parkland. Parameters are $\rho_1 = 20, \rho_2 = 25$, $\alpha_1 = 10, \alpha_2 = 11$, $\mu_1 = 1.5, \mu_2 = 1$, $p_1 = 0.15$ and $p_2 = 0.65$. A tolerance of 10^{-4} is used with a relaxation parameter $\gamma = 0.05$. Note the different scales on the vertical axes between the plots on the right and on the left.

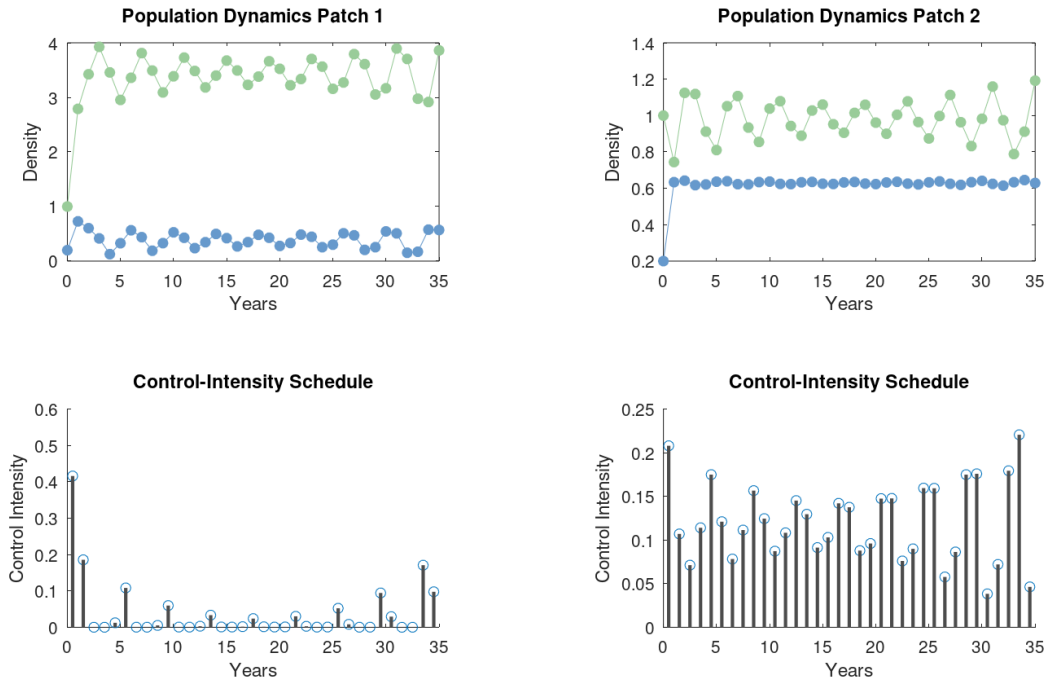

Figure 5.8: Top plot: density of consumer (green) and resource (blue) population on one patch over 35 years. Bottom plots: control intensity when control intensity is applied halfway through each year. Left plots: surrounding stands. Right plots: parkland. Parameters are as in Figure 5.7. Note the different scales on the vertical axes between the plots on the right and on the left.

In this chapter, we determined the optimal-control intensity for both one and two patches. By varying the environments and dispersal asymmetry, we found different control-intensity schedules. We ended by solving for the optimal control of two scenarios inspired by SBWs in adjacent forests.

Chapter 6

Discussion

Overview and Main Findings

In this thesis, we were interested in the long-term behaviour of a semi-discrete two-patch system of consumers and resources. Inspired by the model created by Pachepsky et al. [34], we derived a system where the consumers reproduced discretely, at the beginning of the year, and the resource reproduced continuously. We were mainly interested in three questions. What is the long-term behaviour of our biologically inspired model? What is the impact of dispersal? Which control schedule is most effective at controlling the consumer population? We answer each of these questions by detailing our key results.

In chapter two, we derived the stroboscopic map that describes the consumer density from year to year. In chapter three, we focused on the question of our model's long-term behaviour. The trivial fixed point and semi-trivial fixed points were both characterized in Pachepsky et al. [34] for one patch in isolation. Extending the model to two patches, our conditions for stability of the semi-trivial states are a combination of growth rate and dispersal, which incorporates the effect of patch dynamics. We found that the semi-trivial state can be unstable, which can lead to consumer invasion. We showed that invasion is more likely as the growth rate of either patch increases, and that if invasion is possible in one patch, dispersal means that invasion must also be possible in the second patch. We found that consumer populations benefit from staying in good patches. When the probability of dispersal is equal, we saw that the benefit from remaining in good patches outweighs the detriment of staying in a lower-quality patch. Thus, in general, dispersal is beneficial to consumer populations that are close to extinction.

We continued our exploration of the fixed points and their stability by determining the defining equations for the coexistence state. We found that there were two boundary-coexistence states, one for each of the states where one resource population went extinct. We analyzed the invasion state and found that, unlike the consumer population, the invasion conditions did not depend on dispersal, but rather on the balance between resource growth rate and the consumer presence and pressure on that patch. To analyze the steady states where none of the resource and consumer populations die out, we approached the problem

geometrically. We used the intersections of the conic sections described by the coexistence equilibria to geometrically determine fixed points and their bifurcations. We first found a transcritical bifurcation and found that this bifurcation condition is the same as the invasion condition for the semi-trivial state. Thus, this transcritical bifurcation introduces a positive steady state that passes through the zero state. We also found a saddle-node bifurcation. We determined the conditions for its existence by using the discriminant of the polynomial formed by equating both conic section equations. We ended the chapter by finding dynamics featured in [34] and additional new dynamics such as the boundary-coexistence state and 6-cycles.

In chapter four, we focused our attention on the question of dispersal benefit. We first performed an asymptotic expansion using dispersal as a small parameter and found that the zeroth-order solution on either patch matched the equilibrium found in [34], as expected. We found that the first-order correction was a function of the difference between the zeroth-order correction terms. Also, the benefit to the consumer population on one patch meant detriment to the population on the other patch. This means that, in order for the population to benefit from small dispersal, the population with the higher growth rate must have the lower population without dispersal, or the population with the smaller growth rate must have the larger population without dispersal. We then asked: what happens when dispersal is not restricted to small probabilities? To answer this, we used the H-index, described in Grumbach et al. [20]. We found all four characteristic-response scenarios that were previously reported in the literature, along with the trivial scenario and a response scenario that leads to extinction.

Finally, in chapter five, we extended the model to account for impulsive control of the consumer. This control was a reduction in the consumer density, and was inspired by the aerial spraying of SBWs in Canadian forests. We found that on one patch, the optimal control was simple, with control intensity highest before the final year. When we changed the problem to account for two patches, we found that the control schedule depended on the type of heterogeneity and included feedback from dispersal between the two patches. In the case of asymmetric dispersal, we found that the patch where individuals reside most often is more controlled. Similarly, the better-quality patch receives more control as individuals do better on this patch. These effects are compounded when asymmetry towards the better patch is accounted for. We finish this chapter with an analysis of the optimal control over 35 years of SBW management. Inspired by the varying control strategies in adjacent forests, we determine the optimal control of consumers over two asymmetric patches. For the first experiment, we assumed that there was directed dispersal towards the parkland and that the parkland was of better quality. For the second, we assumed dispersal was mainly away from parklands. We weighted the cost of control on the parkland six times higher than the cost of control on the surrounding privately owned forests. We found that, surprisingly, the optimal outcome was to apply consistent controls to the parkland, even if it was much costlier.

Limitations

The two models studied in the thesis both have limitations that should be acknowledged. First, the Pachepsky model assumes reproduction occurs instantaneously. This is not entirely accurate. The systems we use for inspiration—harp seals, SBWs, and mice—reproduce in short bursts. Harp seals give birth in a highly synchronized birth pulse that lasts on average one week [38]. SBWs reproduce in an 8–12 day burst, and mice in a 10–14 day period. These birth pulses are, when compared to the number of days in a year, relatively short. In the same manner, we assumed that dispersal was instantaneous. While true dispersal is not instantaneous, in the species we have described, dispersal happens over the course of several days. So, although not entirely accurate, we assume birth and dispersal impulses provide a reasonable estimate of these species' dynamics.

Further, we inherit some of the limitations inherent in the model by Pachepsky et al. [34]. The authors note that their model has a very simple structure, with logistic growth and linear functional response. A more complicated model might have a more accurate functional response, such as a Holling Type II functional response. We note that, even with these simplifications, describing the dynamics of this model analytically is challenging. All the analysis in Chapter 3 relies on the solvability of the differential equations, so if they were more complicated, we may not be able to determine the stroboscopic maps. For this reason, we chose to keep the linear functional response and logistic growth as in the Pachepsky model.

Future Directions

There are many exciting future directions for this work. We focus on two of them here.

First, we can naturally extend the framework established to calculate the optimal control to include determining the optimal timing. In our model, we set the time of controls halfway through the year. However, SBWs may be best managed by spraying at a different time in the year. Many studies have shown that optimal harvesting depends on timing [12], and control timing has been shown to establish a pest-free equilibrium in some models [43]. Another consideration is the life cycle of the SBWs, which includes several life stages during the year. Each life stage may have a different attack rate and death rate, affecting possible controls. To address this, one could subdivide the within-year continuous portion into various life stages, which are synchronized because populations emerge at the same time. These ODEs could differ in attack and death rate. Each equation would still be explicitly solvable, and therefore the stroboscopic map could be calculated. Then in the same manner as Chapter 5, we could apply the optimal-control framework to determine the optimal intensity and timing of pesticide application.

Second, we could also include local versus global optimization over two patches. Currently, we only consider the case where the Hamiltonian is minimized over the two patches. This scenario represents one budget for the two forests. We could instead consider two budgets, one dictated by the government responsible for parkland, and the second by the

landowners of private forest around the parkland. We could also consider the management between two provinces with different budgets, such as Quebec and New Brunswick. In this way, each province or party would have a separate objective function, which represents its interest. For the land owners, that may be to optimize the resource density at whatever spraying cost. For the parkland, it may be to reduce consumer density, but at a very high cost of spraying. Once the two Hamiltonians have been established, we can view the problem through the lens of game theory. From here, several options are possible. For reference on Game Theory, we refer to the textbook *An Introduction to Game Theory* [33].

We may decide that the landowners and the province are competitors, and we could frame a Nash equilibrium game-theory problem. We could calculate the Nash equilibrium, where each player maximizes their strategy until no player can achieve a better strategy. In this framework, each manager would create a management plan while anticipating the effects of dispersal and thus the possible control schedules on the other patch, and plan accordingly. For this game, we may ask: Can we stop rapid de-investing in control, where managers give up control since reintroduction of SBWs through dispersal is so common? What control strategies best benefit both managers while optimizing each goal?

We could instead give one manager a power advantage and choose a Stackelberg game. This is what is considered a *nested* optimization, where the leader (the government) makes decisions regarding the follower's (landowners) actions and vice versa. The setup is as follows: first choose a control set for the leader; then find the follower's reaction to the leader's control choice as a function of the leader's control set. Feed that control set back into the leader dynamics. Continue until an equilibrium is found. Because the Stackelberg game has asymmetric influence, we could ask questions such as: Can the leader (government) force the follower (private owners) to help by manipulating the dynamics of SBWs through control? Does the leader benefit and end up with fewer SBWs on their patch?

In summary, this thesis explores effects of dispersal in consumer–resource systems, finding both novel and well-cited results. It identifies new optimal-control strategies applied to a semi-discrete consumer–resource system and extends knowledge about how patch dynamics impact long term stability and population density. By targeting control more efficiently, these strategies reduce unnecessary intervention while still lowering consumer growth. This leads to improved environmental outcomes at lower cost.

Bibliography

[1] Sarah Abel. Dynamic consequences of phenological asynchrony in a consumer–resource model. Master's thesis, University of Ottawa, 2025.

[2] Imane Abouelkheir, Fadwa El Kihal, Mostafa Rachik, and Ilias Elmouki. Optimal impulse vaccination approach for an SIR control model with short-term immunity. *Mathematics*, 7(5):420, 2019.

[3] Michael Allaby. Antechinus. In *A Dictionary of Zoology*. Oxford University Press, Oxford, 5th edition, 2020.

[4] Jéssica C.S. Alves, Sergio M. Oliva, and Christian E. Schaerer. Optimizing impulsive releases: A species competition model. *Applied Mathematical Modelling*, 151:116517, 2026.

[5] Roger Arditi, Claude Lobry, and Tewfik Sari. Is dispersal always beneficial to carrying capacity? New insights from the multi-patch logistic equation. *Theoretical Population Biology*, 106:45–59, 2015.

[6] Stefano Baccarin. Optimal impulse control for cash management with quadratic holding-penalty costs. *Decisions in economics and finance*, 25(1):19–32, 2002.

[7] Carl M. Bender and Steven A. Orszag. *Advanced mathematical methods for scientists and engineers I: Asymptotic Methods and Perturbation Theory*. Springer, New York, 1999.

[8] Arianna Bianchi, Thomas Hillen, Mark A. Lewis, and Yingfei Yi. *The Dynamics of Biological Systems*, volume 4 of *Mathematics of Planet Earth*. Springer International Publishing, 2019.

[9] Peter S. Bullen. The arithmetic, geometric and harmonic means. In *Handbook of Means and Their Inequalities*, pages 61–134. Springer, Dordrecht, 2003.

[10] Hal Caswell. *Matrix Population Models: Construction, Analysis, and Interpretation*. Sinauer Associates, Sunderland, Massachusetts, 2nd edition, 2001.

[11] Catherine Chagnon, Sébastien Dumont, Alexandre Morin-Bernard, Hervé Jactel, Alexis Achim, and Guillaume Moreau. Potential of thinning to increase forest resilience and resistance to drought, pest, windstorm and fire: A meta-analysis. *Forest Ecology and Management*, 590:122788–, 2025.

[12] Begoña Cid, Frank M. Hilker, and Eduardo Liz. Harvest timing and its population dynamic consequences in a discrete single-species model. *Mathematical Biosciences*, 248:78–87, 2014.

[13] Cristian Corona, Abigail C. Leeper, and Jalene M. LaMontagne. Differential defoliation and mortality of white spruce and balsam fir by eastern spruce budworm. *Forest Ecology and Management*, 508:120042, 2022.

[14] Lisette G. de Pillis, Weiqing Gu, K. Renee Fister, Timothy Head, Kevin Maples, Arvind Murugan, Travis Neal, and Karyn Yoshida. Chemotherapy for tumors: An analysis of the dynamics and a study of quadratic and linear optimal controls. *Mathematical Biosciences*, 209(1):292–315, 2007.

[15] Donald L. DeAngelis, Curtis C. Travis, and Wilfred M. Post. Persistence and stability of seed-dispersed species in a patchy environment. *Theoretical population biology*, 16(2):107–125, 1979.

[16] Agriculture Department of Forestry and Lands. *Public Notice Spruce Budworm Early Intervention Control program*. Department of Forestry, Agriculture and Lands, 2025.

[17] Ihza Rizkia Fitri, Farida Hanum, Ali Kusnanto, Toni Bakhtiar, and Sanling Yuan. Optimal pest control strategies with cost-effectiveness analysis. *The Scientific World Journal*, page 6630193, 2021.

[18] Herbert I. Freedman and Paul E. Waltman. Mathematical models of population interactions with dispersal. I: Stability of two habitats with and without a predator. *SIAM Journal on Applied Mathematics*, 32(3):631–648, 1977.

[19] Alvaro Fuentealba, Alain Dupont, Christian Hébert, Richard Berthiaume, Roberto Quezada-García, and Éric Bauce. Comparing the efficacy of various aerial spraying scenarios using Bacillus thuringiensis to protect trees from spruce budworm defoliation. *Forest Ecology and Management*, 432:1013–1021, 2019.

[20] Carolin Grumbach, Femke N. Reurik, Juan Segura, Daniel Franco, and Frank M. Hilker. The effect of dispersal on asymptotic total population size in discrete- and continuous-time two-patch models. *Journal of Mathematical Biology*, 87(4):60, 2023.

[21] Ralph Haygood. Coexistence in MacArthur-style consumer–resource models. *Theoretical Population Biology*, 61(2):215–223, 2002.

[22] Richard A. Holmgren. *A first course in discrete dynamical systems*. Universitext. Springer, 2nd edition, 1996.

[23] Kun Hu and Yuanshi Wang. Dynamics of consumer-resource systems with consumer's dispersal between patches. *Discrete and Continuous Dynamical Systems - Series B*, 27(2):977–1000, 2022.

[24] Rong Huang, Yuanshi Wang, and Hong Wu. Population abundance in predator–prey systems with predator's dispersal between two patches. *Theoretical Population Biology*, 135:1–8, 2020.

[25] Shivani Khare, Kunwer Singh Mathur, and Krishna Pada Das. Optimal control of deterministic and stochastic eco-epidemic food adulteration model. *Results in Control and Optimization*, 14:100336, 2024.

[26] Mark Kot. *Elements of Mathematical Ecology*. Cambridge University Press, Cambridge, UK, 2001.

[27] Valérie Lemesle and Ludovic Mailleret. A note on semi-discrete modelling in the life sciences. *Philosophical Transactions of the Royal Society A: Mathematical, Physical and Engineering Sciences*, 367(1908):4779–4799, 2009.

[28] Suzanne Lenhart and John T. Workman. *Optimal Control Applied to Biological Models*. Mathematical and Computational Biology. Chapman and Hall/CRC, Boca Raton, FL, 2007.

[29] Yuan Lou. On the effects of migration and spatial heterogeneity on single and multiple species. *Journal of Differential Equations*, 223(2):400–426, 2006.

[30] Stephen R. McReynolds and Arthur E. Bryson, Jr. A successive sweep method for solving optimal programming problems. Technical Report 463, Cruft Laboratory, Division of Engineering and Applied Physics, Harvard University, Cambridge, Massachusetts, March 1965.

[31] Jim R. Muirhead, Brian Leung, Colin van Overdijk, David W. Kelly, Kanavillil Nandakumar, Kenneth R. Marchant, and Hugh J. MacIsaac. Modelling local and long-distance dispersal of invasive emerald ash borer *Agrilus planipennis* (coleoptera) in North America. *Diversity and Distributions*, 12(1):71–79, 2006.

[32] Natural Resources Canada, Canadian Forest Service, and Laurentian Forestry Centre. *Spruce budworm*. Natural Resources Canada, Canadian Forest Service, Laurentian Forestry Centre, Québec, 2018.

[33] Martin J. Osborne. *An introduction to game theory*. Oxford University Press, New York, 2004.

[34] Elizaveta Pachepsky, Roger M. Nisbet, and William W. Murdoch. Between discrete and continuous: Consumer–resource dynamics with synchronized reproduction. *Ecology*, 89:280–288, 2008.

[35] Lev S. Pontryagin, Vladimir G. Boltyanskii, Revaz V. Gamkrelidze, and Evgenii F. Mishchenko. *The Mathematical Theory of Optimal Processes*. Interscience Publishers, New York, 1962. Translated from the Russian by Konstantin N. Trirogoff; edited by Lucien W. Neustadt.

[36] Alfonso Ruiz-Herrera and Pedro J. Torres. Effects of diffusion on total biomass in simple metacommunities. *Journal of Theoretical Biology*, 447:12–24, 2018.

[37] Clifford S Sadof, Deborah G McCullough, and Matthew D Ginzel. Urban ash management and emerald ash borer (coleoptera: Buprestidae): facts, myths, and an operational synthesis. *Journal of Integrated Pest Management*, 14(1), 2023.

[38] Becky L. Sjare and Canadian Stock Assessment Secretariat. *Recent estimates of reproductive rates for harp seals in the northwest Atlantic*. Canadian Stock Assessment Secretariat, 2000.

[39] Wladimir A. Smirnoff. Bacillus thuringiensis: A logical weapon for Spruce Budworm control. *The Forestry Chronicle*, 54(6):309–312, 1978.

[40] Steven H. Strogatz. *Nonlinear dynamics and chaos: with applications to physics, biology, chemistry, and engineering*. Studies in nonlinearity. CRC Press, Boca Raton, FL, 2nd edition, 2018.

[41] De Tang and Zhi-An Wang. Population dynamics with resource-dependent dispersal: Single- and two-species models. *Journal of Mathematical Biology*, 86(2):23, 2023.

[42] Bo Zhang, Alex Kula, Keenan M. L. Mack, Lu Zhai, Arrix L. Ryce, Wei-Ming Ni, Donald L. DeAngelis, J. David Van Dyken, and Otso Ovaskainen. Carrying capacity in a heterogeneous environment with habitat connectivity. *Ecology Letters*, 20(9):1118–1128, 2017.

[43] Shujuan Zhang, Juhua Liang, and Sanyi Tang. Optimal application timing of pest control tactics in nonautonomous pest growth model. *Abstract and Applied Analysis*, 2014:650182, 2014.